

THESIS ON NATURAL AND EXACT SCIENCES B156

# **Multi-Scale Wind Wave Modeling in the Baltic Sea**

VICTOR ALARI

**TUT**  
**PRESS**

TALLINN UNIVERSITY OF TECHNOLOGY  
Marine Systems Institute

**Dissertation was accepted for the defense of the degree of Doctor of  
Philosophy in Earth Sciences on June 19, 2013**

**Supervisor:** Dr Urmas Raudsepp, Marine Systems Institute at Tallinn  
University of Technology.

**Opponents:** Dr Gerbrant Ph. Van Vledder, Delft University of Technology, the  
Netherlands

Dr Ülo Suursaar, Estonian Marine Institute, University of Tartu

**Defense of the thesis:** September 2, 2013 at the Marine Systems Institute at  
Tallinn University of Technology, Akadeemia tee 15a, Tallinn, Estonia

Declaration:

I hereby declare that this doctoral thesis, submitted for the doctoral degree at  
Tallinn University of Technology, is my original investigation and achievement  
and has not been submitted for any other academic degree.

*Victor Alari*



European Union  
European Social Fund



Investing in your future

Copyright: Victor Alari, 2013  
ISSN 1406-4723  
ISBN 978-9949-23-511-7 (publication)  
ISBN 978-9949-23-512-4 (PDF)

LOODUS- JA TÄPPISTEADUSED B156

# Mitmemastaapne tuulelainete modelleerimine Läänemeres

VICTOR ALARI



# CONTENTS

<b>LIST OF ORIGINAL PUBLICATIONS.....</b>	<b>6</b>
<b>ABBROPATION OF THE RESULTS .....</b>	<b>7</b>
<b>ABBREVIATIONS.....</b>	<b>8</b>
<b>1. INTRODUCTION .....</b>	<b>9</b>
1.1 BACKGROUND .....	9
1.2 MOTIVATION AND OBJECTIVE .....	10
<b>2. OVERVIEW OF BALTIC SEA WIND AND WAVE VARIABILITY .....</b>	<b>11</b>
2.1 WIND CONDITIONS OVER THE BALTIC SEA .....	12
2.2 BALTIC SEA WAVE VARIABILITY.....	13
<b>3. MATERIALS AND METHODS .....</b>	<b>15</b>
3.1 STUDY AREAS .....	15
3.2 STUDY DESIGNS .....	15
3.3 DESCRIPTION OF SWAN WAVE MODEL .....	18
3.3.1 <i>Source terms</i> .....	19
3.4 OVERVIEW OF SWASH MODEL .....	22
3.5 WAVE INDUCED SHEAR VELOCITY .....	22
3.6 WAVE INDUCED CURRENTS.....	23
<b>4. SENSITIVITY OF SPECTRAL PARAMETERS ON MODEL SETTINGS .....</b>	<b>24</b>
4.1 SURGE IMPACTING WAVE FIELD .....	24
4.2 ROLE OF DEPTH-INDUCED BREAKING .....	27
4.3 TWO WHITECAPPING FORMULATIONS .....	30
<b>5. WAVE PROPAGATION THROUGH ARRAY OF OBSTACLES.....</b>	<b>32</b>
<b>6. WAVE INDUCED FLOW AND SET-UP .....</b>	<b>35</b>
6.1 WAVE INDUCED FLOW .....	35
6.2 WAVE DRIVEN SET-UP.....	37
<b>7. CONCLUSIONS.....</b>	<b>39</b>
<b>REFERENCES .....</b>	<b>41</b>
<b>PUBLICATIONS.....</b>	<b>47</b>
PAPER I.....	47
PAPER II .....	61
PAPER III .....	69
PAPER IV .....	93
PAPER V .....	101
<b>ACKNOWLEDGEMENTS .....</b>	<b>115</b>
<b>ABSTRACT .....</b>	<b>116</b>
<b>RESÜMEE .....</b>	<b>118</b>
<b>ELULOOKIRJELDUS .....</b>	<b>120</b>
<b>CURRICULUM VITAE .....</b>	<b>124</b>

## LIST OF ORIGINAL PUBLICATIONS

The dissertation is based on the following academic publications, which will be referred to in the text by their Roman numerals.

- I. Alari, V., Kõuts, T. 2012. Simulating wave-surge interaction in a non-tidal bay during cyclone Gudrun in January 2005. In: Ocean: Past, Present and Future - 2012 IEEE/OES Baltic International Symposium, BALTIC 2012, art. no. 6249185.
- II. Alari, V., Raudsepp, U. 2012. Simulation of wave damping near coast due to offshore wind farms. Journal of Coastal Research, 28 (1), pp. 143-148.
- III. Raudsepp, U., Laanemets, J., Haran, G., Alari, V., Pavelson, J., Kõuts, T. 2011. Flow, waves and water exchange in the Suur strait, Gulf of Riga, in 2008. Oceanologia, 53 (1), pp. 35-56.
- IV. Alari, V., Raudsepp, U. 2010. Depth induced breaking of wind generated surface gravity waves in Estonian coastal waters. Boreal Environment Research, 15 (3), pp. 295-300.
- V. Alari, V., Raudsepp, U., Kõuts, T. 2008. Wind wave measurements and modelling in Küdema Bay, Estonian Archipelago Sea. Journal of Marine Systems, 74 (SUPPL.), pp. S30-S40.

Some unpublished data is also presented.

### AUTHOR'S CONTRIBUTION

\*\*\* – complete contribution (100 %)

\*\* – leading contribution (> 50 %)

\* – supporting contribution (< 50 %)

Paper	I	II	III	IV	V
Concept	***	***	*	***	**
Design	***	***	*	**	**
Modeling	***	***	*	***	***
Data analysis	***	**	*	**	**
Manuscript preparation	**	**	*	**	**

## **ABBROPATION OF THE RESULTS**

The results have been presented at the following international conferences:

- 1) Baltic Sea Science Congress on 19 – 23 March 2007, Rostock, Germany. Wind wave measurements and modeling in Küdema Bay, Estonian Archipelago Sea.
- 2) Baltic Sea Science Congress on 17 – 21 August 2009, Tallinn, Estonia. On the validation of SWAN, a third-generation spectral wave model, for Estonian coastal sea.
- 3) 12<sup>th</sup> International Workshop on Wave Hindcasting and Forecasting & 3rd Coastal Hazard Symposium on October 30 – November 4 2011, Kohala Coast, Hawaii. Towards an operational wave monitoring and prediction service in Estonia.
- 4) IEEE/OES Baltic 2012 International Symposium on 8 – 11 May 2012, Klaipeda, Lithuania. Simulating wave-surge interaction in a non-tidal bay during cyclone Gudrun in January 2005.

## **ABBREVIATIONS**

DIA	Discrete Interaction Approximation
EMB	Estonian Marine Board
HIRLAM	High Resolution Limited Area Model
RMSD	Root-mean square deviation
SMHI	Swedish Meteorological and Hydrological Institute
SWAN	Simulating Waves Nearshore
SWASH	Simulating Waves till Shoreline
WAM	Wave Model

# 1. INTRODUCTION

## 1.1 Background

Wind waves gain energy, propagate, undergo linear and non-linear transformation, and finally dissipate over a wide range of spatial and temporal scales. As they do so, a non-homogenous distribution of wave energy is formed, leading to zones of increased and decreased energy, while at the same time the wave energy is transported in various propagation directions. The wave fields usually have a large gradient (in any bulk spectral parameter) along physical boundaries, like coastlines, marginal ice zones and shoaling zone.

Spatial variability of wave energy in near-coastal areas is scientifically and technically an important phenomenon, which can be resolved to a certain extent in a feasible manner by the method of multi-scale modeling. A multi-scale model in a geographical space of an oceanographic variable (herein the wave action spectral density) attempts to resolve the underlying natural variations by increasing the density of computational points in areas of interest. Technically this is achieved by nesting techniques or unstructured meshes. It is also necessary that the model's physical and numerical features are suited for capturing the mechanisms of wave transformation on desirable scales, herein the coastal waters.

The need for multi-scale modeling is becoming more and more important, since maritime activities near the coast are increasing as so the awareness of environmental aspects. Furthermore, people settling to live in coastal areas are faced with a flooding danger in lowlands and need accurate forecasts. These can be provided by means of high resolution validated models. Specifically, numerous multi-scale wave modeling studies have been conducted worldwide, in order to provide wave conditions for coastal engineering activities and navigation (Anselmi-Molina et al., 2012; Inghilesi et al., 2012; Rusu and Soares, 2013), to estimate the wave induced flow, water level rise, overtopping (Dietrich et al., 2012; Choi et al., 2013; Zou et al., 2013) and sediment resuspension (Jones et al., 2012; Dalyander et al., 2013). Moreover, multi-scale wind wave modeling has an important role in cross-disciplinary studies (Stevens and Lacy, 2012; Zhang et al., 2012) and just lately, the demand for the utilization of wave energy itself has lead to numerous high resolution model studies (e.g. Neill and Hashemi, 2013; Stopa et al., 2013 and many others). The field of multi-scale wave modeling however is underdeveloped for the applications in the Baltic Sea in any aspects listed above. The author can only name the following researches. Recently Tuomi et al. (2012) used a 0.25 nautical mile grid to study the fetch limited wave growth from an irregular coastline. Soomere (2005) used the same resolution nested in coarser WAM model to study the wind wave statistics in Tallinn Bay. Known unstructured approaches are by Chubarenko et al. (2012), who analyzed the wave regime of

the Vistula lagoon using the SWAN model, with grid size as low as 100 m. Kurennoy and Ryabchuk (2011) modeled the Neva Bay wave climate.

## 1.2 Motivation and objective

Accurate knowledge of near-shore wave spectrum, its spatial variations and implications to other processes is poorly studied and known in the Baltic Sea. Though, a considerable number of academic studies by other authors and engineering projects have indicated the need for detailed knowledge of Baltic Sea near shore wave fields. Lagemaa et al. (2011) pointed out the need to take into account wave induced set-up in extreme weather conditions, while Lilover et al. (2011) suggested estimating the Stokes drift near shore to explain the measured current variability. Patterns of suspended particulate matter (Haran et al., 2010) and species distribution in the Baltic Sea coastal waters depend on the wave fields (Westerbom and Jattu, 2006; Kolesova et al., 2010; Kovtun et al., 2011), whereas movement of shoreline responds to the joint influence of waves, currents and water level (Tönisson et al., 2012). Other examples include: planning of harbors (Elken et al., 2001), offshore wind farms (Paper II) and other infrastructure; assessing backfilling of dredged areas; harbor approach and navigation; marine leisure activities and so forth.

The main objective of this thesis is to study the variability of near-coastal wave fields and particularly their impacts to other processes and processes influencing wave field evolution by using multi-scale wave modeling as a method and Estonian marine waters as a study site. The specific aims are:

- To analyze the sensitivity of significant wave height on temporal variations in water level.
- To quantify the magnitude of depth-induced wave breaking in severe weather conditions.
- To analyze the sensitivity of spectral peak period on two whitecapping formulations.
- To study the effect of arrays of small obstacles to wave field evolution.
- To quantify wave generated near-bed flow due to orbital motions of waves and mean flow generation due to gradients in wave energy.
- To quantify the wave induced setup during cyclone Gudrun in 2005.

This thesis is structured as follows. In Chapter 2 a general overview of the Baltic Sea wind and wave climate is presented. It is followed by materials and methods used in this study in Chapter 3. In Chapter 4 sensitivity of model results to model settings is analyzed. Influence of obstacles to wave field evolution is studied in Chapter 5. In Chapter 6 wave induced setup and flow is analyzed. Main conclusions are summed up in Chapter 7.

## 2. OVERVIEW OF BALTIC SEA WIND AND WAVE VARIABILITY

The Baltic Sea is as a large (spans from 9<sup>0</sup>-30<sup>0</sup> E and 53<sup>0</sup>-66<sup>0</sup> N, total area of 435 000 km<sup>2</sup>) seasonally ice-covered water body containing several topographically and geographically defined sub-basins (Fig. 1). The mean water depth is 55 meters and the maximum water depth reaches 459 meters in the Landsort Deep. The longest possible fetch is about 700 km in the Baltic Proper, 500 km in the Gulf of Finland (along the major axis and continuing in the Baltic Proper), 300 km in the Gulf of Bothnia and Bothnia Sea and 150 km in the Gulf of Riga. While the Gulf of Riga and Bothnia Sea are connected to the Baltic Proper by shallow and narrow straits, which limit wave growth and propagation, the Gulf of Finland has no specific physical border with the Baltic Proper. Therefore long and high waves are steered to the Gulf of Finland under certain meteorological conditions. Ice plays an important role in the fetch geometry of the Baltic Sea (Fig. 2). In typical winters the Gulf of Riga, Gulf of Finland, Gulf of Bothnia and Bothnia Sea are almost totally ice-covered and the Baltic Proper is ice-free, but in severe winters only the central part of Baltic Proper remains ice-free (Vihma and Haapala, 2009; Fig. 2).

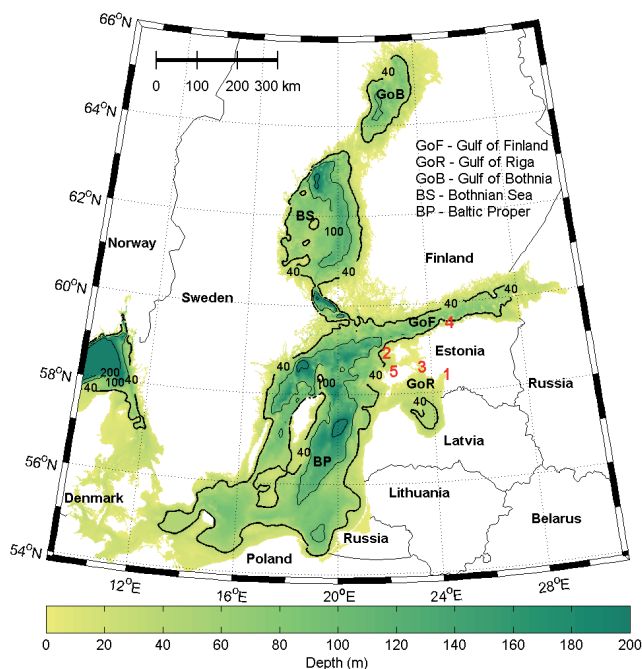


**Figure 1.** Baltic Sea bathymetry (Seifert et al., 1995), smoothed with 6 km filter. Red numbers corresponds to author's original publications study sites.

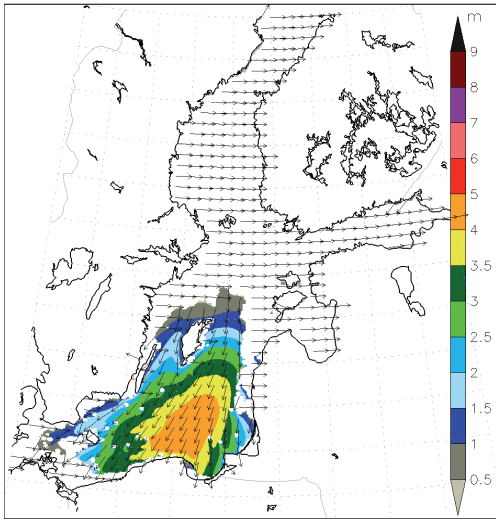


**Figure 2.** Hindcasted significant wave height at 1985-02-18 12:00 UTC (SWAN model, 1.85 km) in ice-covered Baltic Sea. Wave vectors in ice covered regions are not representative.

## 2.1 Wind conditions over the Baltic Sea

The Baltic Sea lies in temperate latitudes and therefore is largely affected by the westerly airflow. This leads to a wind rose, where approximately 50 % of the time the wind blows from sector 180-270<sup>0</sup> (S, SW, W) at coastal stations of western Estonia (Jaagus and Kull, 2011). As the scale of weather patterns usually is much larger compared to the Baltic Sea sub-basin dimensions, the dominating wind direction has a quite uniform spatial distribution, as can be seen for example in fig. 5 by Karagali et al. (2012). In the Gulf of Finland the wind mainly blows from southwest according to Launiainen and Laurila (1984) and the same holds for the Bothnia Sea, while the prevailing direction is south in the Gulf of Bothnia (Tuomi et al., 2011 and references therein). The wind direction in storm conditions (winds with sustained speed over 15 m s<sup>-1</sup>) usually is between 180<sup>0</sup>-360<sup>0</sup> due to the movement of cyclones (Jönsson et al., 2003).

Wind speed in the Baltic Sea area has a clear annual cycle, with monthly mean wind speeds above the yearly average in autumn-winter and below in spring-summer. Although the annual cycles are mainly related to synoptic-scale activity, they are additionally affected by the surface layer stratification, which is most stable during spring and early summer, reducing the near-surface wind speeds (Niros et al., 2002). Depending on the sub-basin and time period chosen for analysis, and also the instrument height, the yearly average wind speeds over the Baltic Sea are 6-8 m s<sup>-1</sup> and monthly values deviate about it up to 1.5 m s<sup>-1</sup> (e.g. Suursaar et al., 2006a; Niros et al., 2002). During the passage of deep

extra-tropical cyclones the 10 minute sustained wind speed has reached  $29 \text{ m s}^{-1}$  at coastal stations facing the Gulf of Riga and Baltic Proper (Suursaar et al., 2009) and probably over  $30 \text{ m s}^{-1}$  in the open sea. In 1967 an overall maximum sustained wind speed of  $35 \text{ m s}^{-1}$  was measured (as it pertains to instrumental measurement history) at weather stations near the entrance of the Gulf of Finland and in the Tallinn meteorological station (Suursaar et al., 2006b).

## 2.2 Baltic Sea wave variability

Instrumental wave measurements in the Baltic Sea started in the 1970s, while only visually observed wave properties were available before (Tuomi et al., 2011). Instrumentally measured maximum significant wave height was 8.2 m in the northern Baltic Proper, 7.4 m in the southern Baltic Proper and 5.2 m in the Gulf of Finland (Tuomi et al., 2011). In the Bothnia Sea the measured maximum significant wave height reached 6.5 m (Tuomi et al., 2011) and in the Gulf of Bothnia 3.1 m (Finnish Meteorological Institute report series, 2012). For the Gulf of Riga long-term instrumental wave measurements are missing but during a 130 day long field campaign Suursaar et al. (2012) measured significant wave heights up to 2 m in northern part of the Gulf. Following the seasonal course of wind, all the maximums have been measured either in autumn or winter. According to a 7 year long model hindcast by Tuomi et al. (2011), the maximum significant wave height can reach over 9 m in the southern and northern Baltic Proper (modeled maximum was 9.7 m during storm Gudrun in 9 January 2005), 7 m in the Bothnia Sea and 6.5 m in the Gulf of Bothnia. The results of a hindcast by the author (unpublished) showed maximum significant wave height of 9.95 m. It is quite interesting to see that in the fetch-limited and shallow Baltic Sea the maximum significant wave heights (Fig. 3) are up to half of what has been measured and modeled in the World Ocean (Hanafin et al., 2012). Needless to mention, the modeled values and especially maxima are greatly influenced by the source term settings of the model, input winds and numerical schemes.

It is evident that the wave field has quite large spatial variability, yet the seasonal changes are even larger. Roughly speaking, monthly mean and monthly maximum wave heights in autumn-winter are twice as big compared to spring-summer months (Tuomi et al., 2011; unpublished author study) but the exact months for maxima and minimums themselves can vary between different sub-basins. For example, in the northern Baltic Proper, the maximum measured significant wave height occurs in December (at the time period between 2001 and 2007) and the seasonal minimum is in June and August, according to Tuomi et al. (2011). On the other hand, in the Gulf of Finland the minimum is in April, which can be explained by the presence of ice cover

The geometry of the Baltic Sea together with prevailing wind directions frequently lead to situations where the wind direction and peak wave direction differ from each other up to  $50^\circ$  in deep water. These slanting fetch cases are

well documented for the Gulf of Finland (Pettersson et al., 2010), but other areas of the Baltic Sea have also fetch restrictions in the upwind direction.

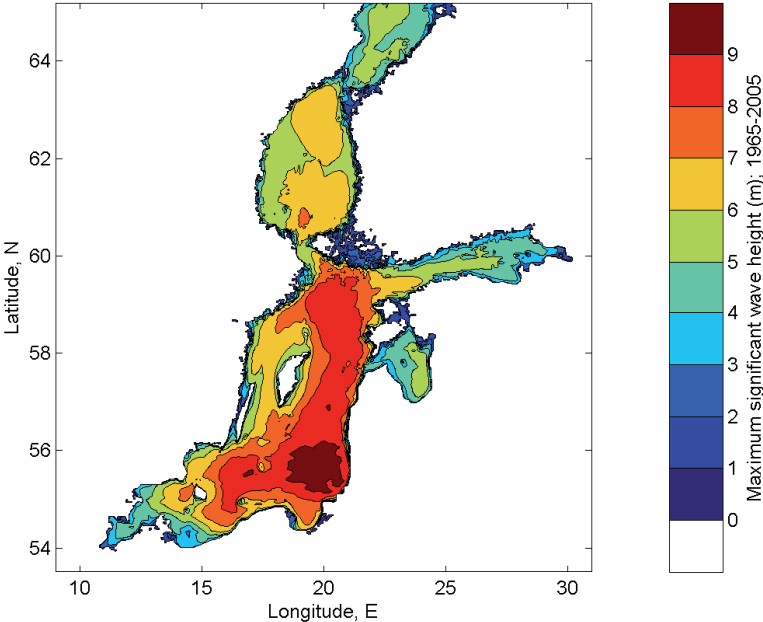


**Figure 3.** Maximum modeled significant wave height in the Baltic Sea between 1965-2005. Simulated with 1 nautical mile SWAN model forced by Luhamaa et al. (2011) winds and ice fields from Rossby Centre SMHI.

## 3. MATERIALS AND METHODS

### 3.1 Study areas

The studies for this thesis were located (Fig. 1) in the Estonian Archipelago Sea (Paper V), Gulf of Finland (Paper IV), Baltic Proper (Paper II) and Gulf of Riga (Papers I and III). In the Gulf of Riga the focus was on the Suur Strait (Paper III) and Pärnu Bay (Paper I). The Suur Strait is a relatively narrow and shallow strait connecting the waters of the Väinameri and the Gulf of Riga. The Suur Strait is the narrowest (6 km) in the Virtsu-Kuivastu region (see fig. 1 in Paper III for further details). Its maximum depth is 21 m and the sill depth is about 5 m near the southern side of the Väinameri basin. It is open to waves from the south. Pärnu Bay is a wider (up to 12 km in narrowest part) and shallow basin in the NE part of the Gulf of Riga. The water depth in the bay interior is less than 10 m and the sea-bed is gently sloping. At the head of the bay lies Pärnu town, being vulnerable to flooding from sea. The bay is fully open to waves from SW.

The Küdema Bay (Paper V) is situated on north-western side of Estonia's largest island Saaremaa (see also fig. 1 in Paper V for further details). The mean width of the bay is 3 km (west–east direction) and its length is 8 km (north–south direction), with a mean depth of 7.5 m. In northern side of the bay the water depth is 20 m at only about 400 m from the coast, so the high waves from NNW may penetrate into the bay.

Tallinn Bay (Paper IV) is sheltered from waves by two islands and numerous shallows. Despite that, NNW winds push high waves into the bay and even W waves propagate to the bay between the mainland and Naissaar Island. Compared to the previous three study sites, the central leg of Tallinn Bay is deep (40 m).

The study sites of Paper II are situated on two shallows (see fig. 1 in Paper II for further details). The water depth at the shallows is 10-20 m, while the surrounding depth on the seaward side is 40 m near the shallows. Wave conditions were the most energetic in these locations compared to other study sites.

### 3.2 Study designs

*Effects of surge upon surface wave field dynamics and wave induced set-up at a natural beach was studied (Paper I) in Pärnu Bay, the Gulf of Riga.* A triply nested SWAN model was implemented in the geographical domain. Each higher resolution run received the boundary data from coarser run, while the coarsest

run started with zero initial and boundary conditions at 00:00 UTC on 8 January 2005 (the whole modeling period was from 00:00 08.01.2005 till 21:00 09.01.2005). The atmospheric forcing used in this paper was based on the dynamically down-scaled winds of the ERA-40 data set. The resolution of the atmospheric forcing grid was 25x25 km with 3 h time step. Two model runs were made, in which surge was neglected and when surge was considered. In the first case, no surge was added to water depth. In the second run, 1 m spatio-temporally constant surge was added to water depth in 400 m grid and time-varying, but spatially constant, water level was added to water depth of the 100 m grid. Model integration time steps varied from 10 to 5 minutes.

For the calculation of wave induced set-up and inundation, the one-dimensional mode of SWASH was used. The SWASH model got its boundary condition in terms of significant wave height and peak period from the 100 m SWAN run. The boundary point for SWASH was outside the zone of intense breaking. The boundary condition was acquired at the time instant when significant wave height was greatest (considering the whole modeling period). The SWASH model was run in non-hydrostatic and depth-averaged mode with 1 m grid resolution and 0.02 s time-step. Breaking was activated and the coefficient for breaking was 0.6. Bottom friction formulation was due to Manning (SWASH team, 2013) with a friction coefficient of 0.019. Model was run 1.5 hours and the set-up and wave height values were extracted from the last five minutes of the calculation.

*The main aim of Paper II was to quantify the absorption and scattering of wave energy by an array of grouped obstacles (wind turbines) located on some shallows in the Baltic Proper. Steady wind speeds of  $8 \text{ m s}^{-1}$  and  $15 \text{ m s}^{-1}$  were selected in this study and blowing from direction SW, W and NW. The modeling of waves was carried out using five or four consequently nested models, depending on the exact location. First the whole Baltic Sea with a 2000-m resolution was modeled. With the boundary conditions from the previous model, waters surrounding Hiiumaa were modeled with a 400-m resolution, and then 100, 50, and 25 m (optional). For every forcing situation, two calculations were made—first without obstacles and second with obstacles. The obstacle was represented as land (0 water depth) and in SWAN the land absorbs all incoming wave energy. Changes in significant wave height were assessed. The diffraction was activated only when the highest spatial resolution was used.*

*Estimating the proportion of surface waves in the flow field and water exchange, and estimating wave-induced shear velocities was the aim in Paper III. A triple-nested wave- model was used for the simulation of waves in the Suur Strait. The coarse grid model covered the whole Baltic Sea with a spatially constant grid size of 2x2 km. No open boundary conditions were implemented for this grid. The model for the Väänameri region had a grid size of 400x400 m, whereas the boundary conditions were obtained from the whole Baltic Sea model. The high resolution model for the Suur Strait area had a grid step of 100x100 m. Hydrodynamic model forcing was obtained from the atmospheric*

model HIRLAM. The modeling period covers time period from 13.11.2008-07.12.2008. In order to take into account the wave-induced currents, a wave-induced force per unit surface area was added to the kinematic wind stress in both the  $x$  and the  $y$  directions. The shear stress calculation methods and wave-induced force calculation methods are presented in Chapters 3.5 and 3.6, respectively.

*The impact of depth induced wave breaking on significant wave height field distribution was studied (Paper IV) in the shallow areas of Tallinn Bay.* Two calculations were made. The first calculation was with depth-induced breaking activated and the second one was with depth-induced breaking not-activated. The analyzed fields represent saturated wave fields corresponding to a NNW storm with wind speed  $23 \text{ m s}^{-1}$ . Calculations of wave field were carried out using a triple nested model. The coarse Baltic Sea model had resolution of  $1'$  along latitudes and  $2'$  along longitudes. The medium grid for the Gulf of Finland had a resolution of  $0.5'$  along latitudes and  $1'$  along longitudes, with the boundary conditions obtained from the coarse Baltic Sea model. The high resolution Tallinn Bay model was  $0.25'$  along latitudes and  $0.5'$  along longitudes and the boundary conditions were obtained from intermediate grid.

*The spatio-temporal wave regime of a semi-sheltered bay was analyzed (Paper V) under spatially homogeneous but temporally variable wind conditions.* The modeling was done for two three-week long time periods in summer and autumn 2005. Since the K udema Bay is open at the northern side, the wave field generated by northerly winds in the Baltic Proper propagates to the bay, and therefore it is important to take into account the wave calculations of the Baltic Proper. The Bothnia Sea was not taken into account, because it is expected that waves in Bothnia Sea do not affect the wave regime in K udema Bay (see Fig. 1). A medium grid between the coarse Baltic Proper area and the small K udema Bay area was also introduced into the computations as a transitional area for waves. Consequently a triple nested model was used, with highest resolution of 0.1 nautical miles. Model time steps varied from 30 minutes on the coarsest grid to 5 minutes in the highest grid.

In all of the studies, 40 spectral frequencies were distributed logarithmically on the frequency range of 0.05–1 Hz. Also wave energies were calculated for 24 equally spaced propagation directions, whereas 36 directions were used in the high resolution grid of Paper I. All studies used a third generation wave model with respect to wave-wave interactions (triad and quadruplet), whitecapping, wind input, bottom friction and depth-induced breaking. Besides Paper V the whitecapping formulation was due to Westhysen et al. (2007). The linear term in wave growth (Eq. 7) was deactivated in Papers III and V. The quadruplet interaction was approximated using the DIA with default settings. The depth-induced breaking coefficient was set to 0.73. A semi-empirical expression for bottom friction was activated, with the bottom friction coefficient of  $0.067 \text{ m}^2\text{s}^{-3}$ . One or more intermediate grids separated the coarsest and most high-resolution grid. This was needed, since when interpolating spectrum data from

coarser resolution to a finer resolution, interpolation errors may occur (SWAN team, 2013) if the grid sizes vary considerable. This was certainly true in the present calculations, as the grid size varied two orders of magnitude between the coarsest and finest grid (2 km and 25-m in Paper II). The influence of currents on waves was neglected in this thesis. One-way grid nesting was used in all studies. SWAN versions 40.41, 40.51 and 40.72 were implemented.

For obtaining the Baltic Sea water depth, three types of data sets were used. The primary one was the digital topography covering the entire Baltic Sea with a resolution of 1 nautical mile (Seifert et al., 1995). The high resolution topographies in Papers I-V were manually digitized from admiralty charts issued by EMB and supplemented by hydrographical surveys by the EMB in Paper III.

### 3.3 Description of SWAN wave model

The SWAN wave model forms the core of this dissertation. SWAN (Booij et al., 1999; SWAN team, 2013) is a third generation phase averaged spectral wave model developed mainly at Delft University of Technology. In SWAN the waves are described with the two-dimensional wave action density spectrum, whereas the evolution of the action density  $N$  is governed by the time dependent wave action balance equation, which in Cartesian coordinates reads:

$$\frac{\partial N}{\partial t} + \left( \vec{c}_g + \vec{U} \right) \cdot \nabla_{x,y} N + \frac{\partial c_\sigma N}{\partial \sigma} + \frac{\partial c_\theta N}{\partial \theta} = \frac{S_{tot}}{\sigma}. \quad (1)$$

The first term represents the local rate of change of action density; the second term denotes the propagation of wave energy in two dimensional geographical space, with  $\vec{c}_g$  being the group velocity and  $\vec{U}$  the ambient current. The third term represents the effect of shifting of the radian frequency due to variations in depth and mean currents. The fourth term represents the depth-induced and current-induced refraction. The quantities  $c_\sigma$  and  $c_\theta$  are the propagation velocities in spectral space  $(\sigma, \theta)$ , with  $\sigma$  and  $\theta$  representing the radian frequency and propagation direction respectively. The right-hand side contains the source term  $S_{tot}$  that represents all physical processes that generate, dissipate or redistribute wave energy in SWAN. In shallow water, six processes contribute to  $S_{tot}$  :

$$S_{tot} = S_{wind} + S_{nl3} + S_{nl4} + S_{wc} + S_{bot} + S_{db}. \quad (2)$$

These terms denote the energy input by wind ( $S_{wind}$ ), the nonlinear transfer of wave energy through three-wave ( $S_{nl3}$ ) and four-wave interactions ( $S_{nl4}$ ), and the dissipation of waves due to whitecapping ( $S_{wc}$ ), bottom friction ( $S_{bot}$ ) and depth-induced wave breaking ( $S_{db}$ ), respectively.

### 3.3.1 Source terms

#### *Depth-induced breaking*

In SWAN the dissipation of wave energy due to depth induced breaking follows the bore based model applied to random waves (Battjes and Jansen, 1978): the energy dissipation rate in a broken wave will be estimated from that in a bore of corresponding height (a tidal bore is a rapidly moving water mass, which travelling against currents will form steep breaking fronts at its leading edge). The key element in this model is the fraction of waves which are breaking or broken ( $Q_b$ ), in terms of the ratio of the root-mean-square wave height actually present, to the maximum wave height ( $H_{max}$ ) which the given depth can sustain:  $H_{max} = \gamma d$ , where  $\gamma$  is the breaker parameter and  $d$  is the total water depth (including wave induced setup, if calculated with SWAN, and surge, if provided by user). Once the fraction of breakers is known, the mean rate of energy dissipation per unit horizontal area can be estimated:  $D_{tot} = \alpha Q_b \bar{\sigma}_{01} H_{max}^2 (8\pi)^{-1}$  where  $\alpha$  is a constant of order one,  $\bar{\sigma}_{01}$  is the mean frequency corresponding to the first moment of the spectrum. The dissipation for a spectral component per unit time reads:

$$S_{db}(\sigma, \theta) = -\frac{D_{tot}}{E_{tot}} E(\sigma, \theta), \quad (3)$$

where  $E_{tot}$  is the total wave energy integrated over all directions and frequencies.

#### *Bottom friction*

Bottom friction in SWAN can be written in the following form:

$$S_{bot}(\sigma, \theta) = -C_b \frac{\sigma^2}{g^2 \sinh^2 kd} E(\sigma, \theta), \quad (4)$$

in which  $C_b$  is the bottom friction coefficient,  $g$  the acceleration due to gravity and  $k$  the wavenumber corresponding to spectral radian frequency.

## Whitecapping

By default in SWAN the whitecapping is represented by the pulse-based model of Hasselmann (1974). A pressure pulse in this model is the whitecap situated in the forward faces of waves, which acts against the rising sea surface, therefore exerting a downward pressure on the upward moving water and hence doing negative work on the wave. Furthermore, breaking of large scale waves induces rapid attenuation of short waves and therefore the dissipation source function should depend on frequency relative to peak (Komen et al., 1994). The pressure induced dissipation and the attenuation of short waves by passage of large whitecaps are sensitive to the extent of whitecap coverage, which itself is assumed to depend on the overall steepness of the wave field (Komen et al., 1994). Combining these three processes, the whitecapping dissipation source term in wave number space reads:

$$S_{wc}(\sigma, \theta) = -\Gamma \bar{\sigma} \frac{k}{\bar{k}} E(\sigma, \theta), \quad (5)$$

where  $\bar{\sigma}$  and  $\bar{k}$  are the mean frequency and mean wavenumber. Coefficient  $\Gamma$  depends on tunable parameters and the ratio of overall wave steepness to steepness of Pierson-Moskowitz (1964) spectrum.

A second approach to model whitecapping in SWAN assumes that breaking only commences once a saturation threshold has been reached, that the breaking is local in frequency space and weakly dependent of wave age (Westhysen et al., 2007). The nonlinear saturation based dissipation term for deep and shallow water by Westhysen et al. (2007) reads:

$$S_{wc}(\sigma, \theta) = -C_{ds} \left[ \frac{B(k)}{B_r} \right]^{p/2} [\tanh(kd)]^{\frac{2-p_0}{4}} \sqrt{gk} E(\sigma, \theta), \quad (6)$$

in which  $B(k)$  is the directionally-integrated spectral saturation. The threshold saturation level  $B_r$  is set to  $1.75 \cdot 10^{-3}$  and the proportionality coefficient  $C_{ds}$  to  $5.0 \cdot 10^{-5}$ . When  $B(k) > B_r$ , waves break and the exponent  $p$  is set to a

calibration parameter  $p_0$ :  $p_0(u_* / c) = 3 + \tanh \left[ 26 \left( \frac{u_*}{c} - 1 \right) \right]$ , in which  $u_*$  is

the wind friction velocity and  $c$  is the phase speed of waves. When  $B(k) \leq B_r$ , there is no wave breaking, but some residual dissipation was necessary. This is accomplished by setting  $p=0$ .

## Wave growth

Wave growth in SWAN is modeled as the sum of exponential growth  $BE$  and linear growth  $A$ :

$$S_{in}(\sigma, \theta) = A + BE(\sigma, \theta). \quad (7)$$

The resonance mechanism by Phillips (1957) e.g. linear growth rate of waves, reads in SWAN:  $A = \frac{1.5 * 10^{-3}}{2\pi g^2} (u_* \max[0, \cos(\theta_{wave} - \theta_{wind})])^4 H$ , where the coefficient  $H$  prevents wave growth at frequencies lower than Pierson Moskowitz frequency (Tolman, 1992). The exponential growth due to feedback mechanism of Miles (1957) is formulated by Komen et al. (1984) and reads

$$B = \max \left[ 0, 0.25 \frac{\rho_a}{\rho_w} \left( 28 \frac{u_*}{c} \cos(\theta_{wave} - \theta_{wind}) - 1 \right) \right],$$

in which  $\rho_a$ ,  $\rho_w$  are the air and water densities, respectively and  $\theta$  donates direction. The wind friction velocity is according to Wu (1982) or alternatively by Zijelma et al. (2012). In papers I-IV the saturation based whitecapping was combined with wind input as described by Yan (1987), with fitting coefficients adapted to describe wave growth in fetch limited conditions (SWAN team, 2013).

### *Quadruplet interactions*

Non-linear four-wave interactions are of paramount importance and form a central part of any third-generation wave model. The primary effect of quadruplet interactions is to carry energy from higher frequencies to lower, while the opposite is true for triads in shallow water. The mechanism also is responsible for self-stabilization of the spectrum. Compared to wind input and dissipation source terms, which have many tuning parameters, the four wave non-linear interaction term is fully known from first principles (Hasselmann, 1962). However, computation of the Boltzmann integral involves cycle intense loops in numerical programs and therefore it's not feasible to implement it in either operational models or long-term hindcasts. Westhysen et al. (2007) pointed that it takes 300 times as much computational effort to compute the non-linear interactions by the "exact" method, compared to method described by Hasselmann et al. (1985), also known as the DIA. The drawback of using only a limited set of wavenumbers is that peakedness of spectrum is underestimated and directional spread overestimated above peak frequencies (Westhysen et al., 2007). See SWAN team (2013) for mathematical implementation.

### *Triad interactions*

In shallow water triad wave interactions becomes the dominant mechanism which transfers energy between wave components. The strength of the transfer

can be qualitatively estimated from Ursell number:

$$Ur = \frac{g}{8\sqrt{2\pi}} \frac{H_{m0} T_{m01}^2}{d^2}, \quad (8)$$

in which  $H_{m0}$  is wave height corresponding to zero'th moment of spectrum (for practical purposes, significant wave height) and  $T_{m01}$  is spectral period corresponding to first moment. In SWAN the interactions only occur, when  $0 < Ur < 1$ . Near unity values indicate strong interaction. The effect of triads is to carry energy from the low-frequency part of the spectrum to the high-frequency part (sum interactions) and to generate bound long waves due to difference interactions (Eldeberky, 1996).

### 3.4 Overview of SWASH model

The SWASH model (used in Paper I for wave setup and inundation calculation) is based on nonlinear shallow water equations including non-hydrostatic pressure and can be applied to simulate non-hydrostatic, free-surface, rotational flows (Zijelma et al., 2011). The model accounts for the following physical phenomena (SWASH team, 2013):

- Advection in spectral and physical space: propagation, frequency dispersion, shoaling and refraction.
- Dissipation: wave breaking and bottom friction.
- Nonlinear wave-wave interactions.
- Turbulence: subgrid turbulence, vertical turbulent mixing.
- Interaction with coastline: wave runup and rundown, moving shoreline, partial reflection and transmission, diffraction.
- Wave-induced currents and wave-current interaction, rapidly varied flows.

Surface gravity wave generation by wind is not accounted for at present.

### 3.5 Wave induced shear velocity

Water depth, significant wave height and peak period dictates the wave generated shear velocities acting on deposited material. In order to calculate the wave induced shear velocity at the seabed, the near bottom excursion amplitude ( $A_b$ ) and orbital velocity ( $U_b$ ) are calculated first as follows:

$$A_b = \frac{H_{m0}}{2 \sinh(k_p d)}, U_b = 2\pi \frac{A_b}{T_p}, \quad (9)$$

where  $k_p$  is wavenumber (corresponding to the peak frequency) and  $T_p$  is the

peak wave period. Shear velocity also depends of the friction coefficient  $f_w$ , which is calculated as follows:

$$f_w = \left\{ \begin{array}{l} 0.3, \frac{A_b}{2.5D} < 1.57 \\ \exp(5.5(\frac{A_b}{2.5D})^{-0.2} - 6.3) \end{array} \right\}, \quad (10)$$

where  $D$  is the diameter of the particulate matter. The wave induced shear velocity ( $u_w$ ) takes the following form:

$$u_w = U_b \sqrt{0.5 f_w}. \quad (11)$$

### 3.6 Wave induced currents

The two dimensional circulation model based on equations for a shallow sea was used to obtain wave induced currents in Paper III. The model has been earlier applied and validated for different regions of the Estonian marine waters (Sipelgas et al., 2006). In order to take into account the wave induced currents in the model, a wave induced force was added to the kinematic wind stress both in  $x$  and  $y$  directions. The wave induced force ( $F_{wave}^x, F_{wave}^y$ ) per unit surface area is calculated as the gradient of the radiation stresses (Holthuijsen, 2007).

$$F_{wave}^x = -\frac{\partial S_{xx}}{\partial x} - \frac{\partial S_{xy}}{\partial y}, \quad F_{wave}^y = -\frac{\partial S_{yx}}{\partial x} - \frac{\partial S_{yy}}{\partial y}, \quad (12)$$

where  $S$  is the radiation stress tensor as given by

$$S_{xx} = \rho_w g \iint \left[ n \cos^2 \theta + n - \frac{1}{2} \right] E d\sigma d\theta, \quad (13a)$$

$$S_{xy} = S_{yx} = \rho_w g \iint n \sin \theta \cos \theta E d\sigma d\theta, \quad (13b)$$

$$S_{yy} = \rho_w g \iint \left[ n \sin^2 \theta + n - \frac{1}{2} \right] E d\sigma d\theta, \quad (13c)$$

where  $n$  is the ratio of group velocity to phase velocity.

## 4. SENSITIVITY OF SPECTRAL PARAMETERS ON MODEL SETTINGS

### 4.1 Surge impacting wave field

Baltic Sea tidal amplitudes in coastal bays are smaller (1-10 cm; Evdokimov, 1974; Feistel et al., 2008) compared to those in oceanic environments, but water level varies over a wide range of spatial and temporal scales. The barotropic surge height is mainly determined by wind stress, volume of water in the Baltic Sea and regional topography and geometry. Measured historical water level maximums are higher on the eastern side of the Baltic Sea compared to western side (Averkjev and Klevanny, 2010) and mainly occur during the passage of intense cyclones in autumn and winter. One of the most vulnerable areas affected by high surge in Estonia is Pärnu (see figs. 1 and 2 in Paper I). The town is at the end of a narrow bay, while river separates it into upper and lower parts. The ground elevation is less than 5 m everywhere in the lower town. More than 40 % of the lower town was flooded during the passage of a severe cyclone Gudrun on 9 January 2005, when surge peaked at 2.78 m above mean water level. The maximum sustained wind speed measured over the Baltic Proper reached  $28 \text{ m s}^{-1}$  (gusts  $37.5 \text{ m s}^{-1}$ ) and prior to the maximum surge, the wind blew mainly from the sector SW-WSW. The impact of the storm generated water level on wave field distribution was already discussed by Tolman (1990) for Dutch tidal inlets, but studies showing the surge impact to wave field distribution in Baltic Sea are lacking.

To get an impression of how strong and uniform the wind was, consider a snapshot at 06:00 UTC (9 January, 2005), when the modeled wind reached its maximum of  $25 \text{ m s}^{-1}$  over the Gulf of Riga (Fig. 4a). Note that the wind speed reduction near the western side of the Baltic Proper is due to shedding by land, but at the eastern side this is probably related to spurious interpolation. Nonetheless, this will not impact the wave field. Modeled wind direction showed good timing (correlation coefficient,  $r=0.93$ ) and overlay ( $\text{RMSD}=7^\circ$ ) with observations, then again the wind speed in the Gulf of Riga was  $2\text{-}3 \text{ m s}^{-1}$  lower compared with the measurements. Due to the fetch, duration and depth limited conditions of wave growth during the storm, a small underestimation of wind has a marginal effect on the wave field. Cyclone Gudrun excited the heaviest wave conditions in Baltic Sea in recent history. Significant wave height reached 9.19 m at 03:00 UTC in the southern Baltic Proper in the modeled dataset and was over 7 m in the entire eastern Baltic Proper. In the Gulf of Riga maximum significant wave height peaked just over 5 m at 06:00 UTC, and basically the entire basin had significant wave height over 4 m (Fig. 4b). Under these wind conditions the Gulf's wave field was depth, fetch and

time limited. Although not shown here, the near bottom orbital velocity was over  $20 \text{ cm s}^{-1}$  in 75 % of the basin, thus likely resuspending most of the sandy and soft bottoms of the Gulf.

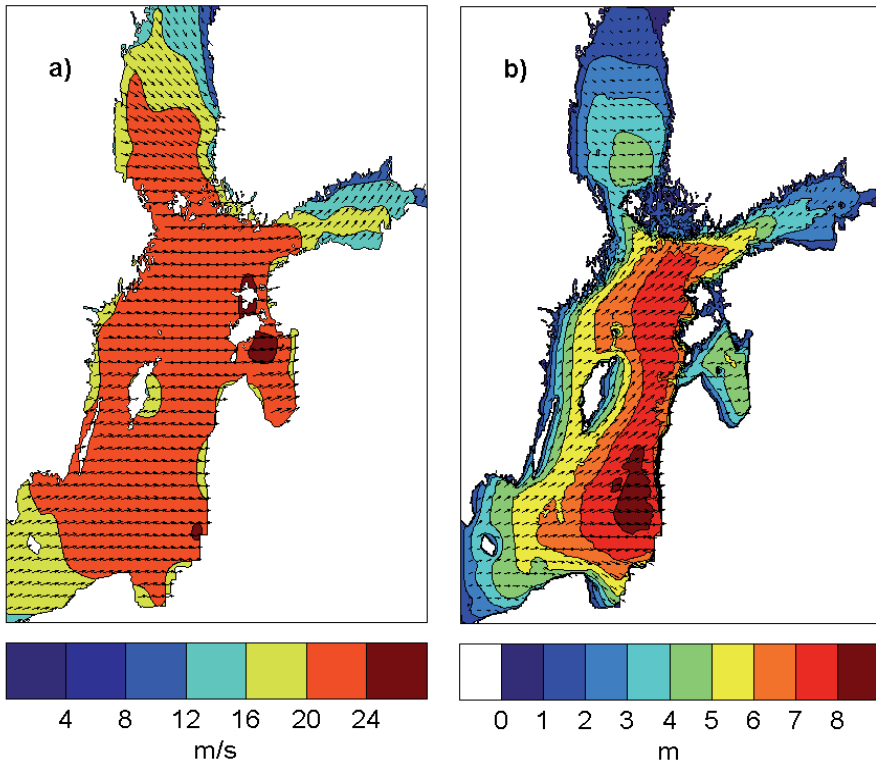


**Figure 4.** Snapshots (06:00 UTC, 09.01.2005) of modeled wind speed and direction (a) and significant wave height and mean wave direction (b) during cyclone Gudrun in the Baltic Sea.

A time-series comparison of significant wave height calculated with and without surge reveals the dependence of significant wave height on surge height and growth stage (Fig. 5). It should be noted that the time-series was selected from the location, which provides initial conditions for further modeling of wave set-up (black dot of Fig. 6b). The difference in significant wave height is less than 5 cm when surge and waves are smaller than 1 m and wind speed below  $10 \text{ m s}^{-1}$ . It implies that in “average” weather conditions a coupled wave-surge model is not necessary. However, as waves and surge grow, the difference peaks at 0.4 m. During that period, the difference in significant wave height shows large variability in the small bay (Fig. 6c). When surge is considered, the significant wave height increases 0.3 m at the entrance where water is deeper than 10, but 1 m in the coastal areas. The effect of having time-varying water

level does not only manifest itself in altering the dissipation due to depth induced breaking (Eq. 3), bottom friction (Eq. 4) and energy transfer due to triad interaction (Eq. 8), but also affects the kinematic part of the transport Eq. (1). Temporally varying water levels shift the radian frequency. However, this was not examined in Paper I.

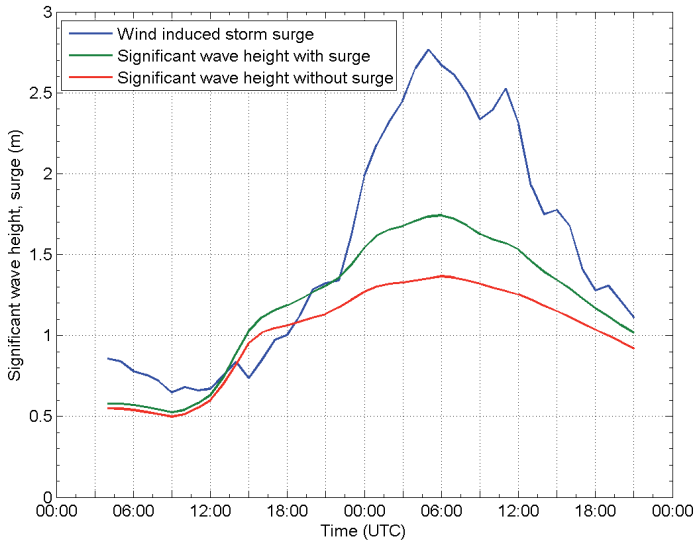


**Figure 5.** Evolution of water level (measurements) and modeled significant wave height in Pärnu Bay on 8-9 January, 2005, during passage of cyclone Gudrun. Spatial location where significant wave height is extracted is shown on Fig. 6b. Blue line: storm surge. Red line: significant wave height without surge. Green line: significant wave height when surge was considered. Adapted from Paper I.

The results of this study are comparable with research done by Liu and Xie (2009) who studied the impacts of Hurricane Hugo passing over Charleston harbor (1989). Pre-landfall of the hurricane the storm surge was 1 m. When this was taken into account in the wave model, it increased significant wave height 0.3 m in water depths less than 4 m, compared to the situation when water level was not taken into account (Liu and Xie, 2009). During landfall the surge was 2.5 m and the significant wave height increased up to 1 m near the coast, when the extra water level was considered (Liu and Xie, 2009).

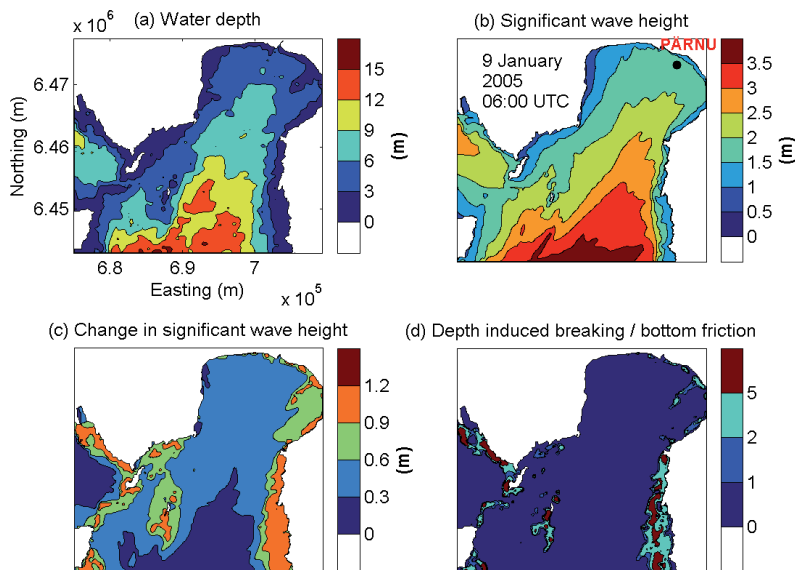


**Figure 6.** (a) Bottom topography (without surge), (b) significant wave height (at peak surge), (c) significant wave height with peak surge minus significant wave height without surge, (d) depth induced breaking dissipation divided by bottom friction dissipation (when peak surge is taken into account). b,c and d are snapshots at 06:00 UTC on 9 January 2005. Adapted from Paper I.

## 4.2 Role of depth-induced breaking

To quantify the impact of depth induced wave breaking, two calculations were made. The first calculation was with depth induced breaking activated and the second one was with depth induced breaking not-activated. The analyzed fields represent saturated wave fields (Paper IV).

Although Tallinn Bay is well sheltered by two islands (Naissaar and Aegna) and many shallows (Fig. 7), high waves may penetrate into the bay in case of NNW winds of  $23 \text{ m s}^{-1}$  (Fig. 8a). Significant wave height may be as high as 3 m in the bay interior and up to 4 m to the west of Naissaar Island. Areas north of Aegna Island and shallows between Aegna and Naissaar islands exhibit significant wave heights less than 3 m. Areas near the peninsulas of Suurupi, Kakumäe, Kopli and Paljassaar exhibit significant wave heights less than 2.5 m. The lowest significant wave heights, less than 1 m, occurred between the mainland and Aegna Island in the case of this forcing.

The results of the SWAN model with depth induced breaking inactive showed an increase in wave height north of Aegna Island and on the north-western coast of Naissaar Island, near the peninsulas of Kopli, Paljassaar and

Kakumäe, and at Naissaar Bank and Uusmadal Bank, as well as at Suurupi (Fig. 8b; see also Fig. 7 for exact locations). The increase in significant wave height north of Aegna was 1.8 m, 1.1 m at Keskmadal Bank, 1.4 m at Naissaar Bank, 2 m at Kakumäe Peninsula, 1.5 m at Kopli and Paljassaare peninsulas. The highest increase occurred near Suurupi Peninsula, where the non-breaking case presents significant wave height increase of 2.3 m. Central Tallinn Bay, also west of Naissaar Island and other areas, where water depth is greater than 20 m showed increase of significant wave height less than 0.5 m when depth-induced breaking was switched off.

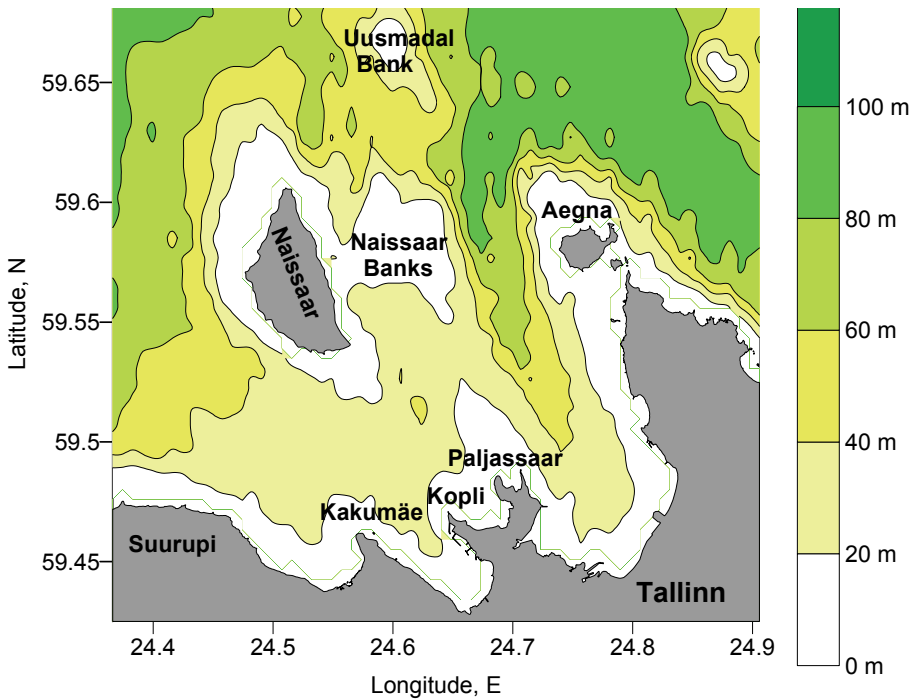


**Figure 7.** Geographical setting and bathymetry of Tallinn Bay. Adapted from Paper IV.

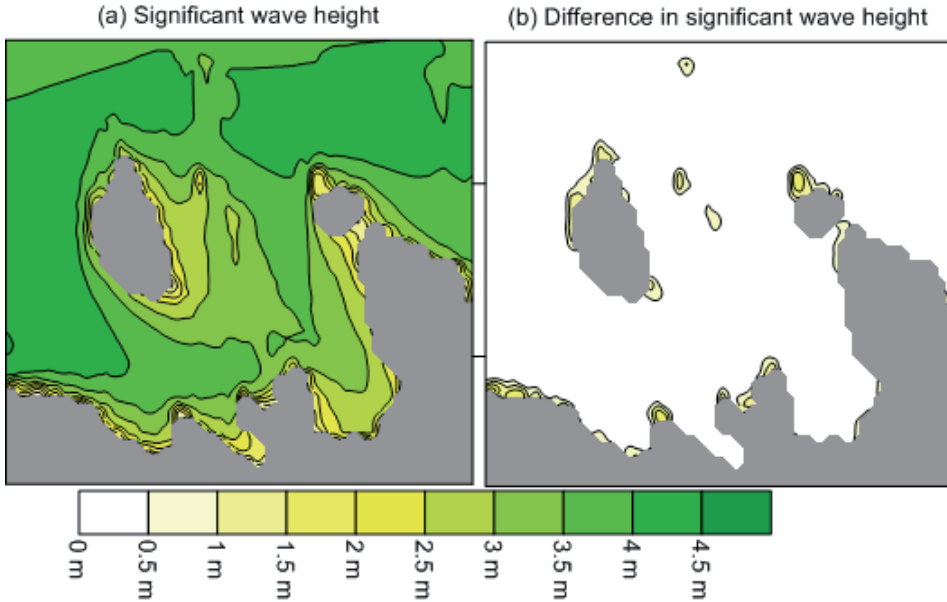


**Figure 8.** (a) Significant wave height in Tallinn Bay and adjacent sea area in case of a  $23 \text{ m s}^{-1}$  NNW storm. (b) Difference in significant wave height between depth-induced breaking not activated and depth induced breaking activated.

Breaking waves appear if significant wave height is at least one fifth of the total water depth and the sea is fully covered with breakers (in spectrum) when significant wave height is comparable to half the water depth. This implies that breaking is modeled as a distribution function and cumulative effect is important. While the dissipation due to bottom friction already starts reducing energy at 70 m water depth (Fig. 9), considerable dissipation due to depth-induced breaking commences from 20 m depths and shallower. The result on Fig. 9 represents the average dissipation for particular source function in a given depth bin (2 m increase) during peak values of cyclone Gudrun. The area covered all of the Estonian coastal waters, and the computational grid was unstructured, where the grid size varied from 100 m near-shore to 15 km in the central Baltic Proper. The distribution function has two distinct peaks for depth-induced wave breaking, representative of different wave climates in different sub-basins (see Fig. 4b for significant wave height variation). Depth induced wave breaking is up to 5 times as intense in the depth range between 4-10 m compared to bottom friction. The depth induced breaking dominance over dissipation due to bottom friction also becomes evident by inspecting Fig. 6d. Therefore, in coastal environments,  $S_{db}$  can't be neglected.

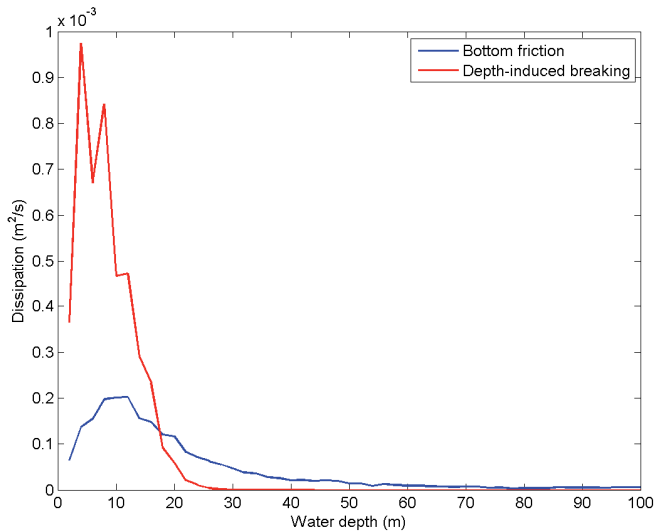


**Figure 9.** Comparison of dissipation due to bottom friction (blue line) and depth-induced wave breaking (red line) as a function of water depth.

### 4.3 Two whitecapping formulations

The model underestimated the peak wave periods in large wave events in Paper V, when the default Komen formulation for whitecapping was used. This underestimation is known in SWAN. For pure wind sea, the energy density at lower frequencies is typically underestimated, whereas energy levels in the tail are generally overestimated. Consequently, both the peak and mean periods are underestimated (Westhuysen et al., 2007). There are several explanations for that. For example, Westhuysen et al. (2007) demonstrates that the peak period underestimation by SWAN is partly due to the use of DIA, which is an approximation of the complete set of quadruplet interactions. Another explanation is based on the definition of the whitecapping source term, which is by default represented in SWAN with the pulse-based, quasi-linear model (Eq. 5). Westhuysen et al. (2007) suggest a new saturation-based model (Eq. 6), which leads to more accurate results in terms of spectral period fit. The Westhuysen et al. (2007) formulation was used in Papers II and III in the case of non-stationary wind and the results were satisfying for peak periods. Improvements of peak period modeling have been reported by other authors also (Mulligan et al., 2008; Teles et al., 2012), when saturation-based dissipation is used.

In Paper V the underestimation of peak periods of small wave events can be spurious. As the wind waves were measured with a pressure transducer at a depth of 4-5 m from the surface, high frequency waves were cut off. The highest

cut-off frequency corresponded to a wave period of 2.6 s. As seen from figs. 6 and 8 in Paper V, the modeled peak period was usually below 3 s in the case of short fetch conditions (S, SSW wind for example), while the measured one was usually above 4 s. The fetch length in case of S wind is 5 km, and with wind speed of 10 m/s the peak period would be only 2.5 s, as calculated with growth laws by Kahma and Calcoen (1992). In that sense in Paper V only wave events corresponding to a long fetch (9 August and 19 November, 2005) can be included in the comparison of measured and modeled waves directly.

In the 9 August case the maximum measured peak period was ~6.2 s and the corresponding values for the model in the default case Komen formulation was ~5.1 s, an 18 % difference. A recalculation of this event with the same wind forcing as in Paper V but instead of using Westhysen et al. (2007) model increased the modeled peak period to 6 s, thus reducing the relative difference to 3 %. Significant wave height also increased by 5 cm.

One might argue that since the model was forced with a temporally varying but spatially homogenous wind, the wind speed was underestimated at the open parts of northern Baltic Proper, thus also contributing to underestimation of peak periods. The wind speed during the 9 August storm in the re-analyzed dataset by Luhamaa et al. (2011) was not higher than the spatially constant wind, which forced SWAN. Another feature which has to be taken into account is the air-sea stability and wind measurement height. The atmospheric surface layer during the 9 August storm was unstable, as the water temperature (measured at 4 m depth in Küdema Bay) was 18.5°C and the air temperature at Vilsandi station was 16°C. The wind measurements were carried out 16 m above sea surface. The model input wind fields usually have to be transformed to 10 m elevation and reduced to neutral conditions, since in the model the air-sea difference is assumed to be zero. Using coefficients from Launiainen and Laurila (1984), it is evident that the measured wind at 16 m elevation was 3 % faster compared to wind which is transformed to 10 m. Combining this result with the reanalysis wind fields, it is unlikely that bulk energy input over the whole northern Baltic Proper was underestimated in the 9 August wind event. This leads to a conclusion that part of the peak period underestimation in Paper V was attributable to the whitecapping formulation. So in other studies (Papers I, II, III and IV) the saturation-based whitecapping formulation was used.

## 5. WAVE PROPAGATION THROUGH ARRAY OF OBSTACLES

A structure which is installed in water will affect the wave and circulation regime and sediment transport. There are plenty of studies published in literature assessing the importance of scour. Only a few technical studies assess the impact of wind turbines or wave farms upon surface waves near the coast (DHI water and Environment, 2007; Millar et al., 2007). The purpose of Paper II was to quantify the effect of these structures on wind waves, which are propagating towards the coast. The main aim was to find out how much these structures will absorb and scatter wave energy. Wind farms are planned to be installed in the coastal waters of Estonia near Hiiumaa, in the NE Baltic Sea (see fig 1 in Paper II for a detailed map). Water is relatively deep off the coast of Hiiumaa, but there are often several shallows, where water depth is less than 20 m.

This study (Paper II) focused on two locations – wind farm 1, situated in the WSW from the Kõpu Peninsula (see fig. 1 in Paper II) and wind farm 2, situated in the NW from Hiiumaa. Coastal areas that could be under impact are the head of Kõpu Peninsula and the northern coast of Hiiumaa. At wind farm 1, 55 turbines were planned to be installed in parallel rows with a minimum distance of 1000 m from each other. The closest turbines at the wind farm 1 will be 5 km from the coast (the head of Kõpu Peninsula) and the distant ones 15 km from the coast of the Kõpu Peninsula. The nearest coast from wind farm 2 is the western part of Tahkuna Peninsula that is 13 km to the SE. The northern coast of the Kõpu Peninsula directly south from wind farm 2 is 20 km away.

For wind farm 1, although there is a fourfold increase of wave heights in case of doubled wind speeds (as expected for fully developed waves) and a linear increase of wave period, the 45° turn of the wind does not change the parameters at any significant level (Table 1). For the SW wind, significant wave height was greater only by 0.2 m compared to the W wind at the wind farm 1. The peak period was only 0.4 s greater. The resulting wavelengths display the same variability. As the fetch length for the W winds is 250 km and for the SW winds 650 km, almost the same variability means that the wave field already has its full development at 250 km in the Baltic Sea in these wind conditions.

At wind farm 2, the change in direction of wind from the NW to the N reduced significant wave height up to 0.5 m and peak period up to 1 s (Table 2). The NW wind generated higher waves since the fetch was longer. However, compared to the wave parameters at wind farm 1, the modelled values of wave parameters were lower at wind farm 2. This is expected as the fetch length was lower in case of wind farm 2.

Table 1: Modelled wave parameters at the wind farm 1 location. Hs – significant wave height; Peak – peak wave period; Wlen – wavelength corresponding to peak wave period.

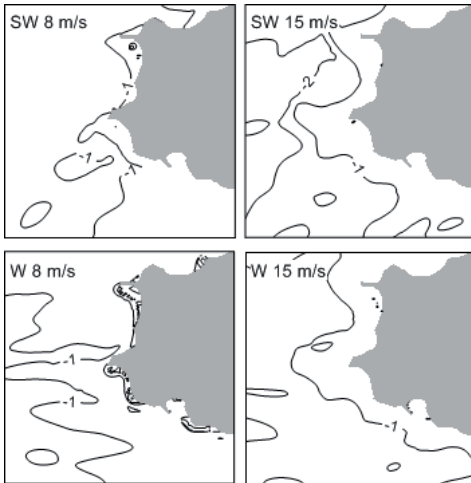
	SW 8 m s <sup>-1</sup>	SW 15 m s <sup>-1</sup>	W 8 m s <sup>-1</sup>	W 15 m s <sup>-1</sup>
Hs [m]	0.9-0.95	3.2-3.8	0.88-0.94	3-3.6
Peak [s]	4.7-4.8	8.5-8.7	4.7-4.8	8.1-8.3
Wlen [m]	33-36	75-110	32-35	70-100

Table 2: Same as Table 1 but for wind farm 2 location.

	NW 8 m s <sup>-1</sup>	NW 15 m s <sup>-1</sup>	N 8 m s <sup>-1</sup>	N 15 m s <sup>-1</sup>
Hs [m]	0.85-0.9	2.8-3.2	0.82-0.84	2.5-2.7
Peak [s]	4.4-4.6	7.4-7.7	4.1-4.2	6.5-6.7
Wlen [m]	29-31	62-84	26-28	52-66

In terms of significant wave height, the absolute reduction near the coast due to wind farm 1 was not more than 2% (Fig. 10). The 1% isoline was closer to the coast in case of the 8 m s<sup>-1</sup> wind compared to the 15 m s<sup>-1</sup> wind. The difference in terms of significant wave height did not exceed 0.5 cm and 1 cm near the coast in case of the 8 m s<sup>-1</sup> and 15 m s<sup>-1</sup> wind, respectively. In the case of the 15 m s<sup>-1</sup> wind, the 1% reduction line coincided with the 10 m isobath. Compared to the impact of wind farm 1, the reduction of significant wave height due to wind farm 2 was even more marginal (see fig. 6 in Paper II) The reduction was less than 0.25 % below the 10 m isobath.

The marginal impact is due to three factors. Firstly, waves meeting an obstacle reflect and bend around it. Only large piles change the wave field considerably. The diffraction and reflection are deemed as significant for  $D/L > 0.1$  or  $D/L > 0.2$ , where  $D$  is the diameter of the monopile and  $L$  is the wavelength. In case of the 8 m s<sup>-1</sup> wind, the ratio is between 0.1-0.2 and in case of the 15 m s<sup>-1</sup> wind, 0.05-0.08 (when the diameter is 5 m, wavelengths from Tables 1 and 2). Thus in these particular cases, diffraction and reflection were negligible. Secondly, the two turbines are not closer than 1 km to each other (at least 10 crests fit between) and therefore very little scatter occurs. And lastly, the wind turbines are distant from the coast.



**Figure 10.** The impact of wind farm 1 to significant wave height. The contour unit is [%] and a negative value shows a decrease of significant wave height. Adapted from Paper II.

The simulation results are directly comparable with other findings from other researchers and consultancies. The loss in significant wave height due to Scorby Sands offshore wind farm was less than 2%. In the latter case a model which was based on an evolution equation solution to the mild slope equation for water waves was used. It differs from the spectral wave model. The model grid size in their experiment was 3 m. Millar et al. (2007) used the SWAN model in order to assess the impact of a wave farm upon wind waves. In their study the interaction of surface waves and wave farms were modelled using the so-called transmission coefficient. The total reduction of significant wave height near the coast was less than 2 cm. The wave damping due to Rodsand offshore wind farm was less than 1% for higher waves (DHI water and Environment, 2007). In their study the energy loss was calculated with the integral wave model WAMIT for a single turbine. The impact of the whole array was further established with the spectral wave model MIKE 21 SW. The shortcoming of this simulation study lies in the assumption that wind farms do not alter wind speed. In general this is not true (Christiansen and Hasager, 2006).

## 6. WAVE INDUCED FLOW AND SET-UP

### 6.1 Wave induced flow

There is no evidence about what role the waves may have on resuspension and what could be the contribution of wave induced currents in the overall water exchange in the Suur Strait (Paper III). Surface wave measurements in the Suur Strait have not been performed, although the role of waves can be important in forcing currents and re-entertaining bottom sediments. Mulligan et al. (2008) have shown the importance of wave induced currents in overall circulation in the small and shallow Lunenburg Bay in hurricane scale winds. Using observation data and model simulations the role of wave induced and current induced shear velocities on resuspension was estimated in Paper III. The magnitude of wave generated currents was also assessed.

Wave induced shear velocity (Eqs. 9, 10 and 11) dominated over current induced shear velocity in the Suur Strait, as calculated from simultaneous wave and current measurements (fig. 8 in Paper III). Long fetch wave events induced sediment resuspension, and the highest shear velocities were obtained during strong ( $15 \text{ m s}^{-1}$ ) southerly wind events. For the current-induced shear velocity, the critical value for resuspension was slightly exceeded only when current speeds of up to  $0.4 \text{ m s}^{-1}$  generated shear velocities of up to  $1.5 \text{ cm s}^{-1}$  in the bottom boundary layer, thus topping the critical resuspension threshold for fine fractioned sand (Kuhrts et al., 2004). On average the wave induced near bed shear velocity was  $1 \text{ cm s}^{-1}$  higher than current induced shear velocity.

The horizontal distribution of wave induced shear velocities (near bed flow due to wave orbital motion) at the peak of the strong ( $15 \text{ m s}^{-1}$ ) southerly wind event showed great variability (Fig. 11). The shear velocities were the highest, exceeding  $6 \text{ cm s}^{-1}$  just outside the Suur Strait and less than the critical value ( $1.4 \text{ cm s}^{-1}$ ) in the deepest area of the Suur Strait.

A comparison of the wind induced currents and wave induced currents (resulting from wave radiation stress as calculated by Eqs. 12 and 13) is shown on Fig. 12. The wind induced currents were much stronger in the strait area and reached  $58 \text{ cm s}^{-1}$  there. However in the strait wave induced currents are negligible. The wave induced currents played an important role in the flow field near the southern coast of Muhu Island, where they were comparable to wind induced currents. Thus, the influence of wave stress is insignificant on long-term water exchange in the Suur Strait, but wave induced currents should be considered while modeling the nearshore hydrodynamics with the emphasis on sediment transport and drift calculations.

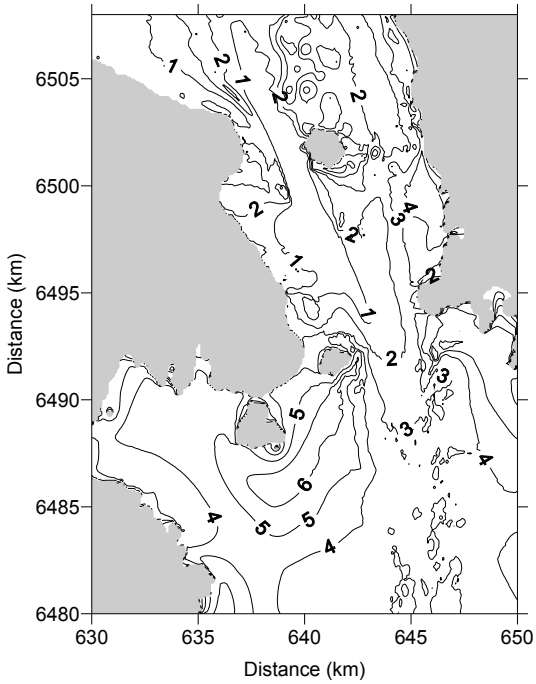


**Figure 11.** Spatial distribution of wave-induced shear velocities ( $\text{cm s}^{-1}$ ) at the peak of the strong southerly wind event on 18 November 2008. Adapted from Paper III.

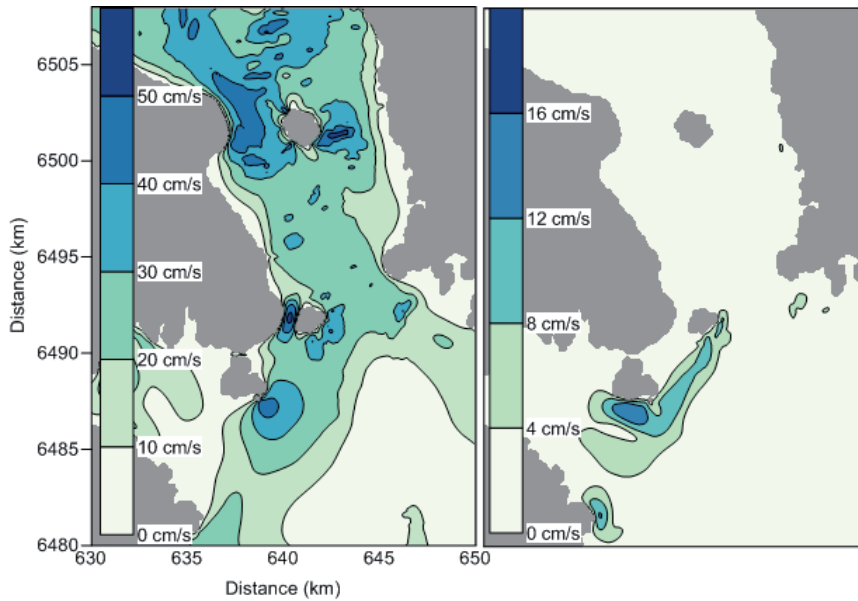


**Figure 12.** Maps of wind induced current speed (left) and wave induced current speed (right) in the Suur Strait at 23:00 UTC on 19 November 2008. Adapted from Paper III.

## 6.2 Wave driven set-up

Wave set-up is driven by the cross-shore gradient in radiation stress that results from rapid energy dissipation due to wave breaking (Longuet-Higgins and Stewart, 1963, 1964). Numerous laboratory experiments have been conducted in the past to study the setup and setdown of waves and to confirm the theory of Longuet-Higgins and Stewart (Bowen et al., 1968; Bowen, 1969). Setups and setdowns were also measured at real field conditions (Guza and Thornton, 1981; Holman and Sallenger, 1985; Hanslow and Nielsen, 1993; Lentz and Raubenheimer, 1999). Guza and Thornton (1981) concluded that the maximum set-up in the surf zone forms 17 % of the significant wave height offshore. Recently, modeling and observational studies have been undertaken to quantify the role of wave induced setup in the whole sea level rise. Kim et al. (2010) predicts a maximum contribution of 40% by the radiation stresses to the peak sea level rises. In the Obidos Lagoon in Portugal, the wave induced setup explained 20 % of the sea level rise during storms (Malhadas et al., 2009). In Paper I the possible wave induced set-up at a natural beach was simulated.

In Pärnu Bay the largest wave induced set-ups were concentrated not to the bay head, but on the sides, where high waves undergo rapid refraction and following depth induced breaking (Fig. 6d). The set-up depends not only on the significant wave height prior to breaking, but on the gradient of dissipation as well. In areas where friction dominates over breaking, the gradient is small. Intense wave breaking together with high significant wave height over 2 m could exert high set-up at Sorgu Island in the middle of Pärnu Bay (barely visible on Fig. 6a). It is a small (500 x 150 m) low-laying island, with typical elevations less than 3.5 m. The island makes an example why such a high resolution (100 m) grid is necessary in coastal areas - the island was not resolved on the 400 m grid. Unstructured mesh approaches (Zijlema, 2010) make it feasible to resolve these islands, without compromising computational times.

At the Pärnu city beach, the transformation of sea state with initial conditions 1.8 m significant wave height and 5.2 s peak period is shown on Fig. 13. This represents the moment, when peak surge and highest significant wave height occurred almost simultaneously. Significant wave height follows the bottom profile very well, with weak dissipation in waters deeper than 6 m. Over the first 2500 meters wave height reduces 0.4 m. Afterwards follows a climb on a slope, in which shoaling commences. When water depth reaches 2.5 m, breaking becomes the dominant mechanism and over the course of next 700 m wave height decreases 1.4 m. This resulted in a 0.51 m maximum setup. The inundation due to static setup is 130 m, as indicated by the slope colored red. The preceding water level rise due to surge caused 600 m of inundation, colored blue on Fig. 13A.

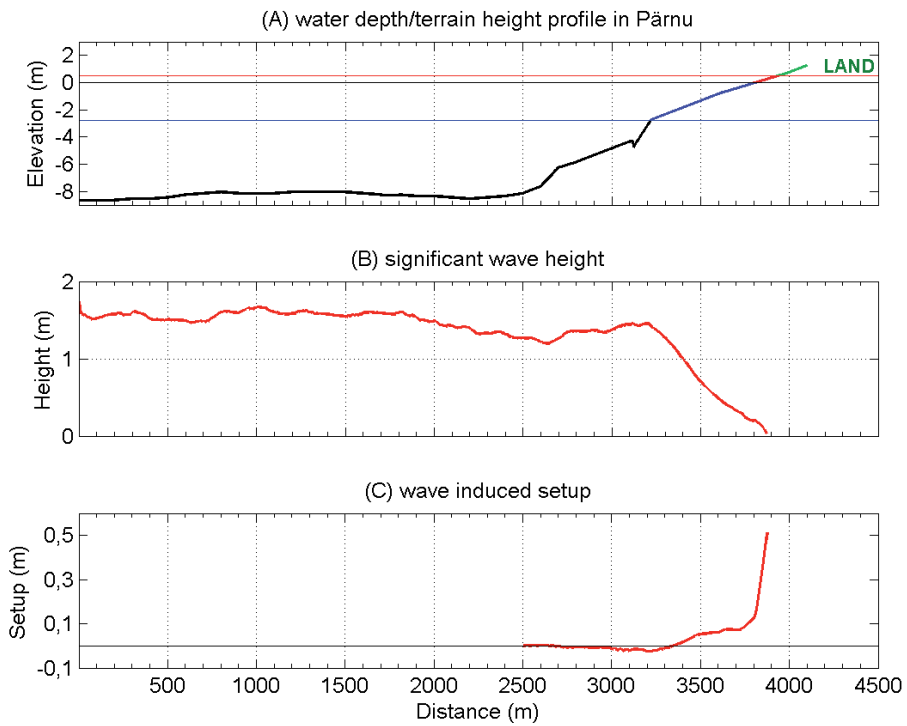


**Figure 13.** Wave transformation near shore (Pärnu town beach, cross-shore profile) as calculated by SWASH model. Panel A; black line is water depth, when a 2.7 m surge is added to topography. Blue slope indicates inundation due to surge and red slope due to wave set-up. The horizontal blue and red lines indicate the location of water in case of no surge and in case of surge plus set-up, respectively. Panel B: spatial evolution of significant wave height (snapshot). Panel C: evolution of wave induced set-down and set-up. Adapted from Paper I.

## 7. CONCLUSIONS

The objective of this dissertation was to improve knowledge of near-coastal wave field variability in the Baltic Sea. The focus was on studying processes which influence wave field evolution and to quantify wave-induced flow and set-up. It was shown that wave fields were heterogeneous on spatial scales, as well as in temporal scales. A multi-scale wave model is necessary when investigating wave field variability, processes influencing wave field evolution and wave field influence to other processes, as it pertains to rapidly varying fields.

The main results of the present dissertation are as follows:

- Water level impacts the significant wave height distribution both in space and time. Significant wave height in a shallow bay increased by taking into account the additional deepening of water due to surge. The increase in significant wave height was correlated with water depth at the time of the maximum surge. Wave height increased less than 0.3 m in areas where water was deeper than 10 m, but up to 1 m when water was shallower than 5 m. During low surges (less than 1 m) wave height increase was not so profound.
- Depth-induced wave breaking is an important mechanism in dissipating wave energy in shallow water. In case of severe storms, depth induced wave breaking reduced significant wave height up to 2.3 m in a semi-sheltered bay, compared to a situation, when this source term is inactive. Considerable dissipation due to depth-induced breaking in high winds commences in the Baltic Sea, when water depth is less than 20 m. Wave breaking dissipation is up to five times as intense in depth range between 4-10 m compared to bottom friction.
- Part of the peak period underestimations was attributable to the whitecapping formulations used. Saturation based, local in wavenumber-space whitecapping provided a better fit of the peak periods compared to default average-wavenumber based whitecapping. Nonlinear saturation based whitecapping reduced the difference between modeled and measured peak periods to 3 %, while the quasi-linear pulse based model underestimated peak period by 18 %.
- An array of small obstacles influenced wave field marginally, reducing significant wave heights in the surf zone less than 1 %. This stems from the low obstacle-to-crest ratio in the particular cases, which limited the diffraction, scattering and breaking of incident wave field.
- Numerical simulations with added wave stress as forcing in a shallow

water model showed a minor influence of wave field to overall water exchange in a narrow channel (Suur Strait) dominated by barotropic currents resulting from sea-level gradients. However, wave induced currents were locally dominating over wind driven currents.

- Wave induced shear velocities considerably exceeded the threshold for resuspension in a narrow channel at time instances, when current induced shear velocity favored deposition.
- The transformation of sea state with initial conditions of 1.8 m significant wave height and 5.2 s peak period resulted in wave induced setup of 0.51 m and additional inundation of 130 m at a coastal area, which is most vulnerable to flooding in Estonia (Pärnu town).

Modeling results indicate that in severe weather conditions a coupled wave-hydrodynamic modeling is needed. Unstructured mesh implementation seems to be a feasible technique to cover wave field evolution over multiple scales, when considering wave modeling of the whole Baltic Sea. It is essential to study further the set-up induced by random wave fields and if necessary, implement this physical forcing in regional sea level forecasting systems. Further studies are also needed to investigate the potential magnitude of wave driven currents across the whole Baltic Sea coastal environments.

## REFERENCES

- Anselmi-Molina, C.M., Canals, M., Morell, J., Gonzalez, J., Capella, J., Mercado, A. 2012. Development of an operational nearshore wave forecast system for Puerto Rico and the U.S. Virgin Islands. *Journal of Coastal Research*, 28 (5), pp. 1049-1056.
- Averkiev, A.S., Klevanny, K.A. 2010. A case study of the impact of cyclonic trajectories on sea-level extremes in the Gulf of Finland. *Continental Shelf Research*, 30 (6), pp. 707-714.
- Battjes, J.A., Janssen, J.P.F.M. 1978. Energy loss and set-up due to breaking of random waves. *Proceedings of the Coastal Engineering Conference*, 1, pp. 569-587.
- Booij, N., Ris, R.C., Holthuijsen, L.H. 1999. A third-generation wave model for coastal regions 1. Model description and validation. *Journal of Geophysical Research C: Oceans*, 104 (C4), pp. 7649-7666.
- Bowen, A.J., Inman, D.L., Simmons, V.P. 1968. Wave setdown and wave setup. *Journal of Geophysical Research*, 73, pp. 2569-2577.
- Bowen, A.J. 1969. Rip currents, 1: theoretical investigations. *Journal of Geophysical Research*, 74, pp. 5468-5478.
- Choi, B.H., Min, B.I., Kim, K.O., Yuk, J.H. 2013. Wave-tide-surge coupled simulation for typhoon Maemi. *China Ocean Engineering*, 27 (2), pp. 141-158.
- Christiansen, M.B., Hasager, C.B. 2006. Using airborne and satellite SAR for wake mapping offshore. *Wind Energy*, 9(5), pp. 437-455.
- Chubarenko, B.V., Leitsina, L.V., Esiukova, E.E., Kurennoy, D.N. 2012. Model analysis of the currents and wind waves in the Vistula Lagoon of the Baltic Sea. *Oceanology*, 52 (6), pp. 748-753.
- Dalyander, P.S., Butman, B., Sherwood, C.R., Signell, R.P., Wilkin, J.L. 2013. Characterizing wave- and current- induced bottom shear stress: U.S. middle Atlantic continental shelf. *Continental Shelf Research*, 52, pp. 73-86.
- DHI Water and Environment, 2007. *The effect of wind turbines on nearshore waves*. Hørsholm, Denmark: DHI, 50p.
- Dietrich, J.C., Trahan, C.J., Howard, M.T., Fleming, J.G., Weaver, R.J., Tanaka, S., Yu, L., Luettich, R.A., Dawson, C.N., Westerink, J.J., Wells, G., Lu, A., Vega, K., Kubach, A., Dresback, K.M., Kolar, R.L., Kaiser, C., Twilley, R.R. 2012. Surface trajectories of oil transport along the Northern Coastline of the Gulf of Mexico. *Continental Shelf Research*, 41, pp. 17-47.
- Eldeberky, Y. 1996. Nonlinear transformation of wave spectra in the nearshore zone, *Ph.D. thesis*, Delft University of Technology, Department of Civil Engineering, the Netherlands.
- Elken, J., Kask, J., Kõuts, T., Liiv, U., Perens, R., Soomere, T. 2001. Hydrodynamical and geological investigations of possible deep harbour sites

- in northwestern Saaremaa Island: overview and conclusions. Proceedings of Estonian Academy of Sciences Engineering, 7, pp. 85–98.
- Evdokimov, S.N., Klevantsov, Y.P., Sustatov, Y.Y. 1974. Analysis of dynamics of waters in the Gulf of Finland. Collected works of the Leningrad Hydrometeorological Observatory, 8, pp. 155–164. [In Russian]
- Feistel, R., Nausch, N., Wasmund, N. 2008. State and Evolution of the Baltic Sea, 1952-2005: A Detailed 50-year Survey of Meteorology and Climate. Physics, Chemistry, Biology, and Marine Environment. John Wiley & Sons, Hoboken.
- Finnish Meteorological Institute report series. [http://www.helcom.fi/BSAP\\_assessment/ifs/ifs2012/en\\_GB/WaveClimate/](http://www.helcom.fi/BSAP_assessment/ifs/ifs2012/en_GB/WaveClimate/)
- Guza, R.T., Thornton, E.B. 1981. Wave setup on a natural beach. Journal of Geophysical Research, 86, pp. 4133–4137.
- Hanafin, J.A., Quilfen, Y., Ardhuin, F., Sienkiewicz, J., Queffelec, P., Obrebski, M., Chapron, B., Reul, N., Collard, F., Corman, D., De Azevedo, E.B., Vandemark, D., Stutzmann, E. 2012. Phenomenal sea states and swell from a north atlantic storm in february 2011: A comprehensive analysis. Bulletin of the American Meteorological Society, 93 (12), pp. 1825-1832.
- Hanslow, D., Nielsen, P. 1993. Shoreline set-up on natural beaches. Journal of Coastal Research, 15, pp. 1–10.
- Haran, G., Raudsepp, U., Alari, V., Uiboupin, R., Sipilgas, L., Erm, A. 2010. Operational observations methods during offshore sand mining - Case study in Tallinn Bay, the southern Gulf of Finland. In IEEE/OES US/EU Baltic International Symposium, Baltic 2010, art. no. 5621660.
- Hasselmann, K. 1962. On the non-linear transfer in a gravity wave spectrum, part 1. General theory. Journal of Fluid Mechanics, 12, pp. 481-500.
- Hasselmann, K. 1974. On the spectral dissipation of ocean waves due to white capping. Boundary-Layer Meteorology, 6 (1-2), pp. 107-127.
- Hasselmann, S., Hasselmann, K., J.H. Allender, J.H., Barnett, T.P. 1985. Computations and parameterizations of the nonlinear energy transfer in a gravity wave spectrum. Part II: Parameterizations of the nonlinear transfer for application in wave models, Journal of Physical Oceanography, 15, 11, pp. 1378-1391.
- Holman, R.A., Sallenger, A.H. 1985. Set-up and swash on a natural beach. Journal of Geophysical Research, 90, pp. 945–953.
- Holthuijsen L.H. 2007. Waves in oceanic and coastal waters, Cambridge University Press, New York, 404 pp.
- Inghilesi, R., Catini, F., Bellotti, G., Franco, L., Orasi, A., Corsini, S. 2012. Implementation and validation of a coastal forecasting system for wind waves in the Mediterranean Sea. Natural Hazards and Earth System Science, 12 (2), pp. 485-494.
- Jaagus, J., Kull, A. 2011. Changes in surface wind directions in Estonia during 1966-2008 and their relationships with large-scale atmospheric circulation. Estonian Journal of Earth Sciences, 60 (4), pp. 220-231.

- Jones, E.M., Kämpf, J., Fernandes, M. 2012. Characterisation of the wave field and associated risk of sediment resuspension in a coastal aquaculture zone. *Ocean and Coastal Management*, 69, pp. 16-26.
- Jönsson, A., Broman, B., Rahm, L. 2003. Variations in the Baltic Sea wave fields. *Ocean Engineering*, 30 (1), pp. 107-126.
- Kahma, K.K., Calkoen, C.J., 1992. Reconciling discrepancies in the observed growth of wind-generated waves. *Journal of Physical Oceanography*, 22, pp. 1389–1405.
- Karagali, I., Peña, A., Badger, M., Hasager, C.B. 2012. Wind characteristics in the North and Baltic Seas from the QuikSCAT satellite. *Wind Energy*. Article in Press.
- Kim, S.Y., Yasuda, T., Mase, H. 2010. Wave set-up in the storm surge along open coasts during Typhoon Anita. *Coastal Engineering*, 57, pp. 631–642.
- Kolesova, N., Raudsepp, U., Alari, V. 2010. Dominant zoobenthic species in the northwestern coastal sea of Estonia - Potential role of abiotic stresses. In *IEEE/OES US/EU Baltic International Symposium, Baltic 2010*, art. no. 5621647.
- Komen, G.J., Hasselmann, S., Hasselmann, K. 1984. On the existence of a fully developed wind-sea spectrum, *Journal of Physical Oceanography*, 14, pp. 1271-1285.
- Komen G. J., Cavaleri L., Donelan M., Hasselmann S., Janssen P.A.E.M. 1994. *Dynamics and modelling of ocean waves*. Cambridge University Press, Cambridge, 532 pp.
- Kovtun, A., Torn, K., Martin, G., Kullas, T., Kotta, J., Suursaar, Ü. 2011. Influence of abiotic environmental conditions on spatial distribution of charophytes in the coastal waters of West Estonian Archipelago, Baltic Sea. *Journal of Coastal Research*, (SPEC. ISSUE 64), pp. 412-416.
- Kuhrts, C., Fennel, W., Seifert, T. 2004. Model studies of transport of sedimentary material in the western Baltic. *Journal of Marine Systems*, 52 (1-4), pp. 167-190.
- Kurennoy, D., Ryabchuk, D. 2011. Wind wave conditions in Neva Bay. 2011. *Journal of Coastal Research*, (SPEC. ISSUE 64), pp. 1438-1442.
- Lagemaa, P., Elken, J., Kõuts, T. 2011. Operational sea level forecasting in Estonia. *Estonian Journal of Engineering*, 17 (4), pp. 301-331.
- Launiainen J., Laurila T. 1984, Marine wind characteristics in the northern Baltic Sea, *Finnish Mar. Res.*, 250, pp. 52–86.
- Lentz, S., Raubenheimer, B. 1999. Field observations of wave setup. *Journal of Geophysical Research*, 104, pp. 25867–25875.
- Lilover, M.-J., Pavelson, J., Kõuts, T. 2011. Wind forced currents over the shallow Naissaar Bank in the Gulf of Finland. *Boreal Environment Research*, 16 (SUPPL. A), pp. 164-174.
- Longuet-Higgins, M.S., and R.W. Stewart, R.W. 1963. A note on wave set-up. *Journal of Marine Research*, 21, 4.

- Longuet-Higgins, M.S., and R.W. Stewart, R.W. 1964. Radiation stresses in water waves; a physical discussion, with applications. *Deep-Sea Research*, 11, pp. 529–562.
- Liu, H., Xie, L. 2009. A numerical study on the effects of wave-current-surge interactions on the height and propagation of sea surface waves in Charleston Harbor during Hurricane Hugo 1989. *Continental Shelf Research*, 29 (11-12), pp. 1454-1463.
- Luhamaa, A., Kimmel, K., Männik, A., Rõõm, R. 2011. High resolution re-analysis for the Baltic Sea region during 1965-2005 period. *Climate Dynamics*, 36 (3), pp. 727-738.
- Malhadas, M.S., Leitão, P.C., Neves, A.S.R. 2009. Effect of coastal waves on sea level in Óbidos Lagoon, Portugal. *Continental Shelf Research*, 29(9), 1240-1250.
- Miles, J.W. 1957. On the generation of surface waves by shear flows. *Journal of Fluid Mechanics*, 3, pp. 185-204.
- Millar, D.L., Smith, H.C.M., Reeve, D.E., 2007. Modelling analysis of the sensitivity of shoreline change to a wave farm. *Ocean Engineering*, 34, pp. 884–901.
- Mulligan, R.P., Bowen, A.J., Hay, A.E., Van Der Westhuysen, A.J., Battjes, J.A. 2008. Whitecapping and wave field evolution in a coastal bay. *Journal of Geophysical Research C: Oceans*, 113 (3), art. no. C03008.
- Neill, S.P., Hashemi, M.R. 2013. Wave power variability over the northwest European shelf seas. *Applied Energy*, 106, pp. 31-46.
- Niros, A., Vihma, T., Launiainen, J. 2002. Marine meteorological conditions and air-sea exchange processes over the northern Baltic Sea in 1990s. *Geophysica*, 38 (1-2), pp. 59-87.
- Pettersson, H., Kahma, K.K., Tuomi, L. 2010. Wave directions in a narrow bay. *Journal of Physical Oceanography*, 40 (1), pp. 155-169.
- Phillips, O.M. 1957. On the generation of waves by turbulent wind. *Journal of Fluid Mechanics*, 2, pp. 417-445.
- Pierson, W.J., Moskowitz, L. 1964. A proposed spectral form for fully developed wind seas based on the similarity theory of S.A. Kitaigorodskii. *Journal of Geophysical Research*, 69, 24, pp. 5181-5190.
- Rusu, L., Soares, C.G. 2013. Evaluation of a high-resolution wave forecasting system for the approaches to ports. *Ocean Engineering*, 58, pp. 224-238.
- Seifert, T., Kayser, B., Tauber, F., 1995. Bathymetry data of the Baltic Sea. *Baltic Sea Research Institute, Warnemünde*.
- Sipelgas, L., Raudsepp, U., Kõuts, T. 2006. Operational monitoring of suspended matter distribution using MODIS images and numerical modeling. *Advances in Space Research*, 38 (10), pp. 2182-2188.
- Soomere, T. 2005. Wind wave statistics in Tallinn Bay. *Boreal Environment Research*, 10 (2), pp. 103-118.
- Stevens, A.W., Lacy, J.R. 2012. The influence of wave energy and sediment transport on seagrass distribution. *Estuaries and Coasts*, 35 (1), pp. 92-108.

- Stopa, J.E., Filipot, J.-F., Li, N., Cheung, K.F., Chen, Y.-L., Vega, L. 2013. Wave energy resources along the Hawaiian Island chain. *Renewable Energy*, 55, pp. 305-321.
- Suursaar, Ü., Jaagus, J., Kullas, T. 2006a. Past and future changes in sea level near the Estonian coast in relation to changes in wind climate. *Boreal Environment Research*, 11 (2), pp. 123-142.
- Suursaar, Ü., Kullas, T., Otsmann, M., Saaremäe, I., Kuik, J., Merilain, M. 2006b. Cyclone Gudrun in January 2005 and modelling its hydrodynamic consequences in the Estonian coastal waters. *Boreal Environment Research*, 11 (2), pp. 143-159.
- Suursaar, Ü., Kullas, T., Szava-Kovats, R. 2009. Wind and wave storms, storm surges and sea level rise along the Estonian coast of the Baltic Sea. *WIT Transactions on Ecology and the Environment*, 127, pp. 149-160.
- Suursaar, Ü., Kullas, T., Aps, R. 2012. Currents and waves in the northern Gulf of Riga: Measurement and long-term Hindcast. *Oceanologia*, 54 (3), pp. 421-447.
- SWAN team, 2013. <http://swanmodel.sourceforge.net/>
- SWASH team, 2013. <http://swash.sourceforge.net/>
- Teles, M.J., Pires-Silva, A.A., Belo-Pereira, M. 2012. Simulations of wave conditions on an open beach configuration: Wind resolution, seaward forcing and whitecapping effects. *European Journal of Environmental and Civil Engineering*, 16 (8), pp. 927-942.
- Tolman, H.L. 1990. Wind wave propagation in tidal inlets. *PhD thesis*, Delft University of Technology, Department of Civil Engineering, the Netherlands.
- Tolman, H.L. 1992. Effects of numerics on the physics in a third-generation wind-wave model. *Journal of Physical Oceanography*, 22 (10), pp. 1095-1111.
- Tuomi, L., Kahma, K.K., Pettersson, H. 2011. Wave hindcast statistics in the seasonally ice-covered Baltic Sea. *Boreal Environment Research*, 16 (6), pp. 451-472.
- Tuomi, L., Kahma, K.K., Fortelius, C. 2012. Modelling fetch-limited wave growth from an irregular shoreline. *Journal of Marine Systems*, 105-108, pp. 96-105.
- Tõnisson, H., Suursaar, Ü., Suuroja, S., Ryabchuk, D., Orviku, K., Kont, A., Sergeev, Y., Ravis, R. 2012. Changes on coasts of western Estonia and Russian Gulf of Finland, caused by extreme storm Berit in November 2011. In *Ocean: Past, Present and Future - 2012 IEEE/OES Baltic International Symposium, BALTIC 2012*, art. no. 6249193.
- Vihma, T., Haapala, J. 2008. Geophysics of sea ice in the Baltic Sea: A review. *Progress in Oceanography*, 80 (3-4), pp. 129-148.
- Westerbom, M., Jattu, S. 2006. Effects of wave exposure on the sublittoral distribution of blue mussels *Mytilus edulis* in a heterogeneous archipelago. *Marine Ecology Progress Series*, 306, pp. 191-200.

- Westhuysen, A.J., Zijlema, M., Battjes, J.A. 2007. Nonlinear saturation-based whitecapping dissipation in SWAN for deep and shallow water. *Coastal Engineering*, 54 (2), pp. 151-170.
- Wu, J. 1982. Wind-stress coefficients over sea surface from breeze to hurricane. *Journal of Geophysical Research*, 87, C12, pp. 9704-9706.
- Yan, L. 1987. An improved wind input source term for third generation ocean wave modelling, Scientific report WR-No 87-8, De Bilt, the Netherlands.
- Zhang, Z., Falter, J., Lowe, R., Ivey, G. 2012. The combined influence of hydrodynamic forcing and calcification on the spatial distribution of alkalinity in a coral reef system. *Journal of Geophysical Research C: Oceans*, 117 (4), art. no. C04034.
- Zijlema, M. 2010. Computation of wind-wave spectra in coastal waters with SWAN on unstructured grids. *Coastal Engineering*, 57 (3), pp. 267-277.
- Zijlema, M., Stelling, G., Smit, P. 2011. SWASH: An operational public domain code for simulating wave fields and rapidly varied flows in coastal waters. *Coastal Engineering*, 58 (10), pp. 992-1012.
- Zijlema, M., Van Vledder, G., Holthuijsen, L.H. 2012. Bottom friction and wind drag for wave models. *Coastal Engineering*, 65, pp. 19-26.
- Zou, Q.-P., Chen, Y., Cluckie, I., Hewston, R., Pan, S., Peng, Z., Reeve, D. 2013. Ensemble prediction of coastal flood risk arising from overtopping by linking meteorological, ocean, coastal and surf zone models. *Quarterly Journal of the Royal Meteorological Society*, 139 (671), pp. 298-313.

## **PUBLICATIONS**

### **Paper I**

Alari, V., Kõuts, T. 2012. Simulating wave-surge interaction in a non-tidal bay during cyclone Gudrun in January 2005. In: Ocean: Past, Present and Future - 2012 IEEE/OES Baltic International Symposium, BALTIC 2012, art. no. 6249185.



# Simulating wave-surge interaction in a non-tidal bay during cyclone Gudrun in January 2005

V. Alari, and T.Kõuts

Marine Systems Institute at Tallinn University of Technology  
12618 Akadeemia Rd 15a Tallinn  
Estonia

**Abstract**—Cyclone Gudrun (Erwin) crossed the Baltic Sea in 8-9 January 2005. The maximum sustained wind speed measured over the Baltic Proper reached 28 m/s (gusts 37.5 m/s) and prior the high surge (2.75 m in Pärnu city), wind blew mainly from the sector SW-WSW. The hydrodynamic consequences, coastal damages and wave conditions in Baltic Proper and Gulf of Finland resulting from windstorm Gudrun have been analyzed previously. Lacking was the knowledge of wave-surge interaction and the role of wave induced setup. The aim of this paper is to study the effects of surge upon surface wave field dynamics and to reconstruct the possible wave induced set-up at a natural beach by means of numerical modeling. Modeling system consisting of a spectral wave model SWAN and non-hydrostatic depth-averaged free surface flow model SWASH was implemented. Spectral model was implemented to describe wave conditions in the Baltic Sea during the passage of cyclone and for providing boundary data to SWASH model, which in turn is used to calculate setup and inundation. Modeling relies profoundly on the quality of modeled wind fields - hence the accuracy of downscaled ERA40 wind fields during cyclone Gudrun is analyzed. We conclude an overall good level of agreement between modeled winds and observations and suggest using it in further modeling studies. Significant wave height in Pärnu bay increases up to 1 m by taking into account the additional deepening of water due to surge. The transformation of waves over the swash zone results in wave induced setup of 0.51 m and additional inundation of 130 m.

## I. INTRODUCTION

The Baltic Sea (BS) is a large, brackish and shallow inland sea located in north-eastern Europe (Fig. 1). Although BS is nearly tideless with amplitudes of  $M_2$  and  $K_1$  waves 0.01–0.02 m [1], water level varies over a wide range of spatial and temporal scales due to interaction with atmosphere. The barotropic surge height is mainly determined by tangential wind stress, volume of water in the BS and regional topography and geometry; though, in some cases sea surface deformation caused by deep meso-scale baric lows moving rapidly over the sea is important forcing factor [2]. Measured historical water level maximums are higher on the eastern side of the BS compared to western side [3] and mainly occur during the passage of intense cyclones in spring and winter. The most vulnerable area affected by high surge in Estonia is the town of Pärnu in Pärnu bay (Fig. 1).

The city is at the end of a narrow bay, and it is separated by a river into upper and lower parts. The ground elevation is less than 5 m everywhere in the lower city. More than 40 % of the lower town was flooded during the passage of a severe cyclone Gudrun (or Erwin as named by university of Berlin) on 9 January 2005, when surge peaked at 2.78 m above mean sea level (to see inundation, compare Fig. 2a and 2b). Cyclone started its life cycle as a low pressure system near Newfoundland US, gained more strength as crossing the Atlantic, reached its nadir point 960 hPa near Oslo Norway [4] and continued to travel across the Scandinavian Peninsula, crossing the Bothnian Bay (Fig. 3). The maximum sustained wind speed measured over the Baltic Proper reached 28 m/s (gusts 37.5 m/s) and prior to the maximum surge, wind blew mainly from the sector SW-WSW. The hydrodynamic consequences [4], the coastal damages [5] and wave conditions in Baltic Proper and Gulf of Finland [6] resulting from windstorm Gudrun have been analyzed previously. Lacking is the knowledge of wave-surge interaction and the role of wave induced setup during the particular storm.

Setup, the super-elevation of the mean water level, is driven by the cross-shore gradient in radiation stress that results from wave breaking [7,8]. Many laboratory experiments have been conducted in past to study the setup and setdown of waves and to confirm the theory of Longuet-Higgins and Stewart (see for example: [9,10,11]). As the uniform beach profile is rare in nature, the setups and setdowns were also measured at real field conditions (see: [12,13,14,15]). [12] concluded that the maximum set-up in surf zone forms 17 % of the significant wave height offshore. Recently, modeling and observational studies have been undertaken to quantify the role of wave induced setup in the whole sea level rise. [16] predicts maximum contribution of 40% by the radiation stresses to the peak sea level rises. In the Obidos Lagoon in Portugal, the wave induced setup explains 20 % of the sea level rise during storms [17].

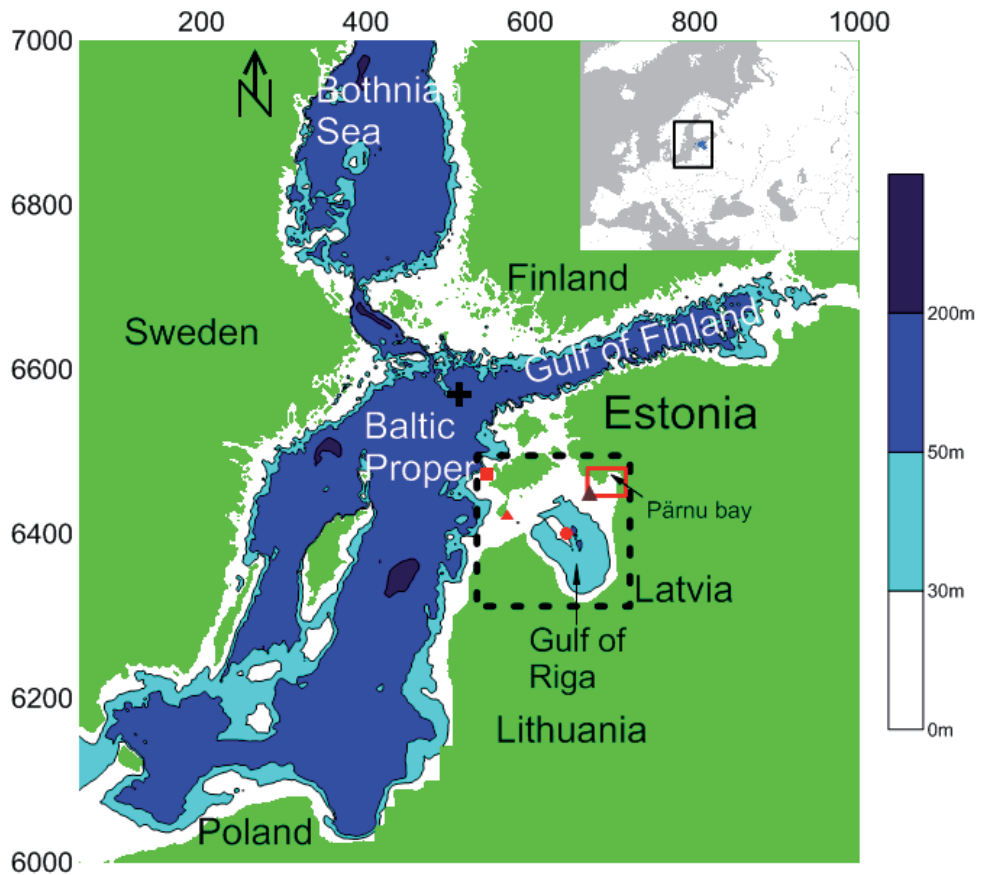


Fig.1. Study area in UTM-34 coordinates (km). Dashed rectangle is the boundary for 400 m grid and red rectangle is the boundary of 100 m grid. The whole big figure itself is the coarsest modeling domain with 2000 m resolution. Colorbar indicates water depth. The meteorological stations are following: (■) Vilsandi, (▲) Sörve, (●) Ruhnu, (▲) Kihnu. Black cross in the northern Baltic Proper is wave measurement station owned by FIMR.

The aim of this paper is to study the effects of surge upon surface wave field dynamics and to reconstruct the possible wave induced set-up at a natural beach by means of numerical modeling. The aims profoundly rely on the quality of modeled wind fields, hence the accuracy of downscaled ERA40 wind fields during cyclone Gudrun is also analyzed. Study is structured as following. In section 2 we describe the modeling system and its configuration. Following we present results of modeling and discuss them in context of other studies. Conclusions and further study prospects wrap up.



Fig.2. Pärnu city in a normal day (upper panel) and at 06:00 UTC on 9 January 2005. The maximum flood height is 2.75 m. The red dot represents sea level monitoring station. North up. Figure by Estonian Land Board.

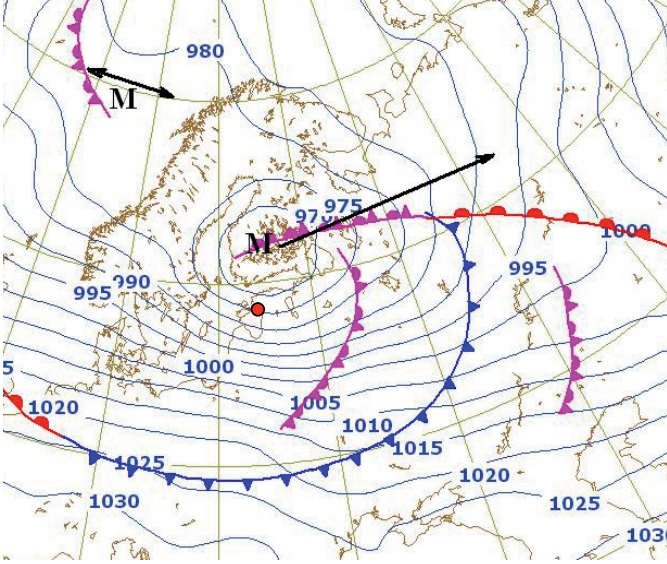


Fig. 3. Meteorological situation over Europe at 06:00 UTC on 9 January 2005. M represents low pressure system; magenta, red and blue lines represent occluded, warm and cold fronts, respectively. The isobars are given at 5 hPa incensement. Red dot represents Pärnu Bay. Figure by Estonian Meteorological and Hydrological Institute.

## II. MODELING SYSTEM

### A. Model descriptions

Modeling system consisting of a spectral wave model SWAN and non-hydrostatic depth-averaged free surface flow model SWASH was implemented. We will describe the models to outline the physical phenomena's which they account for. The SWAN wave model was implemented to describe wave conditions in the Baltic Sea during the passage of cyclone Gudrun and for providing boundary data to SWASH model, which in turn is used to calculate setup and inundation. Although [18] implemented SWAN directly to calculate the wave-induced set-up, the phenomenon of set-up requires hydrodynamic modeling when dealing with real coasts.

*SWAN*. It is a third generation phase averaged spectral wave model developed at Delft University of Technology [19]. In SWAN, the waves are described with the two-dimensional wave action density spectrum, whereas the evolution of the action density  $N$  is governed by the time dependent wave action balance equation, which reads:

$$\frac{\partial N}{\partial t} + (\vec{c}_g + \vec{U}) \cdot \nabla N + \frac{\partial c_\sigma N}{\partial \sigma} + \frac{\partial c_\theta N}{\partial \theta} = \frac{S_{tot}}{\sigma}. \quad (1)$$

The first term represents the local rate of change of action density; the second term denotes the propagation of wave energy in two dimensional geographical space, with  $\vec{c}_g$  being the group velocity and  $\vec{U}$  the ambient current. The third term represents the effect of shifting of the radian frequency due to variations in depth and mean currents. The fourth term represents the depth-induced and current-induced refraction. The quantities  $c_\sigma$  and  $c_\theta$  are the propagation velocities in spectral space  $(\sigma, \theta)$ , with  $\sigma$  and  $\theta$  representing the radian frequency and propagation direction respectively. The right-hand side contains the source term  $S_{tot}$  that represents all physical processes that generate, dissipate or redistribute wave energy. In shallow water, six processes contribute to  $S_{tot}$ :

$$S_{tot} = S_{wind} + S_{nl3} + S_{nl4} + S_{wc} + S_{bot} + S_{db} \quad (2)$$

These terms denote the energy input by wind ( $S_{wind}$ ), the nonlinear transfer of wave energy through three-wave ( $S_{nl3}$ ) and four-wave interactions ( $S_{nl4}$ ), and the dissipation of waves due to whitecapping ( $S_{wc}$ ), bottom friction ( $S_{bot}$ ) and depth-induced wave breaking ( $S_{db}$ ), respectively. The model has been validated for Estonian coastal sea close to present study area [20].

*SWASH*. SWASH [21] is a general-purpose numerical tool for simulating non-hydrostatic, free-surface, rotational flows. The governing equations are the nonlinear shallow water equations including non-hydrostatic pressure and provide a general basis for describing complex changes to rapidly varied flows typically found in coastal flooding resulting from e.g. dike breaks and tsunamis, and wave transformation in both surf and swash zones due to nonlinear wave-wave interactions, interaction of waves with currents, and wave breaking as well as runup at the shoreline [21]. The model is essentially applicable in the coastal regions up to the shore (Simulating Waves till Shore). The model has been validated with a series of analytical and laboratory test cases. In general the level of agreement between predictions and observations is quite favorable, particularly in view of the fact that a wide range of wave conditions and topographies were modeled [21].

The model accounts for the following physical phenomena:

- propagation, frequency dispersion, shoaling, refraction and diffraction,
- nonlinear wave-wave interactions (including surf beat and triads),
- wave breaking,
- wave runup and rundown,
- moving shoreline,
- bottom friction,
- partial reflection and transmission,
- wave-induced currents and wave-current interaction,
- vertical turbulent mixing,
- subgrid turbulence,
- mass and momentum conservation.

Surface gravity wave generation by wind is not accounted at present.

## B. Input data

*Wind*. The atmospheric forcing used in present modeling study is based on the dynamically down-scaled winds of the ERA40 data set. The resolution of the atmospheric forcing grid is 25x25 km with 3 h time step. Data was made available by ECCOSUPPORT project. The period used is 00:00 UTC 8 January 2005-21:00 UTC 9 January 2005. Wind was further converted to UTM-34 zone and interpolated to regular Cartesian grids corresponding to the coarse computational grid of SWAN.

*Bottom topography and terrain elevation*. For obtaining the Baltic Sea water depth, two datasets were used. The digital topography covering entire Baltic Sea with a resolution of 1 nautical mile is by [22] with the data available in internet. The topography of Pärnu Bay was manually digitized from marine charts issued by Estonian Marine Board with the coastline extracted from Coastline Generator, a freeware in internet. Both datasets were converted to UTM-34 zone and regular grids were generated. A 1 D profile was constructed for a certain section of the Pärnu city beach zone, which was extended to positive elevations of land by manually digitizing terrain elevation data, acquired from Estonian Land Board geoportal.

*Water level*. We use water level measurements taken in Pärnu harbor (see Fig. 2 the red dot) for model input and for analysis. According to [23], automatic temperature and air pressure compensation ensure an accuracy of 1 cm in terms of water column above the sensor. Also, automatic measurements are regularly checked by the readings of the staff gauge.

## C. Setup of models

*SWAN*. A triply nested SWAN model is implemented in geographical domain, with the boundaries shown in Fig 1. Each higher resolution run receives the boundary data from coarser run, while the most coarsest run starts with zero initial and boundary conditions at 00:00 UTC on 8 January 2005. The basic parameters of model runs are listed in Table 1. In the most nested grid the number of spectral directions was increased to 36 to ensure better representation of refraction. Two model runs were made, in which surge was neglected and when surge was considered. In the first case, no surge was added to water depth. In the second run, 1 m spatio-temporally constant surge was added to water depth in 400 m grid and time-varying, but spatially constant, water level was added to water depth of the 100 m grid.

TABLE 1. SWAN CONFIGURATION

	Coarse grid	Medium grid	Most nested grid
Run period (UTC)	08.01.2005 00:00-09.01.2005 21:00	Same	Same
Location of origin of x-direction (km) in UTM-34	50	503.4	675
Location of origin of y-direction (km) in UTM-34	6000	6314	6440
Nr. of meshes in x-direction	475	517	344
Nr. of meshes in y-direction	500	460	375
Mesh size in x-direction (km)	2	0.4	0.1
Mesh size in y-direction (km)	2	0.4	0.1
Model time step (min)	10	5	5
Spectral directions	24	24	36
Spectral frequencies (0.05-1 Hz)	40	40	40
Surge effect	No	Constant 1 m	Time varying water level (from measurements), but constant over 100 m grid.
Wind	Yes	Yes	Yes

The third-generation mode respect to wind-input, quadruplet interactions and whitecapping was used. For wind-input and whitecapping dissipation, the formulation by [24] was used; in case of wind-input, both the linear and exponential growth term was activated. Triads, bottom friction and depth-induced breaking were also activated. The quadruplet interaction was approximated using the Discrete Interaction Approximation (DIA). The breaking of waves is controlled by the ratio of maximum individual wave height over depth and is set to be 0.73.

*SWASH*. We use only one-dimensional mode of SWASH for practical purposes. The elevation data of Pärnu city in digital format is not yet available and the digitalization of the whole coastal terrain is pointless, as the digital data becomes available soon. Secondly, 1D configuration allows greater confidence in interpreting results.

The model gets its boundary condition in terms of significant wave height and peak period from the most nested SWAN run. The direction of wave propagation and the 1 D profile matches, as does the water depth in 1 D profile forcing boundary and in the grid point, where wave parameters are extracted from SWAN. The boundary condition is acquired at time instant, when significant wave height is greatest (considering the whole modeling period). The profile was constructed so that the forcing boundary extends out from the breaking zone.

The model is run in non-hydrostatic and depth-averaged mode, with the advection approximation being strictly momentum conservative. 1 m grid resolution and 0.02 s time step was used. Breaking is activated and the coefficient for breaking is 0.6. Bottom friction formulation is due to Manning with a friction coefficient of 0.019. Model is run to spin up 1.5 hours and the set-up and wave height values are extracted from the last five minutes of the calculation.

### III. RESULTS AND DISCUSSION

#### A. Accuracy of modeled wind field

To test the accuracy of the modeled wind field in the Baltic Proper we compare it with measurements taken at Vilsandi weather station (see Fig. 1) and with some instantaneous measurement values of other weather stations (Ruhnu, Kihnu, Sõrve; Fig. 1). All of the stations are fully open to marine wind directions and therefore well reflect the meteorological regime of the Baltic Proper and Gulf of Riga. To get the impression of how strong and uniform the wind was, consider a snapshot at 03:00 UTC, when

modeled wind reached its maximum of 25 m/s over the Gulf of Riga (Fig. 4). Note that the wind speed reduction near western side of Baltic Proper is due to shedding by land, but at the eastern side this is probably related to spurious interpolation. Nonetheless, this will not impact the wave field.

The modeled wind speed at Vilsandi results higher compared with measurements during first 8 hours of measurements (Fig. 5). However, this small overestimation will not affect wave fields in the morning of 9 January due to short “memory” time of waves and due to fact that much more energy is transferred to wave field during the passage of Gudrun.

The average measured wind (10 min averages prior to time) peaked 22.9 m/s at 04:00 (9 January) and the modeled wind peaked at 03:00. The model does not capture the sudden drop in wind speed in the evening of 8 January. This drop is most probably caused by the income of a warm front and after the warm front has left the wind speed will increase again. There may be several reasons for the model not capturing the drop, one of them the 3 h time resolution. Prior to the maximum surge event the model represents very well wind direction, with root-mean square difference of only 7°. Correlation between modeled and measured wind is 0.95. About 6 hours after the maximum surge the measured wind turns faster compared with model. This fact combined with the overestimation of wind speed by the model after the maximum surge suggests that the simulated cyclone is moving slower compared to measurements.

Further evidence of the accuracy of wind field in the Baltic Proper is that measured significant wave height was 7.2 m at FIMR measurement station (Fig. 1) at 03:00 UTC [6] and modeled value was 7.03 m in this study.

Considering the Gulf of Riga, in Sörve the sustained maximum wind speed reached 28 m/s at 09:00 UTC, and the model predicted 22 m/s, while in Ruhnu the measured maximum was 26 m/s (at 06:00 UTC) and model predicted 24 m/s. In Kihnu the values were 25.2 m/s and 21 m/s, for measurements and model at 03:00 UTC, respectively. This demonstrates that in the Gulf of Riga the wind speed definitely was not overestimated. Overall, the modeled wind well matches the measured ones prior to the maximum wind induced surge and it is justified to use this wind as a representation of meteorological situation at that time.

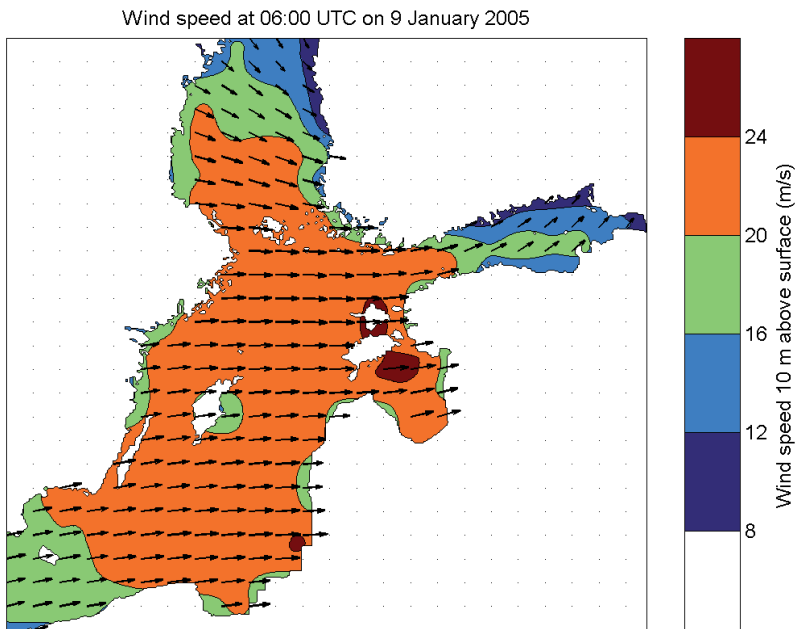


Fig. 4. Snapshot of model input wind. Every 20<sup>th</sup> vector is plotted.

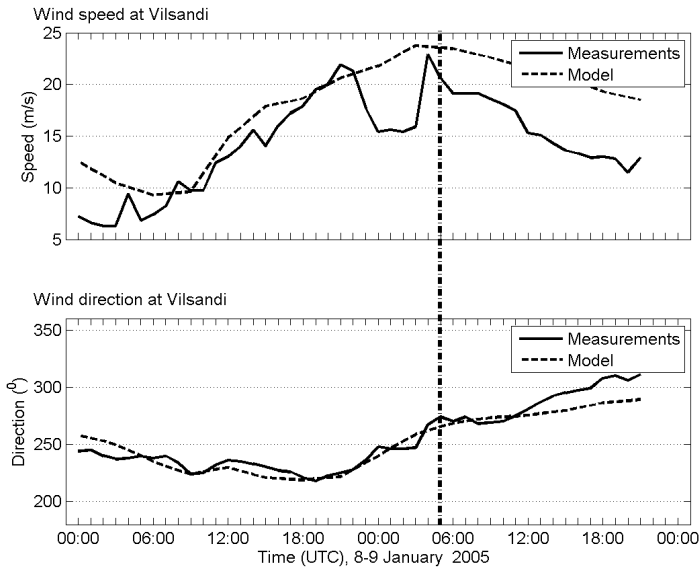


Fig. 5. Model-data comparison of wind speeds and directions. Dashed vertical line marks the timing of maximum surge in Pärnu Bay.

### B. Wave conditions

Cyclone Gudrun excited probably the hardest wave conditions in Baltic Sea during recent history. Significant wave height reached 9.13 m at 03:00 UTC in the southern Baltic Proper and was over 7 m in the entire eastern Baltic Proper. In the Gulf of Riga maximum significant wave height peaked just over 5 m at 06:00 UTC, and basically the entire basin had significant wave height over 4 m. Under these wind conditions the Gulf was both depth and fetch limited. Although not shown here, the near bottom orbital velocity was over 20 cm/s in 75 % of the basin, thus resuspending most of the sandy and soft bottoms of the Gulf.

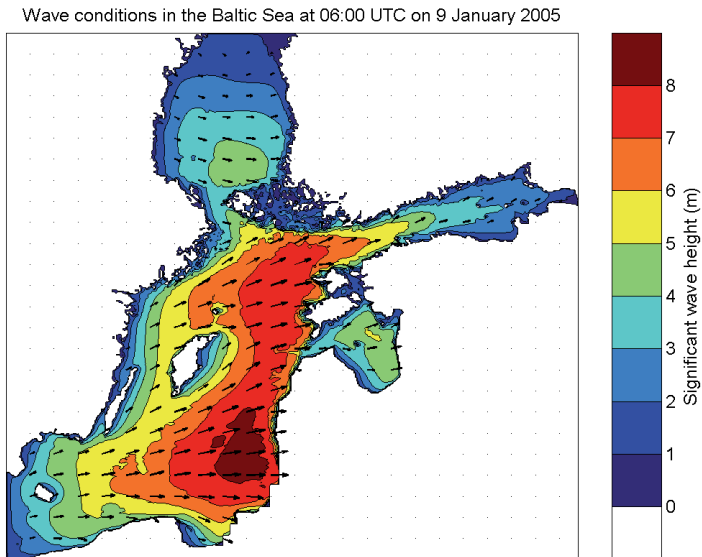


Fig. 6. Snapshot of modeled significant wave height. Every 20<sup>th</sup> vector is plotted.

### C. Surge impacting wave fields

A time-series comparison of significant wave height calculated with and without surge reveals the dependence of significant wave height of surge height and growth stage (Fig. 7). It should be noted that the time-series represents output in a coordinate, which provides initial conditions for further modeling of wave set-up. The difference is less than 5 cm when surge and waves are smaller than 1 m and wind speed below 10 m/s. It implies that for practical purposes in normal weather conditions the coupled model is not necessary. However, as waves and surge grow, the difference peaks at 0.4 m. During that period, the difference in significant wave height shows large variability in the small bay (Fig. 8c). At the entrance where water is deeper than 10 m significant wave height “grows” (e.g. dissipates less due to bottom friction and depth induced breaking) up to 0.3 m when the surge is considered, while adjacent coastal areas face wave height increase nearly 1 m; near Pärnu city wave height increases also up to 1 m.

The results of this study are comparable with research done by [25] who studied the impacts of Hurricane Hugo passing over Charleston harbor in 1989. Pre landfall the storm surge was 1 m and when this was taken into account in significant wave height modeling, it had additional 0.3 m in water depths less than 4 m. During the landfall, simulated offshore significant wave height was 3 m, storm surge 2.5 m and additional significant wave height up to 1 m.

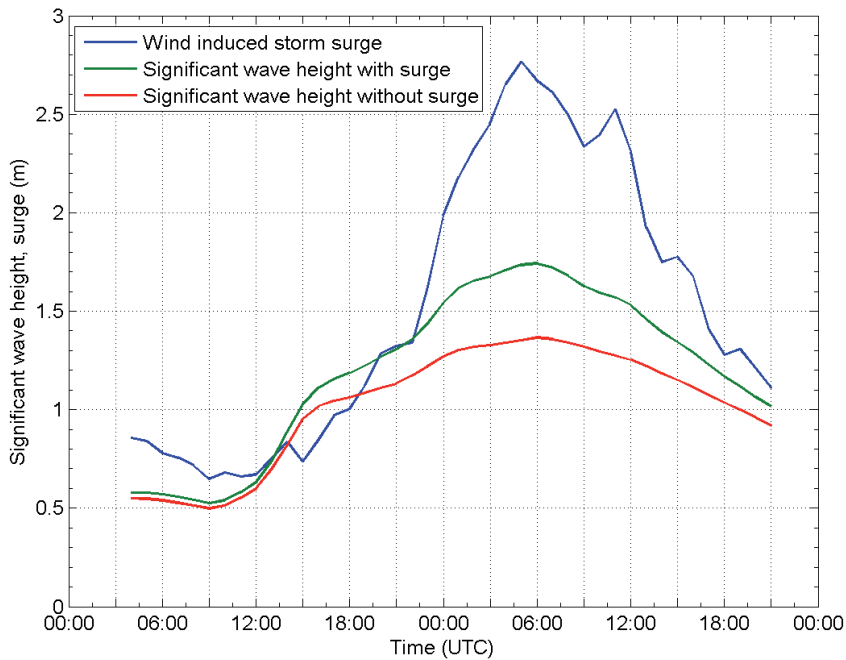


Fig. 7. Evolution of water level (measurements) and modeled significant wave height near Pärnu city during cyclone. Location where significant wave height is extracted is shown on Fig. 8b

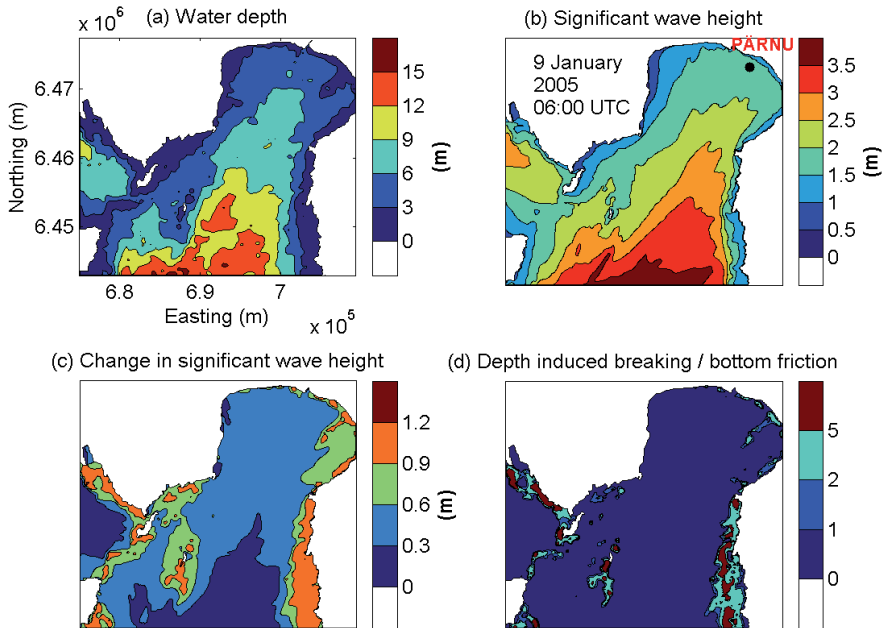


Fig. 8. (a) Bottom topography (without surge), (b) significant wave height (at peak surge), (c) significant wave height with peak surge minus significant wave height without surge, (d) depth induced breaking dissipation divided by bottom friction dissipation (when peak surge is taken into account). b,c and d are snapshots at 06:00 UTC. Black dot on panel b represents the point, where time-series from previous figure is extracted. It also donates the forcing boundary to SWASH model.

#### D. Wave induced set-up

Fig. 8d suggests that in Pärnu Bay the largest wave induced set-ups are concentrated not to bay head, but on the sides, where high waves undergo rapid refraction and following depth induced breaking. The set-up depends not only on the significant wave height prior breaking, but on the gradient of dissipation as well. In areas where friction dominates over breaking, the gradient is small. Intense wave breaking together with high significant wave height over 2 m could exert high set-up at Sorgu Island in the middle of the Pärnu Bay (barely visible on Fig. 8). It is a small (500\*150 m) low-laying island, with typical elevations less than 3.5 m. Although it is not habited, it is a nice recreational area and under environmental protection. The island makes a perfect example why such a high resolution (100 m) grid is necessary in coastal areas - the island is not resolved on the 400 m grid anymore. However, further modeling studies should implement unstructured grids, which avoid the impracticalities of nesting.

Moving to Pärnu city beach, the transformation of sea state with initial conditions 1.8 m significant wave height and 5.2 s peak period is shown on Fig. 9. This represents the time moment, when peak surge and highest significant wave height occurred almost simultaneously. Significant wave height follows the bottom profile very well, with weak dissipation in waters deeper than 6 m. Over the first 2500 meters wave height reduces 0.4 m. Afterwards follows a climb on a slope, in which shoaling commences. When water depth reaches 2.5 m, breaking becomes dominant mechanism and over the course of next 700 m wave height decreases 1.4 m. This results in a 0.51 m maximum setup. The inundation due to static setup is 130 m, as indicated by slope colored red. The preceding water level rise due to surge caused 600 m of inundation, colored blue on Fig. 9a.

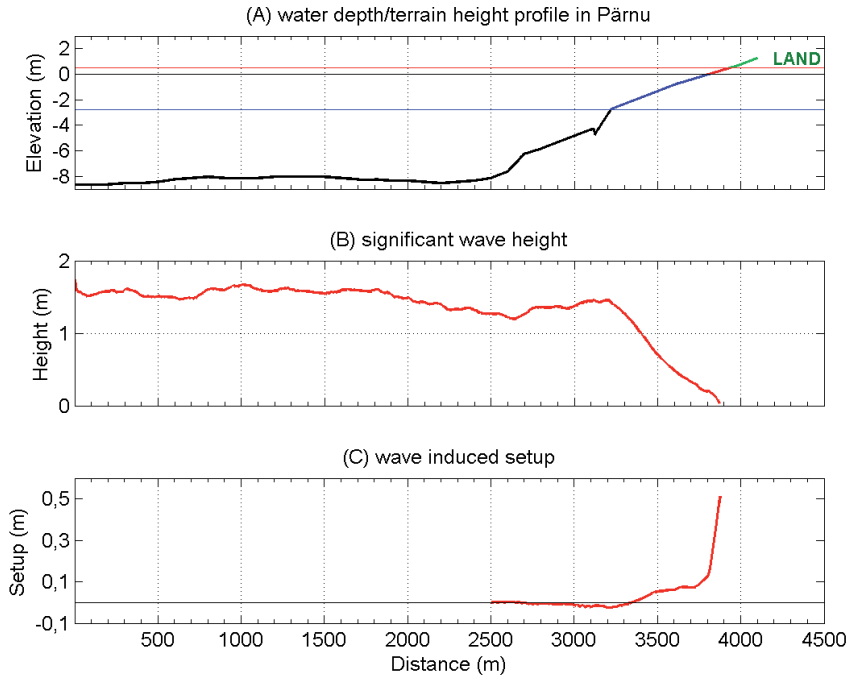


Fig. 9. Wave transformation near coast. Red slope on (a) is inundated area due to wave set-up and blue is due to surge.

#### E. Future modeling

In Pärnu bay the possible water level increase due to climate change will be balanced by the post-glacial land uplift. However, studies indicate the declining trends of sea ice days in the study area. In Kihnu the number of days covered by ice has declined up to 70 days compared to situation in 1950s [26]. At the same time the percentages of W and SW winds have clear positive trends, while SE, E and NE winds are characterized by negative tendencies in winter [27]. If these trends would continue in future, the probability of high surges and waves in Pärnu bay would also increase. Taking that for granted, and considering capabilities of modern models and modeling power, tightly coupled air-wave-surge models should be used in Baltic Sea for forecast and hindcast purposes.

### IV. CONCLUSION

We studied wave-surge interaction and wave induced set-up in Pärnu bay during the passage of a severe cyclone (Gudrun, 8-9 January 2005), by implementing a spectral wave model and a non-hydrostatic circulation model. The validity of input wind was analyzed, since model results depend profoundly on the quality of forcing fields.

Modeled wind direction showed good timing ( $R=0.93$ ) and overlay ( $RMSE=7^0$ ) with observations, then again wind speed in the Gulf of Riga was 2-3 m/s lower compared with some measurements. Due to the fetch, duration and depth limited conditions of wave growth during the storm, a small underestimation of wind has marginal effect on the wave field. We conclude an overall good level of agreement between downscaled ERA40 winds and observations and suggest using it in further modeling studies. To even more minimize the uncertainty of wind field quality at severe weather, following studies should make use of the Synthetic Aperture Radar technology.

Significant wave height in Pärnu bay increases by taking into account the additional deepening of water due to surge. The additional significant wave height is correlated with water depth at the time of the maximum surge. Wave height increases less than 0.3 m in areas where water is deeper than 10 m, but up to 1 m when water is shallower than 5 m. During low surge (less than 1 m) wave height increase is not so profound. In order to accurately describe hydrodynamic processes and resulting sediment transport in coastal zone, coupled wave-surge interaction is essential at high energy conditions.

The transformation of sea state with initial conditions 1.8 m significant wave height and 5.2 s peak period over the swash zone results in wave induced setup of 0.51 m and additional inundation of 130 m. It is essential to study the wave induced set-up in Pärnu Bay further and if necessary, implement this physical forcing in regional sea level forecasting system.

#### ACKNOWLEDGMENT

We are grateful to Estonian Meteorological and Hydrological Institute for providing the wind data from Vilsandi weather station and for Estonian Land Board for providing the flooding map. This study was supported by grant 8968 funded by the Estonian Science Foundation.

#### REFERENCES

- [1] Suursaar, Ü., Kullas, T., Otsmann, M., Kõuts, T. 2003: Extreme sea level events in the coastal waters of western Estonia. *Journal of Sea Research*, 331, 1 – 9.
- [2] Wisniewski, B., Wolski, T. 2011. Physical aspects of extreme storm surges and falls on the Polish coast. *Oceanologia*, 53 (1-TI), 373–390.
- [3] Averkjev, A.S., Klevanny, K.A. 2010. A case study of the impact of cyclonic trajectories on sea-level extremes in the Gulf of Finland. *Continental Shelf Research*, 30, 707–714.
- [4] Suursaar, Ü., Kullas, T., Otsmann, M., Saaremäe, I., Kuik, J., Merilain, M. 2006. Cyclone Gudrun in January 2005 and modelling its hydrodynamic consequences in the Estonian coastal waters. *Boreal Environment Research*, 11, 143-149.
- [5] Tõnisson, H., Orviku, K., Jaagus, J., Suursaar, Ü., Kont, A., Ravis, R. 2008. Coastal damages on Saaremaa Island, Estonia, caused by the extreme storm and flooding on January 9, 2005. *Journal of Coastal Research*, 24(3), 602 - 614.
- [6] Soomere, T., Behrens, A., Tuomi, L., Nielsen, J.W. 2008. Wave conditions in the Baltic Proper and in the Gulf of Finland during windstorm Gudrun. *Natural Hazards and Earth System Sciences*, 8(1), 37 - 46.
- [7] Longuet-Higgins, M.S., and R.W. Stewart, R.W. 1963. A note on wave set-up. *Journal of Marine Research*, 21, 4.
- [8] Longuet-Higgins, M.S., and R.W. Stewart, R.W. 1964. Radiation stresses in water waves; a physical discussion, with applications. *Deep-Sea Research*, 11, 529–562.
- [9] Saville, T. 1961. Experimental determination of wave set-up. *Proc. 2nd Technical Conf. on Hurricanes, Beach Erosion Board*.
- [10] Bowen, A.J., Inman, D.L., Simmons, V.P. 1968. Wave setdown and wave setup. *Journal of Geophysical Research*, 73, 2569–2577.
- [11] Bowen, A.J. 1969. Rip currents, I: theoretical investigations. *Journal of Geophysical Research*. 74, 5468–5478.
- [12] Guza, R.T., Thornton, E.B. 1981. Wave setup on a natural beach. *Journal of Geophysical Research*, 86, 4133–4137.
- [13] Holman, R.A., Sallenger, A.H. 1985. Set-up and swash on a natural beach. *Journal of Geophysical Research*, 90, 945–953.
- [14] Hanslow, D., Nielsen, P. 1993. Shoreline set-up on natural beaches. *Journal of Coastal Research*, 15, 1–10.
- [15] Lentz, S., Raubenheimer, B. 1999. Field observations of wave setup. *Journal of Geophysical Research*, 104, 25,867–25,875.
- [16] Kim, S.Y., Yasuda, T., Mase, H. 2010. Wave set-up in the storm surge along open coasts during Typhoon Anita. *Coastal Engineering*, 57, 631–642.
- [17] Malhadas, M.S., Leitão, P.C., Neves, A.S.R. 2009. Effect of coastal waves on sea level in Óbidos Lagoon, Portugal. *Continental Shelf Research*, 29(9), 1240-1250.
- [18] Wolf, J. 2008. Coupled wave and surge modeling and implications for coastal flooding. *Advances in Geosciences*, 17, 19-22.
- [19] Booij, N., Ris, R.C., Holthuijsen, L.H. 1999. A third – generation wave model for coastal regions. I. Model description and validation. *Journal of Geophysical Research*, C104, 7649 – 7666.
- [20] Raudsepp, U., Laanemets, J., Haran, G., Alari, V., Pavelson, J., Kõuts, T. 2011. Flow, waves and water exchange in the Suur Strait, Gulf of Riga, in 2008. *Oceanologia*, 53(1), 35–56.
- [21] Zijlema, M., Stelling, G., Smit, P. 2011. SWASH: An operational public domain code for simulating wave fields and rapidly varied flows in coastal waters. *Coastal Engineering*, 58, 992-1012.
- [22] Seifert, T., Kayser, B., and Tauber F., 2001. *Bathymetry data of the Baltic Sea*. Baltic Sea Research Institute, Warnemünde.
- [23] Lagema, P., Elken, J., Kõuts, T. 2011. Operational sea level forecasting in Estonia. *Estonian Journal of Engineering*, 17(4), 301–331.
- [24] Van der Westhuysen A.J., Zijlema M., Battjes J.A., 2007, *Nonlinear saturation-based whitewashing dissipation in SWAN for deep and shallow water*. Coastal Engineering, 54, 151–170.
- [25] Liu, H., Xie, L. A numerical study on the effects of wave–current–surge interactions on the height and propagation of sea surface waves in Charleston Harbor during Hurricane Hugo 1989. *Continental Shelf Research*, 29, 1454–1463
- [26] Jaagus, J. 2006. Trends in sea ice conditions in the Baltic Sea near the Estonian coast during the period 1949/1950-2003/2004 and their relationships to large-scale atmospheric circulation. *Boreal Environment Research*, 11, 169-183.
- [27] Jaagus, J., Kull, A. 2011. Changes in surface wind directions in Estonia during 1966-2008 and their relationships with large-scale atmospheric circulation. *Estonian Journal of Earth Sciences*, 60(4), 220-231.

## **Paper II**

Alari, V., Raudsepp, U. 2012. Simulation of wave damping near coast due to offshore wind farms. *Journal of Coastal Research*, 28 (1), pp. 143-148.



# Simulation of Wave Damping Near Coast due to Offshore Wind Farms

Victor Alari and Urmas Raudsepp

Marine Systems Institute  
Tallinn University of Technology  
12618 Akadeemia tee 15a  
Tallinn, Estonia  
victor.alari@phys.sea.ee



www.cerf-jcr.org

## ABSTRACT

ALARI, V. and RAUDSEPP, U., 0000. Simulation of wave damping near coast due to offshore wind farms. *Journal of Coastal Research*, 00(0), 000-000. West Palm Beach (Florida), ISSN 0749-0208.

Two hundred wind turbines with an annual productivity of 2.3 TWh, which could produce up to 30% of the energy Estonia needs, are scheduled to be constructed on separate shallows in the NW Estonian coastal waters (the Baltic Sea), 5–20 km off shore. With numerical modeling, we have established a potential impact of the wind farms on wave heights. We concluded that the impact exists in terms of the reduction of significant wave height, but it is very marginal, not more than 1% below 10-m isobaths. This is due to a very small ratio between the turbine diameter and dominant wavelength and the favorable setup of turbines with respect to each other and the coast.

**ADDITIONAL INDEX WORDS:** *wind turbines, wave damping, SWAN, Baltic Sea.*



## INTRODUCTION

The ever growing need for energy and the decreasing availability of nonrenewable energy sources has put the use of alternative energy sources at the forefront. Apart from nuclear energy, which now generates 6.5% of world's energy, renewable energy—solar, geothermal, water, wind, and biomass—is steadily increasing, now generating up to 13.1% of global energy consumption (IEA, 2007). As renewable energy supplies increase, we begin to look not only toward the increasing need for energy, but toward the reduction of environmental effects as well; climate change due to excess CO<sub>2</sub> is a well-documented fact (IPCC, 2007).

In Estonia (Figure 1) up to 5.1% of energy will be produced from renewable energy sources by the end of 2010 (European Commission, 2007). This number will grow in the future, since nearly 200 wind turbines are scheduled to be installed in the shallows near Hiiumaa. The total power of these arrays would be 600–1000 MW, and the productivity 2.3–2.5 TWh/year (Nelja Energia, 2010). This is about 30% of the total Estonian electricity requirement, maximally. In comparison, in the leading wind energy country, Denmark, only 19.7% of the domestic need is covered by wind energy (Danish Energy Agency, 2007). In addition to the aforementioned 200 turbines, which will most likely be installed in coming years, another 500 MW of arrays could be installed in some shallows in the coastal waters of the northern Estonia as well (Erm *et al.*, 2009).

Every structure that is installed in water will affect the wave

and circulation regime and the sediment transport. There are plenty of studies published in scientific literature assessing the importance of scour. Only a handful of studies assess the impact of wind turbines or wave farms upon surface waves near the coast (CEFAS, 2005; DHI Water and Environment, 2007; Millar, Smith, and Reeve, 2007). In scientific papers, however, no studies are published that assess the importance of the whole array of wind turbines upon wind waves. The purpose of this study is to quantify the effect of these structures on wind waves, which propagate toward the coast. The main aim is to find out how much these structures will absorb and scatter wave energy.

Wind farms are scheduled to be installed in the coastal waters of Estonia near Hiiumaa, the NE Baltic Sea. Basically, when planning offshore wind farms, they should be located some distance away from the shore to reduce the effect on land. Construction costs can be reduced if an offshore wind farm is located in shallows. Water is relatively deep off the coast of Hiiumaa, but there are several shallows where water depth is less than 20 m.

This study focuses on two locations—wind farm 1, situated WSW from the Kõpu Peninsula (Figure 1), and wind farm 2, situated NW from Hiiumaa (Figure 1). Coastal areas that could be affected are the head of Kõpu Peninsula (where the so-called surf paradise is located) and the northern coast of Hiiumaa. At wind farm 1, 55 turbines will be installed in parallel rows with a minimum distance of 1000 m from each other. The closest turbines at the wind farm 1 will be 5 km from the coast (the head of Kõpu Peninsula) and the farthest ones 15 km from the coast of the Kõpu Peninsula. The nearest coast from wind farm 2 is the western part of Tahkuna Peninsula, which is 13 km to the SE. The northern coast of the Kõpu Peninsula directly south of the wind farm 2 is 20 km away.

DOI: 10.2112/JCOASTRES-D-10-00054.1 received 26 March 2010; accepted in revision 23 September 2010.

Published Pre-print online 3 December 2010.

© Coastal Education & Research Foundation 2010

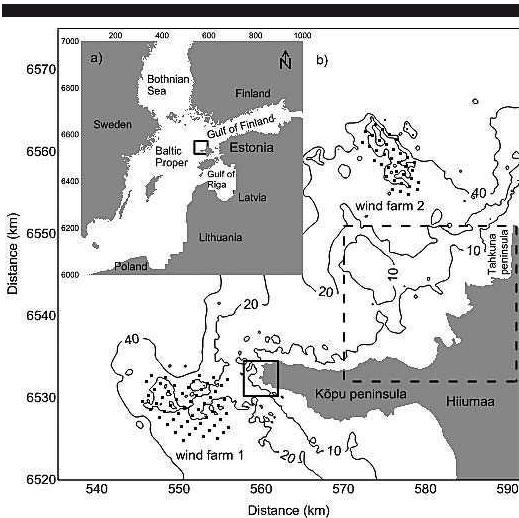


Figure 1. (a) The Baltic Sea, its subbasins and countries residing. The black box is the boundary of Figure 1b. Note that (a) represents the 2000-m grid as well. North up; (b) A detailed location of the wind farms. The black continuous box represents the impact area of wind farm 1 and the dashed black box represents the impact area of wind farm 2. The contour levels are the water depth in meters. Every black-filled circle represents a wind turbine. North up.

In Section 2 the model is described, set up, and validated. Main findings are presented and discussed in Section 3; key conclusions are outlined in Section 4.

## METHODS

### Model Description

The Simulating Waves Nearshore (SWAN) model is used to assess a potential effect of wind farms upon wave heights. SWAN is a third-generation phase averaged spectral wave model developed at the Delft University of Technology, the Netherlands (Booij, Ris, and Holthuijsen, 1999). In SWAN, waves are described with a two-dimensional wave action density spectrum, whereas the evolution of the action density,  $N$ , is governed by the time-dependent wave action balance equation, which in Cartesian coordinates reads

$$\frac{\partial N}{\partial t} + (\bar{c}_g + \bar{U}) \cdot \nabla N + \frac{\partial c_\sigma N}{\partial \sigma} + \frac{\partial c_\theta N}{\partial \theta} = \frac{S_{\text{tot}}}{\sigma}. \quad (1)$$

The first term represents the local rate of change in action density; the second term denotes the propagation of wave energy in the two-dimensional geographical space with  $\bar{c}_g$  the group velocity, and  $\bar{U}$  the ambient current. The third term represents the effect of shifting the relative frequency due to variations in depth and mean currents. The fourth term represents the depth-induced and current-induced refraction. The quantities  $c_\sigma$  and  $c_\theta$  are the propagation velocities in spectral space ( $\sigma$ ,  $\theta$ ), with  $\sigma$  and  $\theta$  representing the relative

frequency and the direction of propagation, respectively. The right-hand side contains the source term  $S_{\text{tot}}$  that represents all physical processes that generate, dissipate, or redistribute wave energy. In shallow water, six processes contribute to  $S_{\text{tot}}$

$$S_{\text{tot}} = S_{\text{wind}} + S_{n13} + S_{n14} + S_{\text{wc}} + S_{\text{bot}} + S_{\text{db}}. \quad (2)$$

These terms denote, respectively, the energy input by wind ( $S_{\text{wind}}$ ), the nonlinear transfer of wave energy through three-wave ( $S_{n13}$ ) and four-wave interactions ( $S_{n14}$ ), and the dissipation of waves due to white-capping ( $S_{\text{wc}}$ ), bottom friction ( $S_{\text{bot}}$ ), and depth-induced wave breaking ( $S_{\text{db}}$ ).

### Model Setup

The model (version 40.72) was run in the third-generation mode with the saturation-based whitecapping model, which estimates the whitecapping of wind sea locally in the wave spectrum and therefore gives realistic estimates of peak periods (Van der Westhuysen, Zijlema, and Battjes, 2007). In every model run, 40 frequencies distributed logarithmically in the range of 0.05–1 Hz were used and 24 spectral directions were included. The diffraction was activated only when the highest spatial resolution was used.

Steady wind speeds of 8 m/s and 15 m/s were selected. The first value is the annual average wind speed offshore (Soomere, 2003), while the second represents strong wind events that occur at least once per month in autumn and spring (Soomere and Keevallik, 2003). All presented wave fields are saturated. In the case of wind farm 1 winds from the SW and west were selected. The head of the Kõpu Peninsula is located NE from wind farm 1. Thus, waves generated by winds blowing from the north, east, and south do not propagate toward the coast. Even the waves coming from the NW do not make landfall at the head of the Kõpu Peninsula.

Wind farm 2 is orientated so that the waves from the north and NW could reach the coasts of Hiiumaa. Thus, the impact of wind farm 2 is assessed for winds blowing from those directions.

The modeling of waves at wind farm 1 has been carried out using five consequently nested models. First the whole Baltic Sea with a 2000-m resolution is modeled. With the boundary conditions from the previous model, waters surrounding Hiiumaa are modeled with a 400-m resolution, and then 100, 50, and 25 m. The same scheme applies also for wind farm 2, but the highest model resolution is 50 m, not 25 m. The details of the grids are listed in Tables 1, 2, and the coarsest model boundaries visualized in Figure 1.

The Baltic Sea bottom topography by Seifert, Kayser, and Tauber (2001) and the marine charts provided by the Estonian Maritime Administration were used to create the model topographies. The model grids are all Cartesian, and the coordinate system used is Universal Transverse Mercator (UTM-34). The scattered data were interpolated to the model grid. The land mass of Hiiumaa was blanked using a digitized coastline that was extracted from Google Earth. Water depths lower than 0.1 m were replaced with a value of 0.1 m. In the case of the 2000-m model, some small bays in the southern Baltic Sea were artificially masked to reduce the model calculation time. It has no effect on the wave heights near

Table 1. The location of the origin of the computational grid, number of meshes of the computational grid, mesh sizes of the computational grid for wind farm 1 impact calculations.

	2000 m	400 m	100 m	50 m	25 m
Location of origin of $x$ direction (km)	50	524	535.2	541	543
Location of origin of $y$ direction (km)	6000	6500	6510	6521	6524
No. meshes in $x$ direction	475	140	348	420	760
No. meshes in $y$ direction	500	150	400	380	480

Hiiuuaa. Model bathymetry was smoothed at the boundaries of nested model grids to avoid spurious waves.

For every forcing situation, two calculations are made—first without farms and second with farms. For every wind turbine, the closest point is located in the grid and the value at that grid point is replaced with 0, *e.g.*, it is represented as land. In SWAN the land absorbs all incoming wave energy. Here we assess the changes in significant wave height. Let  $Hs_1$  be the calculation made without farms and  $Hs_2$  be the calculations with farms in nodes  $(i, j)$ . The impact is defined

$$\Delta Hs(i, j) = \frac{Hs_2(i, j) - Hs_1(i, j)}{Hs_1(i, j)} \times 100\%. \quad (3)$$

If  $\Delta Hs(i, j) < 0$ , the impact is in terms of reduction, and when  $\Delta Hs(i, j) > 0$ , it shows an increase. The diameter of the windmill structure (monopile) is not more than 5 m in reality. Assuming a linear dependence between the differences of calculated height, in the case of a 25-m grid step, the results obtained with Eq. 3 are divided by a factor of 5, and in the case of a 50-m grid size, results are divided by a factor of 10.

### Model Validation

Subsurface pressure sensors were deployed in the locations of wind farms 1 and 2 in the summer of 2007. Although the pressure gauges remained in the water for 23 days, the first 10 days were selected for the comparison. The second half of the measurements displayed a very low wave activity. Subsurface pressure was converted to surface spectra using the method described by Alari, Raudsepp, and Kõuts (2008).

The model was forced with high-resolution limited area model (HIRLAM) wind fields (resolutions  $1' \times 1.6'$  in latitudes and longitudes respectively). During the verification period, wind speed did not exceed 12–13 m/s and wind blew mainly from the SW–west.

The temporal variability of the measured significant wave heights and peak periods are similar at both locations (Figures 2 and 3). The mean significant wave height and the mean peak period were greater at wind farm 1 compared with wind farm 2 (Table 3). The waves generated by the SW winds refract around the Kõpu Peninsula and lose energy. It results

Table 2. Same as Table 1 but for wind farm 2 impact calculations. The 2000-m grid has the same setup as described in Table 1.

	400 m	100 m	50 m
Location of origin of $x$ direction (km)	560	566.4	570
Location of origin of $y$ direction (km)	6532	6532	6532
No. meshes in $x$ direction	90	256	420
No. meshes in $y$ direction	110	380	700

in a lower significant wave height and peak period at wind farm 2 compared with the location of wind farm 1. The simulated significant wave height matches the measurements equally well at both locations. The root mean square errors (RMSEs) are 0.2 m and 0.23 m, respectively, but the scatter in terms of height is smaller at wind farm 1 (Table 3). There are time slices when significant wave height is better represented at one location than at the other. The timing of period is somewhat better represented at wind farm 2, but the scatter is basically the same for both sites. Usually, the model fails to reproduce peak periods in both locations synchronously.

## RESULTS AND DISCUSSION

It is helpful to recognize significant wave height and wavelength in the vicinity of wind turbines prior to the construction. Since the field distribution of the parameters are quite homogenous at the wind farm areas, the results are summarized in Tables 4 and 5, instead of in figures.

For wind farm 1, although there is a fourfold increase of wave heights in the case of doubled wind speeds and a linear increase of wave period, the  $45^\circ$  turn of the wind does not change the parameters at any significant level. For the SW wind, significant wave height is greater only by 0.2 m compared with the west wind at wind farm 1. The peak period is only 0.4 seconds greater. The resulting wavelengths display the same variability. Since the fetch length for the west winds is 250 km and for the SW winds 650 km, almost the same

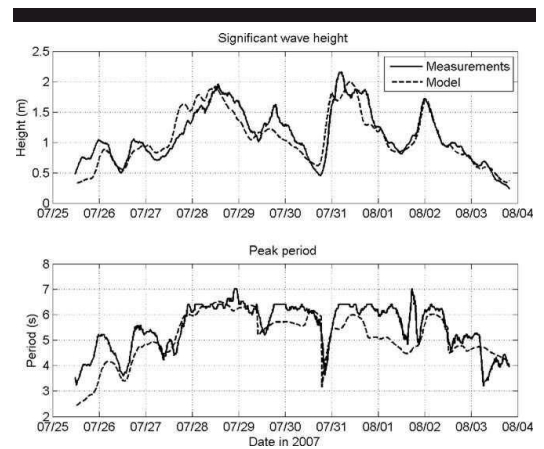


Figure 2. Model-data comparison at the location of wind farm 1.

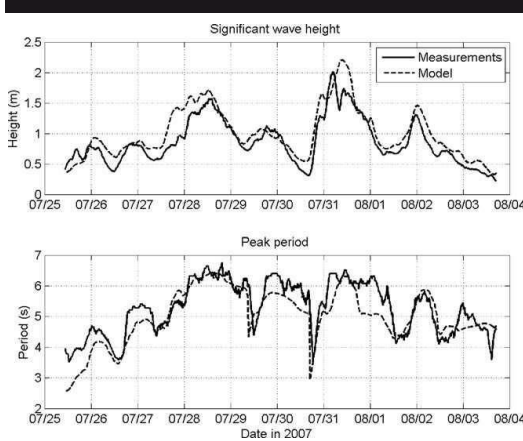


Figure 3. Model-data comparison at the location of wind farm 2.

variability means that the wave field is already full developed at 250 km.

At wind farm 2, the turning of wind from the NW to the north reduces significant wave height up to 0.5 m and peak period up to 1 second. The NW wind generates higher waves since the fetch is longer. However, compared with the wave parameters at wind farm 1, the modeled values of wave parameters are lower at wind farm 2. This is expected since the fetch length is lower in case of wind farm 2.

As an illustration, a field distribution of significant wave heights in the case of 15 m/s, the SW winds are presented in Figure 4. The variability on significant wave heights and wavelengths at the farm locations suggests that dissipation due to bottom friction occur in areas where significant wave height is lower than the mean value, but where wavelengths stay at the mean value. In places where significant wave height is greater than the mean value and wavelengths shorter than the mean value, shoaling exceeds dissipation. The 15 m/s wind induces greater dissipation and shoaling compared with the 8 m/s wind.

In terms of significant wave height, the absolute reduction near the coast due to the wind farm 1 is not more than 2%

Table 3. The statistics of the validation of the wave model. R is the correlation coefficient, scatter index (SI) is defined as the ratio between RMSE and the mean of measurements.

	Wind farm 1	Wind farm 2
Water depth (m)	14	11
Data points	1350	1350
Hs mean (m)	1.12	0.86
Peak mean (s)	5.56	5.27
RMSE Hs (m)	0.2	0.23
RMSE Peak (s)	0.7	0.58
R Hs	0.88	0.9
R Peak	0.81	0.86
SI Hs	0.18	0.27
SI Peak	0.13	0.11

Table 4. Modeled wave parameters at the wind farm 1 location. Hs—significant wave height; Peak—peak wave period; Wlen—wavelength corresponding to peak wave period.

	SW 8 m/s	SW 15 m/s	West 8 m/s	West 15 m/s
Hs (m)	0.9–0.95	3.2–3.8	0.88–0.94	3–3.6
Peak (s)	4.7–4.8	8.5–8.7	4.7–4.8	8.1–8.3
Wlen (m)	33–36	75–110	32–35	70–100

(Figure 5). The 1% isoline is closer to the coast in the case of the 8 m/s wind compared with the 15 m/s wind. The difference in terms of significant wave height does not exceed 0.5 cm and 1 cm near the coast in the case of the 8 m/s and 15 m/s wind, respectively. In the case of the 15 m/s wind, the 1% reduction line coincides with the 10-m isobath. Compared with the impact of wind farm 1, the reduction of significant wave height due to wind farm 2 is even more marginal (Figure 6). The reduction is less than 0.25% below the 10-m isobath.

A very low impact is due to three factors. First, waves meeting an obstacle reflect and bend around it. Only large piles change the wave field considerably. Depending on an author (see, for example, Coastal Engineering Manual 2003), the diffraction and reflection are evaluated as significant for  $D/L > 0.1$  or  $D/L > 0.2$ , where  $D$  is the diameter of the monopile and  $L$  is the wavelength. In case of the 8 m/s wind, the ratio is between 0.1 and 0.2, and in case of the 15 m/s wind, it is between 0.05 and 0.08 (when the diameter is 5 m, wavelengths from Tables 4 and 5). Thus in our cases, diffraction and reflection are negligible. Second, the two turbines are not closer than 1 km to each other (at least 10 crests fit between) and therefore very little scatter occurs. And last, the wind turbines are distant from the coast (Figure 2).

A 25-m grid step might be a slight overkill for practical forecasts and hindcasts, and one might think that the results obtained with such a high resolution are not valid anymore, since the grid size is up to four times lower than the peak wavelength. However, when comparing the output, significant wave height, and wavelength with the output of the 100-m and 400-m grid, the results do not deviate (not illustrated here). The dissipation and shoaling is captured as well (of course, the 25-m grid shows more detail—Figure 4).

A question arises: is the linear scaling between 25 m to 5 m reliable? Do we get the same results with different scaling, say from between 100 m and 5 m? We also performed a numerical experiment with the 100-m grid, when the diameter of the turbine was 100 m. After scaling it down to 5 m, *e.g.*, dividing the impact by a factor of 20, we obtained the same result: in the case of the 15 m/s west wind, the reduction was 1% at 10-m isobath. However, the 100-m case displayed some 0.5% to 1%

Table 5. Modeled wave parameters at the wind farm 2 location. Hs—significant wave height; Peak—peak wave period; Wlen—wavelength corresponding to peak wave period.

	NW 8 m/s	NW 15 m/s	North 8 m/s	North 15 m/s
Hs (m)	0.85–0.9	2.8–3.2	0.82–0.84	2.5–2.7
Peak (s)	4.4–4.6	7.4–7.7	4.1–4.2	6.5–6.7
Wlen (m)	29–31	62–84	26–28	52–66

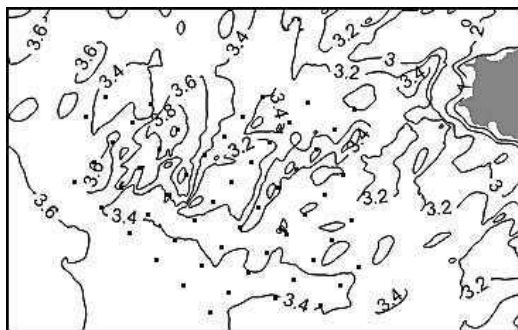


Figure 4. The field distribution of saturated wave field of significant wave height at wind farm 1. The contour unit is in meters. Every black-filled circle represents a wind turbine.

increase of the significant wave height grid point next to shore, which in reality might not exist.

The model results of this study are directly comparable with other findings from other researchers and consultancies. The loss in significant wave height due to Scorby Sands offshore wind farm was less than 2% (CEFAS, 2005). In the latter case a model that was based on an evolution equation solution to the mild slope equation for water waves was used. It differs from the spectral wave model. The model grid size in their experiment was 3 m. Millar, Smith, and Reeve (2005) used the SWAN model in order to assess the impact of a wave farm

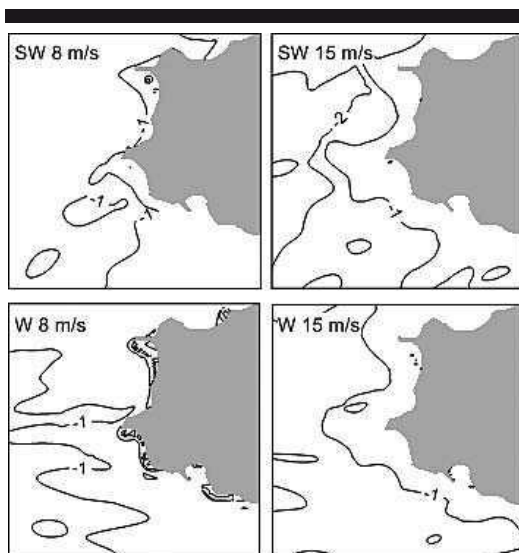


Figure 5. The impact of wind farm 1. The contour unit is [%] and a negative value shows a decrease of significant wave height.

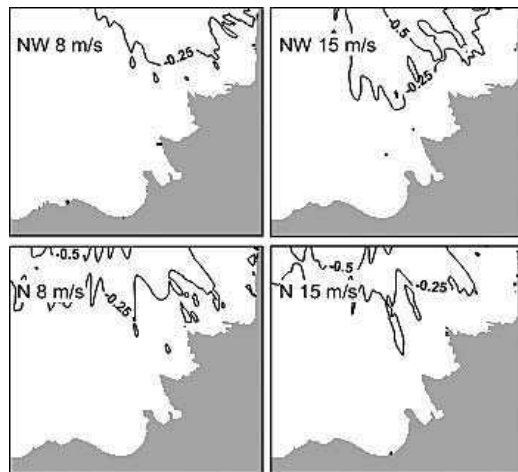


Figure 6. The impact of wind farm 2. The contour unit is [%] and a negative value shows a decrease of significant wave height.

upon wind waves. In their study the interaction of surface waves and wave farms were modeled using the so-called transmission coefficient. Applying a realistic transmission coefficient, the total reduction of significant wave height near the coast was less than 2 cm. The wave damping due to Rødsand offshore wind farm was less than 1% for higher waves (DHI Water and Environment, 2007). In the study made by DHI (2007), the energy loss was calculated with the integral wave model WAMIT for a single turbine. The impact of the whole array was further established with the spectral wave model MIKE 21 SW.

The shortcoming of this simulation study and of the ones mentioned in the latter paragraph lies in the assumption that wind farms do not alter wind speed. In general this is not true (Christiansen and Hasager, 2006). However, establishing the exact loss of wind speed in a wind farm in the present situation needs a detailed study, which is not in the scope of this paper. In our opinion the changes in the wave fields due to a 10% loss of wind behind the farm established by Christiansen and Hasager (2006) will be superposed by the nearshore wave transformation processes.

Also, we have to emphasize here that although the presence of wind farms has a negligible effect on the wave field, the presence of vertical piles in water motion induces von Karman vortex shedding behind the structure. This vortex shedding provides some disturbances in the water column, particularly at the sea bottom, and may induce substantial effects on the local benthic communities at sea bottom.

## CONCLUSIONS

A modeling study was undertaken in order to quantify the possible effects of offshore wind farms on the reduction of wave height near coast. The model was successfully verified against

the measurements at the locations where wind turbines would be installed. The impact of wind farms was assessed by calculating the ratio of difference of significant wave height with and without wind turbines to significant wave height without turbines. It is concluded that the reduction of significant wave height near the coast below 10-m isobaths does not exceed 1%. From a practical point of view, the developers of wind farms and the habitants/tourists on the coast should not be concerned.

### ACKNOWLEDGMENTS

This study was supported by the grants 7000 and 7283 funded by the Estonian Science Foundation and by the grant EMP53.

### LITERATURE CITED

- Alari, V.; Raudsepp, U., and Kõuts, T., 2008. Wind wave measurements and modelling in Küdema Bay, Estonian Archipelago Sea. *Journal of Marine Systems*, 74, S30–S40.
- Booij, N.; Ris, R.C., and Holthuijsen, L.H., 1999. A Third-Generation wave model for coastal regions. 1. Model description and validation. *Journal of Geophysical Research*, C104, 7649–7666.
- Christiansen, M.B. and Hasager, C.B., 2006. Using airborne and satellite SAR for wake mapping offshore. *Wind Energy*, 9(5), 437–455.
- Coastal Engineering Manual, 2003. Part VI, Chapter 5, pp. 242–245, Vicksburg, Mississippi: U.S. Army Corps of Engineers.
- Danish Energy Agency, 2007. *Energy Statistics 2007*. Copenhagen: Danish Energy Agency, 29p.
- CEFAS (Centre for Environment, Fisheries, and Aquaculture Science), 2005. Assessment of the significance of changes to the inshore wave regime as a consequence of an offshore wind array, project AE1227. Lowestoft, UK: CEFAS. <http://www.cefasc.co.uk/our-science/assessing-human-impacts/offshore-renewable-energy/assessment-of-the-significance-of-changes-to-the-inshore-wave-regime-as-a-consequence-of-an-offshore-wind-array.aspx> (accessed October 6, 2010).
- DHI Water and Environment, 2007. The effect of wind turbines on nearshore waves. Hørsholm, Denmark: DHI, 50p.
- Erm, A.; Alari, V.; Kõuts, T.; Lilover, M.-J.; and Kask, A., 2009. A pilot study of hydrodynamical and geological conditions at some possible offshore wind farms in Estonian coastal waters. In: *Proceedings of European Seminar: Offshore Wind and Other Marine Renewable Energies in Mediterranean and European Seas* (Brindisi, Italy, May 21–23), pp. 49–63.
- European Commission, 2007. Estonia—Renewable energy fact sheet. Brussels: European Commission, 3p [http://ec.europa.eu/energy/energy\\_policy/doc/factsheets/renewables/renewables\\_ee\\_en.pdf](http://ec.europa.eu/energy/energy_policy/doc/factsheets/renewables/renewables_ee_en.pdf) (accessed October 6, 2010).
- IPCC (Intergovernmental Panel on Climate Change), 2007. Climate change, a synthesis report. Core Writing Team, Pachauri, R.K. and Reisinger, A. (eds.). Geneva, Switzerland: IPCC, 104p.
- IEA (International Energy Agency), 2007. Renewables in global energy supply: An IEA fact sheet. Paris: OECD/IEA, 34 p.
- Millar, D.L.; Smith, H.C.M., and Reeve, D.E., 2007. Modelling analysis of the sensitivity of shoreline change to a wave farm. *Ocean Engineering*, 34, 884–901.
- Nelja Energia, 2010. Hiiumaa offshore wind farm. <http://www.4energia.ee/en/projects/hiiumaa-offshore-wind-farm/> (accessed October 6, 2010).
- Seifert, T.; Kayser, B., and Tauber F., 2001. *Bathymetry data of the Baltic Sea*. Warnemünde, Germany: Baltic Sea Research Institute.
- Soomere, T., 2003. Anisotropy of wind and wave regimes in the Baltic Proper. *Journal of Sea Research*, 49, 305–316.
- Soomere, T. and Keevallik, S., 2003. Directional and extreme wind properties in the Gulf of Finland. Proceedings of the Estonian Academy of Sciences, Engineering, 9, 73–90.
- Van der Westhuysen, A.J.; Zijlema, M., and Battjes, J.A. 2007. Nonlinear saturation-based whitecapping dissipation in SWAN for deep and shallow water. *Coastal Engineering*, 54, 151–170.

### **Paper III**

Raudsepp, U., Laanemets, J., Haran, G., Alari, V., Pavelson, J., Kõuts, T. 2011. Flow, waves and water exchange in the Suur strait, Gulf of Riga, in 2008. *Oceanologia*, 53 (1), pp. 35-56.



**Flow, waves and water  
exchange in the Suur  
Strait, Gulf of Riga, in  
2008\***

OCEANOLOGIA, 53 (1), 2011.  
pp. 35–56.

© 2011, by Institute of  
*Oceanology PAS.*

**KEYWORDS**

Flow  
Water exchange  
Waves  
Modelling  
Shear velocity  
Strait  
Baltic Sea

URMAS RAUDSEPP\*  
JAAN LAANEMETS  
GETLI HARAN  
VICTOR ALARI  
JUSS PAVELSON  
TARMO KÕUTS

Marine Systems Institute,  
Tallinn University of Technology,  
12618 Akadeemia 15a, Tallinn, Estonia;

e-mail: raudsepp@phys.sea.ee

\*corresponding author

Received 23 June 2010, revised 26 August 2010, accepted 23 November 2010.

**Abstract**

Wind, flow and wave measurements were performed in November–December in 2008 in the relatively narrow and shallow Suur Strait connecting the waters of the Väinameri and the Gulf of Riga. During the measurement period wind conditions were extremely variable, including a severe storm on 23 November. The flow speed along the strait varied between  $\pm 0.2 \text{ m s}^{-1}$ , except for the  $0.4 \text{ m s}^{-1}$  that occurred after the storm as a result of the sea level gradient. The mean and maximum

---

\* The work was partially supported by the Estonian Science Foundation (Grant 7283) and by the Estonian Road Administration project Perspective Development Plan for the Transportation of Passengers and Cargo across the Suur Strait and Strategic Environmental Impact Assessment.

The complete text of the paper is available at <http://www.iofan.gda.pl/oceanologia/>

significant wave heights were 0.53 m and 1.6 m respectively. Because of their longer fetch, southerly winds generated higher waves in the strait than winds from the north. All wave events caused by the stronger southerly winds induced sediment resuspension, whereas the current-induced shear velocity slightly exceeded the critical value for resuspension only when the current speed was  $0.4 \text{ m s}^{-1}$ . A triple-nested two-dimensional high resolution (100 m in the Suur Strait) circulation model and the SWAN wave model were used to simulate water exchange in 2008 and the wave-induced shear velocity field in the Suur Strait respectively. Circulation model simulations demonstrated that water exchange was highly variable, that cumulative transport followed an evident seasonal cycle, and that there was a gross annual outflow of  $23 \text{ km}^3$  from the Gulf of Riga. The horizontal distribution of wave-induced shear velocity during the strong southerly wind event indicated large shear velocities and substantial horizontal variability. The shear velocities were less than the critical value for resuspension in the deep area of the Suur Strait.

## 1. Introduction

Shallow and narrow straits play an important role in water and material exchange between the open sea and coastal water basins, lagoons and bays. In shallow straits wind forcing generates current and sea level differences between sub-basins, which in turn influences currents. Wind-generated waves can also contribute to the flow in shallow straits. High resolution model studies of the transport of sedimentary material have shown that despite strong currents, wave action dominates the forcing of sediment transport in shallow sea areas (Seifert et al. 2009).

The Suur Strait is a relatively narrow and shallow strait connecting the waters of the Väinameri and the Gulf of Riga. The Suur Strait is the narrowest (6 km) in the Virtsu-Kuivastu region (Figure 1). Its maximum depth is 21 m and the sill depth is about 5 m near the southern side of the Väinameri basin. Besides the Irbe Strait, the Suur Strait is an alternative gateway to the Gulf of Riga, but with a cross-section that is almost nine times smaller. The gulf (area about  $140 \times 150 \text{ km}^2$ , volume  $406 \text{ km}^3$  and mean depth 23 m) annually receives an average of ca  $32 \text{ km}^3$  freshwater from rivers (mainly from the Daugava).

The first current velocity measurements in the Suur Strait date back to 1908 (Mardiste 1995). In the 1990s prolonged measurement series were carried out in the Suur Strait (Suursaar et al. 1995, Suursaar et al. 1996, Suursaar et al. 1998). In the observation series of the Suur Strait, two current directions dominated:  $130\text{--}160^\circ$  (inflow to the Gulf of Riga) and  $340\text{--}350^\circ$  (outflow from the Gulf of Riga), which were in relatively good agreement with the axis of the strait. A maximum flow speed of about  $1 \text{ m s}^{-1}$  was recorded in both along-axis directions during ice-free conditions in the winter of 1994/95. In spring and summer the flow speeds were about

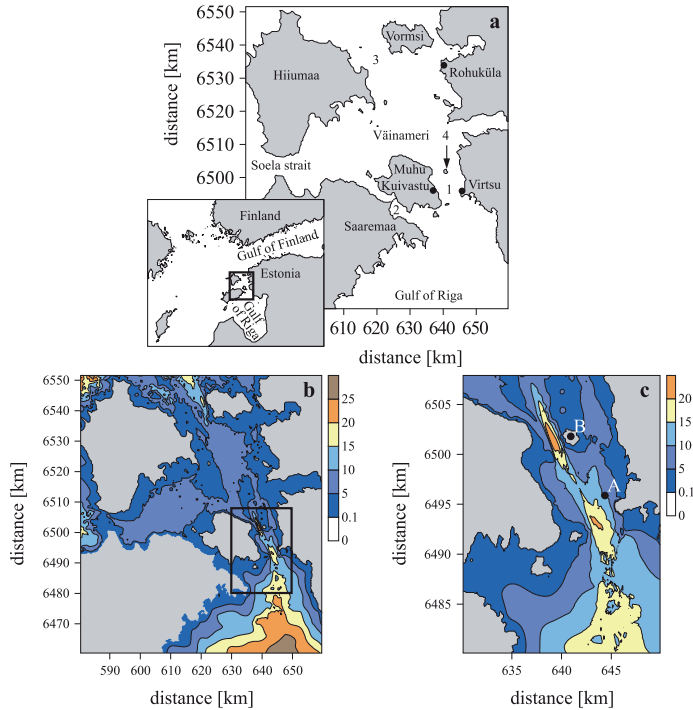


**Figure 1.** Study area (a). 1 – Suur Strait; 2 – Väike Strait; 3 – Hari Strait; 4 – Kessulaid. The bottom topography of the Vainameri region used in the 400 m resolution wave model (b). The black rectangle represents the borders of the 100 m model. The high resolution bottom topography of the Suur Strait (c). The filled circles (A) and (B) mark the positions of the buoy station and the weather station respectively. Coordinate system UTM-34. Colour scale: depth in metres

half as fast as the winter ones without ice cover. In winter with ice cover the flow speeds were relatively small:  $0.05\text{--}0.15\text{ m s}^{-1}$  (mean) and up to  $0.35\text{ m s}^{-1}$  (maximum).

Water exchange through the Suur Strait has been estimated from direct current velocity measurements and from model simulations. The yearly inflow to the Gulf of Riga has been estimated at between  $110$  and  $159\text{ km}^3$ , while the yearly outflow is between  $133$  and  $201\text{ km}^3$  (Suursaar et al. 1996, Otsmann et al. 2001). These estimates give a gross outflow from the Gulf of Riga of between  $10$  and  $53\text{ km}^3$ . On the basis of these estimates, the flow

through the Suur Strait plays an important role (up to 32%) in the water balance of the Gulf of Riga (Suursaar et al. 1996).

Surface wave measurements in the Suur Strait have not been carried out, although the role of waves can be important in forcing currents, and more likely, in resuspending bottom sediments. Mulligan et al. (2008) have shown the importance of wave-induced currents in the overall circulation in the small and shallow Lüneburg Bay during the passage of a hurricane.

There is still no evidence for the effect waves may have on resuspension and what the contribution of wave-induced currents in the overall water exchange in the Suur Strait could be. The objectives of this paper were (1) to simulate flow velocity and surface wave fields in the Suur Strait and to validate these with in situ observations; (2) using simulation results, to estimate the proportion of surface waves in the flow field and water exchange through the Suur Strait; and (3) using observation data and model simulations, to estimate wave-induced and current-induced shear velocities.

This paper is structured as follows. In section 2, the field data, circulation model and wave model are briefly described, and the wave and current shear velocities are calculated. In section 3, the model results are presented, discussed and compared with the measurements. The conclusions are drawn in section 4.

## 2. Data and methodology

### 2.1. Field measurements

Current velocity and wave measurements in the Suur Strait were performed in November–December 2008. A buoy station equipped with a Sensordata current meter SD-6000 and a pressure sensor was deployed on 13 November near Virtsu ( $58^{\circ}34.95'N$ ;  $23^{\circ}29.30'E$ , Figure 1c). The water depth at the location of the buoy station was 9 m. The current meter was at a depth of 3.5 m and the wave gauge at 2.5 m. The current speed and direction recording interval was 5 min, that of the wave gauge 0.25 s. Current measurements lasted until 4 December and wave measurements until 6 December. The method for reconstructing surface elevation spectra from sub-surface pressure recordings is described in detail by Alari et al. (2008).

Wind speed and direction were recorded with the Väisälä Weather Transmitter WXT520 installed at a height of 30 m at the Kessulaid weather station (Figure 1c). It recorded wind data at 5 min intervals from 21 November to 13 December. We used a height correction factor of 0.91 to reduce the recorded wind speed to the reference height of 10 m (Launiainen & Laurila 1984).

## 2.2. Description of the circulation model

We used a two-dimensional circulation model based on the hydrodynamic equations for a shallow sea. The model had been applied earlier to different regions of the Estonian coastal sea (Sipelgas et al. 2006). The model consists of vertically integrated motion equations

$$\frac{\partial u}{\partial t} + u \frac{\partial u}{\partial x} + v \frac{\partial u}{\partial y} - fv = -g \frac{\partial \eta}{\partial x} + \frac{F_w^x}{h} - \frac{F_b^x}{h} + \frac{F_{\text{wave}}^x}{h} + G^x, \quad (1)$$

$$\frac{\partial v}{\partial t} + u \frac{\partial v}{\partial x} + v \frac{\partial v}{\partial y} + fu = -g \frac{\partial \eta}{\partial y} + \frac{F_w^y}{h} - \frac{F_b^y}{h} + \frac{F_{\text{wave}}^y}{h} + G^y$$

and a continuity equation

$$\frac{\partial \eta}{\partial t} + \frac{\partial uh}{\partial x} + \frac{\partial vh}{\partial y} = 0, \quad (2)$$

where  $(u, v)$  are the vertically averaged velocities in the water column in the Cartesian coordinates,  $(F_w^x, F_w^y)$  are the kinematic wind stresses,  $(F_b^x, F_b^y)$  are the bottom friction stresses,  $(F_{\text{wave}}^x, F_{\text{wave}}^y)$  are the wave-induced forces,  $(G^x, G^y)$  are the horizontal turbulent viscosities in the  $(x, y)$  directions,  $f$  is the Coriolis parameter,  $g$  is the acceleration due to gravity,  $\eta$  is the sea surface elevation (deviation from the equilibrium depth) and  $h(x, y)$  is the depth.

In order to take into account the wave-induced currents, a wave-induced force per unit surface area is added to the kinematic wind stress in both the  $x$  and the  $y$  directions. The wave-induced force per unit surface area [ $\text{N m}^{-2}$ ] is calculated as the gradient of the radiation stresses (SWAN 2008).

The friction at the bottom is calculated using the quadratic relationship from the flow speed

$$F_b^x = C_D |\vec{u}| u, \quad F_b^y = C_D |\vec{u}| v, \quad (3)$$

where  $C_D (= 2.5 \times 10^{-3})$  is the bottom friction coefficient, and  $\vec{u}$  is the current velocity. The bottom friction coefficient is taken to be constant, since reliable data on sea bottom irregularities are lacking. The wave-induced force per unit surface area is the gradient of radiation stresses. It reads:

$$F_{\text{wave}}^x = \frac{1}{\rho_0} \left( -\frac{\partial S_{xx}}{\partial x} - \frac{\partial S_{xy}}{\partial y} \right), \quad F_{\text{wave}}^y = \frac{1}{\rho_0} \left( -\frac{\partial S_{yx}}{\partial x} - \frac{\partial S_{yy}}{\partial y} \right), \quad (4)$$

where  $\rho_0$  is the reference density and  $S$  is the radiation stress tensor as given by

$$S_{xx} = \rho_0 g \int n \cos^2 \theta + n \frac{1}{2} E d\sigma d\theta, \quad (5)$$

$$S_{xy} = S_{yx} = \rho_0 g \int n \sin \theta \cos \theta E d\sigma d\theta,$$

$$S_{yy} = \rho_0 g \int \left[ n \sin^2 \theta + n - \frac{1}{2} \right] E d\sigma d\theta,$$

where  $n$  is the ratio of the group velocity to the phase velocity.  $E(\sigma, \theta)$  denotes the two-dimensional wave spectrum in frequency and directional space respectively.

The terms of horizontal turbulence are calculated using the constant eddy viscosity coefficient  $A_H$ :

$$G^x = A_H \left( \frac{\partial^2 u}{\partial x^2} + \frac{\partial^2 u}{\partial y^2} \right), \quad G^y = A_H \left( \frac{\partial^2 v}{\partial x^2} + \frac{\partial^2 v}{\partial y^2} \right). \quad (6)$$

The eddy viscosity coefficient for all grids is  $50 \text{ m}^2 \text{ s}^{-1}$ .

The kinematic wind stress components are calculated as:

$$F_x^w = \frac{\tau_x^w}{\rho_0} = \frac{\rho_a}{\rho_0} c_d u_w |\vec{u}_w|, \quad (7)$$

$$F_y^w = \frac{\tau_y^w}{\rho_0} = \frac{\rho_a}{\rho_0} c_d v_w |\vec{u}_w|,$$

where  $\vec{u}_w$  is the wind velocity vector,  $u_w$  and  $v_w$  are wind components,  $\tau_x^w$  and  $\tau_y^w$  are wind stress components,  $c_d (= 1.3 \times 10^{-3})$  is the drag coefficient, and  $\rho_a$  is the air density.

Thus, the numerical model takes into account bottom topography, the Earth's rotation, friction at the sea bottom and horizontal eddy viscosity. Temperature and salinity fields are not calculated in the model. Consequently, the baroclinic component of currents is not taken into account; in the Väinameri region this is of minor importance compared to wind forcing and sea level changes (Otsmann et al. 2001).

The model did not include the river runoff into the Gulf of Riga because of its minor role in the water exchange through the Suur Strait. According to previous modelling studies, the river inflow affects mainly the flows in the Irbe Strait because the Suur Strait has a smaller cross-section and a higher resistance (Otsmann et al. 1997, Otsmann et al. 2001, Suursaar et al. 2002: Figure 3f).

A triple-nested circulation model was used for the simulation of currents and water exchange in the Suur Strait. The coarse grid model covered the whole Baltic Sea with a spatially constant grid size of  $2 \times 2 \text{ km}$ . Digital

topography was taken from Seifert et al. (2001). No open boundary conditions were implemented for this grid. The model for the Väinameri region had a grid size of 400x400 m (Figure 1b), whereas the boundary conditions for water transport were obtained from the whole Baltic Sea model. The high resolution model for the Suur Strait area had a grid step of 100x100 m (Figure 1c), and boundary conditions were obtained from the Väinameri model. One-way grid nesting was used for both model domains. For the Väinameri and the Suur Strait models, transport was used as a boundary condition. In the Väinameri and Suur Strait models, bottom topography was based on marine charts, the data being obtained from hydrographical surveys by the Estonian Maritime Administration.

Hydrodynamic model forcing was obtained from the atmospheric model HIRLAM (High Resolution Limited Area Model) version of the Swedish Meteorological and Hydrological Institute in the form used for the forcing of the HIROMB (High Resolution Operational Model of the Baltic Sea) model. Wind velocity components were interpolated to all three model grids. The HIRLAM winds were compared with the measured local wind data at the Kessulaid station. The wind velocity interpolated from the HIRLAM data was smaller than that of the wind measurements at Kessulaid by a factor of 1.4 and were therefore multiplied by this factor.

### 2.3. Description of the wave model

The SWAN wave model was implemented to describe wave conditions in the Väinameri. The SWAN model is a third-generation, phase-averaged spectral wave model developed at the Delft University of Technology (Booij 1999). In SWAN, the waves are described with the two-dimensional wave action density spectrum, whereas the evolution of the action density  $N$  is governed by the time-dependent wave action balance equation, which reads:

$$\frac{\partial N}{\partial t} + \nabla \times \left[ \left( \vec{c}_g + \vec{U} \right) N \right] + \frac{\partial c_\sigma N}{\partial \sigma} + \frac{\partial c_\theta N}{\partial \theta} = \frac{S_{\text{tot}}}{\sigma}. \quad (8)$$

The first term represents the local rate of change of action density; the second term denotes the propagation of wave energy in two-dimensional geographical space, with  $\vec{c}_g$  being the group velocity and  $\vec{U}$  the ambient current. The third term represents the effect of shifting of the radian frequency due to variations in depth and mean currents. The fourth term represents the depth-induced and current-induced refraction. The quantities  $c_\sigma$  and  $c_\theta$  are the propagation velocities in spectral space  $(\sigma, \theta)$ , with  $\sigma$  and  $\theta$  representing the radian frequency and propagation direction respectively. The right-hand side contains the source term  $S_{\text{tot}}$  representing all the

physical processes that generate, dissipate or redistribute wave energy. In shallow water, six processes contribute to  $S_{\text{tot}}$ :

$$S_{\text{tot}} = S_{\text{wind}} + S_{nl3} + S_{nl4} + S_{wc} + S_{\text{bot}} + S_{db}. \quad (9)$$

These terms denote the energy input by wind ( $S_{\text{wind}}$ ), the nonlinear transfer of wave energy through three-wave ( $S_{nl3}$ ) and four-wave interactions ( $S_{nl4}$ ), and the dissipation of waves due to whitecapping ( $S_{wc}$ ), bottom friction ( $S_{\text{bot}}$ ) and depth-induced wave breaking ( $S_{db}$ ) respectively. Extensive details on the formulations of these processes can be found, for example, in Komen et al. (1994).

For the present calculations with SWAN, the same bottom topography and meteorological forcing was used as in the circulation model. The third-generation model was used with respect to wind-input, quadruplet interactions and whitecapping. Triads, bottom friction and depth-induced breaking were also activated. For wind-input and whitecapping dissipation, the formulation by Van der Westhuysen et al. (2007) was used; in the case of wind-input, only the exponential growth term was activated. The quadruplet interaction was approximated using the Discrete Interaction Approximation (DIA). Wave breaking is governed by the ratio of the maximum individual wave height to the depth and was set at 0.73. A semi-empirical expression for bottom friction (see Holthuijsen 2007) was also activated.

#### 2.4. Wave and current shear velocities

Sediment resuspension by waves commences when fluid flow forces, such as shear stress (or shear velocity), exceed the resisting forces such as gravity and bottom friction (Van Rijn 2007). Water depth, significant wave height and peak period dictate wave-generated shear velocities acting on deposited material. In order to calculate the wave-induced shear velocity at the bottom, the near-bottom excursion amplitude and orbital velocity were calculated using the respective formulas by Kuhrtts et al. (2004):

$$A_b = \frac{H_s}{2 \sinh\left(\frac{2\pi h}{\lambda}\right)}, \quad (10)$$

$$U_b = 2\pi \frac{A_b}{T_p},$$

where  $H_s$  is the significant wave height,  $\lambda$  is the wavelength (corresponding to the peak wave period),  $T_p$  is the peak wave period and  $h$  is the water

depth. The shear velocity also depends on the friction coefficient  $f_w$ , which is calculated as follows:

$$f_w = \left\{ \begin{array}{l} 0.3, \frac{A_b}{2.5d} < 1.57 \\ \exp\left(5.5\left(\frac{A_b}{2.5d}\right)^{-0.2}\right) - 6.3 \end{array} \right\}, \quad (11)$$

where  $d$  is the diameter of the particulate matter. The shear velocity therefore takes the following form:

$$u_s = U_b \sqrt{0.5f_w}. \quad (12)$$

The current induced shear velocity was also calculated according to Kuhrts et al. (2004).

### 3. Results and discussion

#### 3.1. Wind conditions

Moderate southerly winds dominated during the measurement period (Figures 2a and b), and the mean wind speed was  $7.0 \pm 3.5 \text{ m s}^{-1}$ . Long-term analyses of winds at Vilsandi meteorological station showed an angular

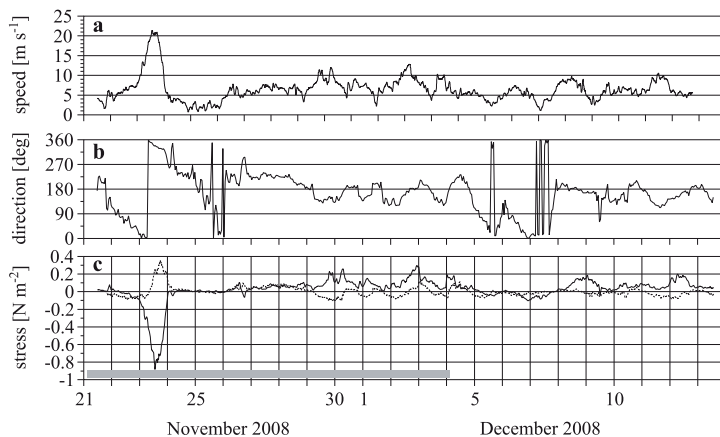


**Figure 2.** Wind speed (a), direction (b) and along-strait wind stress component (solid curve) and cross-strait wind stress component (dotted curve) calculated from wind data (c). The  $x$ -axis is positive eastwards, the  $y$ -axis is positive northwards. The shaded rectangle on the  $x$ -axis shows the period of current measurements. The data are smoothed with a 1 h running mean

distribution of directions with two peaks (Soomere & Keevallik 2003): the dominant wind direction is SW, and secondarily N or NNW, which means that our measurements represent the prevailing winds in the area. A strong storm passed through the study area on 23 November, when the maximum NNW wind speed was  $23 \text{ m s}^{-1}$  and up to  $30 \text{ m s}^{-1}$  during gusts.

The along- and cross-strait components of the wind stress were calculated in the Suur Strait (eq. (7)). Five wind impulses with an absolute along-strait wind stress component  $\geq 0.2 \text{ N m}^{-2}$  could be identified, whereas during the storm of 23 November the maximum along-strait wind stress values were ca  $-0.9 \text{ N m}^{-2}$  (Figure 2c).

### 3.2. Flow in the strait

The cross-strait flow velocity component  $u$  and the along-strait flow velocity component  $v$  were calculated from current meter data (Figure 3). The along-strait velocity component describes water exchange in the strait, whereas the inflow to the strait means northward motion, i.e. positive  $v$  values.

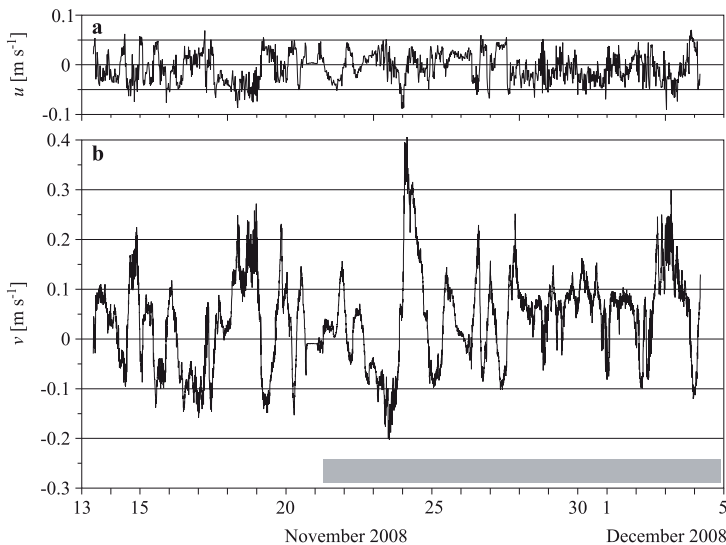


**Figure 3.** The cross-strait flow velocity component  $u$  (a) and the along-strait velocity component  $v$  (b) calculated from the measured current data in the Suur Strait. The shaded rectangle on the  $x$ -axis shows the period of wind measurements

During the severe storm on 23 November the southward flow speed was up to  $0.2 \text{ m s}^{-1}$ , the flow being from the Väänameri to the Gulf of Riga (Figure 3b). The highest along-strait flow speeds were measured after the passage of the storm and were up to  $0.4 \text{ m s}^{-1}$  (directed northwards). The somewhat lower flow speed than previously reported by Otsmann et al. (2001) was due to the closer location of our buoy station to the coast. Cross-strait flow speeds were small and varied mainly between  $-0.05$  and  $+0.05 \text{ m s}^{-1}$  (Figure 3a).

The correlation between the along-strait wind stress and the flow speed was low ( $r = 0.53$ ), indicating the important role of the along-strait sea level gradient in flow generation. From the sea level changes measured at the Virtsu and Rohuküla stations (Figure 1a), it can be seen that on the morning of 23 November, the sea level difference between Virtsu and Rohuküla started to increase rapidly and was about  $0.4 \text{ m}$  on the morning of 24 November (Figure 4). This is most likely the reason why during the gale the southward flow speeds were relatively small and during the rapid decrease in wind speed on 24 November, a strong northward flow was forced by the along-strait sea level gradient.

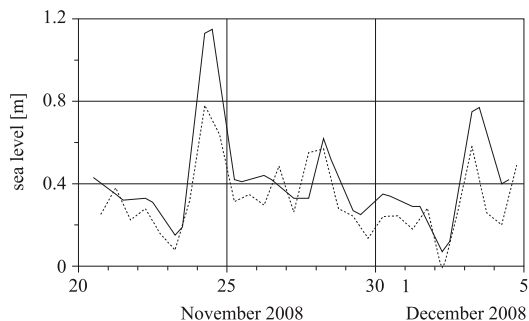


**Figure 4.** The course of sea level at Virtsu (solid curve) and Rohuküla (dotted curve) stations. (Data from the Estonian Meteorological and Hydrological Institute)

The flow in the Suur Strait was also characterized by well-expressed oscillations with different periods (Figure 3b). Otsmann et al. (2001) found from the spectral analysis of current measurements that the duration of the only significant oscillation period in the Suur Strait was  $12.43 \text{ h}$ , which is close to the  $M_2$  (lunar semi-diurnal) tidal period ( $12.42 \text{ h}$ ). They also modelled the flow in the straits as the superposition of two Helmholtz oscillators with resonance periods of about  $13$  and  $24 \text{ h}$ . These

oscillations appeared as a response of the system both to rapid changes in the wind forcing and to the sea level changes in the boundaries of the study area.

### 3.3. Wave characteristics

The mean significant wave height during the measurements was 0.53 m and the maximum significant wave height was 1.6 m (Figure 5a). Six events when the significant wave height grew to over 1 m were observed during the measurement period. The mean peak period during the measurements was 4.5 s and varied between 2.3 s and 8 s (Figure 5b). The peak period grew during the larger wave events. The maximum wave height was 2.5 m during the measurement campaign.

The first stronger wave event occurred in the evening of 14 November, when the significant wave height reached 1.35 m and the maximum peak period reached about 7 s. The wind was blowing from the south at a speed of  $12 \text{ m s}^{-1}$  (HIRLAM data). The fetch length of southerly waves was about 170 km. The strongest wave event occurred on 18 November, during which the significant wave height reached 1.6 m and the peak wave period was

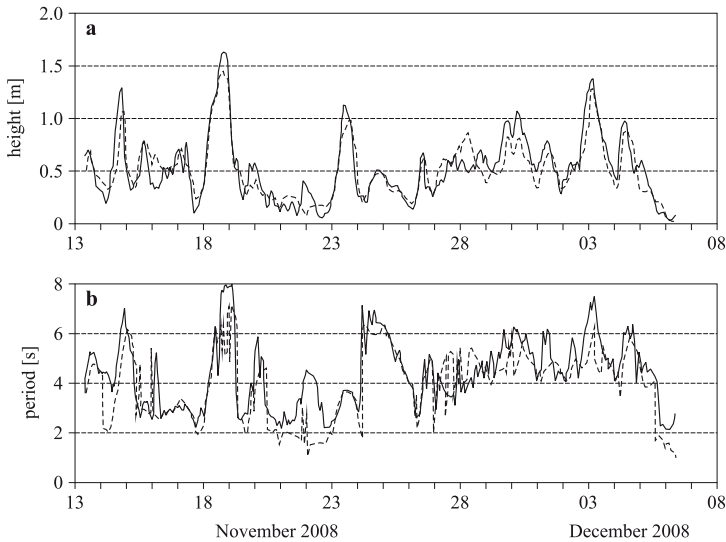


**Figure 5.** Measured (solid line) and modelled (dashed line) wave parameters: the significant wave height (a) and the peak period (b). The horizontal axis represents dates in November–December

8 s. This event was the result of southerly winds blowing at speeds of up to  $15 \text{ m s}^{-1}$  (HIRLAM data).

Although the strongest wind was measured on 23 November ( $23 \text{ m s}^{-1}$  from the NNW (Figures 2a and b)), it did not generate the highest waves – the significant wave height remained below 1.2 m and the peak wave period was 3.7 s. At the end of November, an SSE wind with a speed up to  $11 \text{ m s}^{-1}$  excited waves with a significant height of 1.1 m and a period of 6 s. The southerly wind of  $13 \text{ m s}^{-1}$  on the night of 3 December resulted in a significant wave height of about 1.4 m, with a peak wave period of 7 s.

On the afternoon of 24 November a swell was measured, where the significant wave height was between 0.4 and 0.5 m and the associated peak wave period was over 7 s. The speed of the wind, blowing from the SW, measured at the Kessulaid weather station was  $< 5 \text{ m s}^{-1}$ . The wave spectrum during this time was shifted towards lower frequencies compared to the spectra from stormy conditions (Figure 6). At first glance, we could explain this swell as a consequence of the strong,  $23 \text{ m s}^{-1}$ , NNW wind on 23 November. But the wind dropped some 12 h (Figure 2) before the first signs of swell. Therefore, it is rather unlikely that long swells could flow into the Suur Strait from the rather shallow Vainameri area. Examining the HIRLAM wind field for this period (24 November), one could see a SW

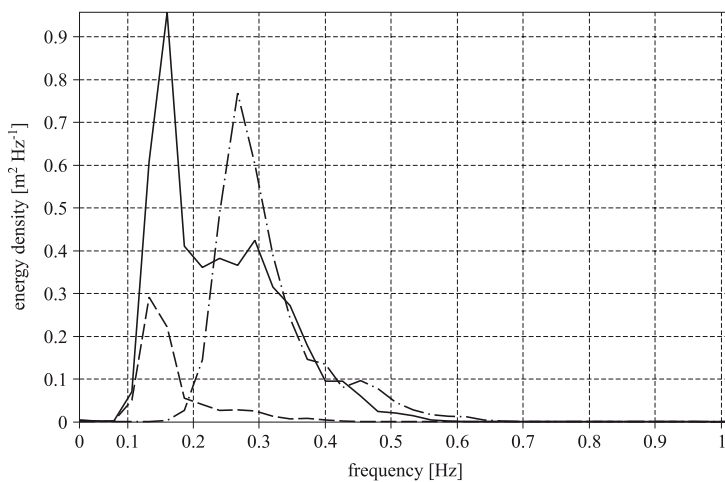


**Figure 6.** The wave field spectra during the observation period: a long fetch and the S wind on 14 November (solid line), a short fetch and the NNW storm wind on 23 November (dash-dot line) and the swell (dashed line)

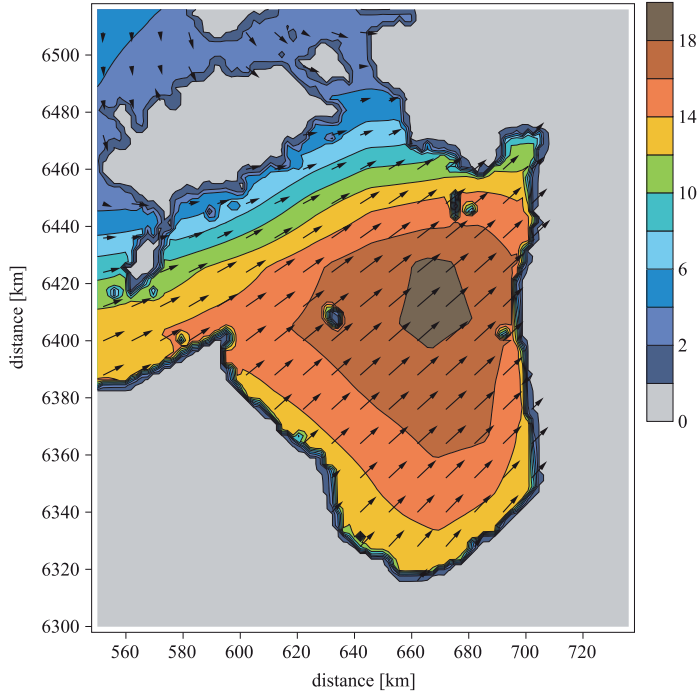


**Figure 7.** Wind field of HIRLAM (speed and direction) over the Gulf of Riga on 24 November at 11.00 UTC. Colour scale: wind speed in  $\text{m s}^{-1}$

storm in the Gulf of Riga with wind speeds of up to  $18 \text{ m s}^{-1}$  (Figure 7). The wind speed decreased significantly towards the Väänameri and matched the measured value at Kessulaid. Thus, the swell at the measurement site can be explained as having been generated by the SW storm in the open Gulf of Riga.

The wave field is described by the long fetch (the S wind), the short fetch (the NNW wind) and the swell spectrum during the observation period (Figure 6). As one can see, the southerly wind on 14 November generated a rather broad spectrum, which had its maximum at 0.16 Hz and a secondary, lower peak at 0.3 Hz. The NNW wind on 23 November,  $23 \text{ m s}^{-1}$ , on the other hand, generated a spectrum where the peak frequency was 0.27 Hz. This was because the NNW winds had a shorter fetch than the southerly winds, so that its spectrum was shifted towards higher frequencies. For the swell coming from the south, the spectrum peak was located at 0.13 Hz and the tail of the spectrum contained less energy.

### 3.4. Shear velocity

The wave-induced and current-induced shear velocities were calculated from the measured time series of waves and currents (Figure 8). The critical shear velocity for the resuspension of grains 0.25 mm in size, which corresponds to the fine sand common to the Väänameri, is  $1.4 \text{ cm s}^{-1}$  (Kuhrts et al. 2004). All wave events when the wind was blowing from the south induced sediment resuspension, and the highest shear velocities were obtained during the strong ( $15 \text{ m s}^{-1}$ ) southerly wind event on 18 November. Note that the extreme northerly wind event on 23 November did not induce shear velocities larger than the critical value, but it is possible that the swell the next day led to resuspension. For the current-induced shear velocity, the critical value for resuspension was slightly exceeded only on 24 November, when current speeds of up to  $0.4 \text{ m s}^{-1}$  generated shear velocities of up to  $1.5 \text{ cm s}^{-1}$  in the bottom boundary layer. The root mean square difference between the wave- and current-induced shear velocities was  $1.05 \text{ cm s}^{-1}$ .

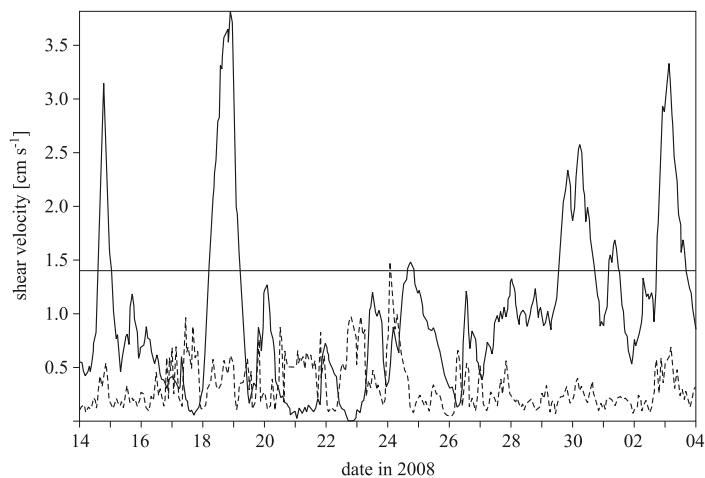


**Figure 8.** The wave-induced (solid line) and current-induced (dashed line) shear velocities calculated from the measured wave and current time series. The horizontal line marks the critical shear velocity ( $1.4 \text{ cm s}^{-1}$ ) for resuspension

The triple-nested wave model with the same bathymetry and forcing as the circulation model was used. The model results were validated using the wave measurements. The modelled and measured significant wave heights

coincided rather well – the corresponding correlation coefficient was 0.89 and the scatter index (root mean square difference between the simulated and measured significant wave height divided by the mean measured significant wave height) was 0.28. The correlation coefficient was 0.76 and the scatter index was 0.24 for peak periods.

The horizontal distribution of wave-induced shear velocities at the peak of the strong ( $15 \text{ m s}^{-1}$ ) southerly wind event showed great variability (Figure 9). Shear velocities were the highest, exceeding  $6 \text{ cm s}^{-1}$ , in the

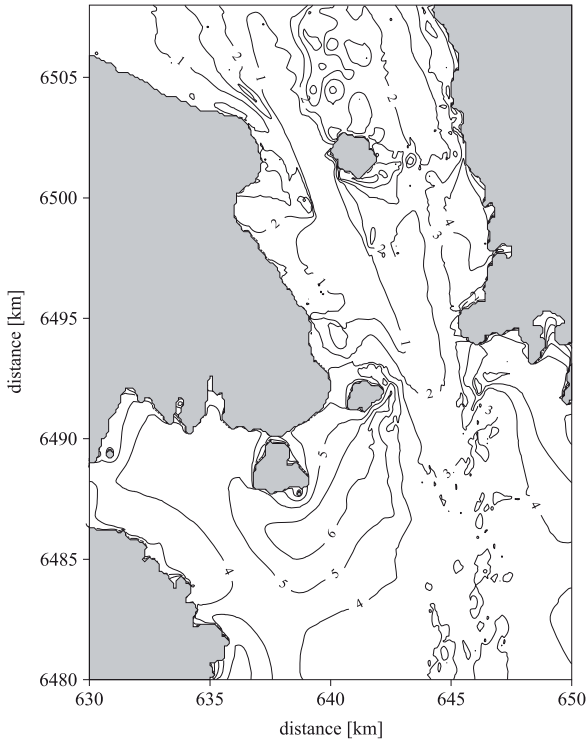


**Figure 9.** The map of wave-induced shear velocities at the peak of the strong southerly wind event on 18 November

southern part of the Suur Strait and were less than the critical value for resuspension in its deepest area. Thus, wave-induced shear velocities were generally related to the bottom topography of the strait.

### 3.5. Water exchange

The flow velocity measurements in the Suur Strait in November–December were used for the validation of the circulation models (100 m and 400 m grid step). Only the validation of the high resolution 2D circulation model with the 100 m grid step is presented because the model with the 400 m grid step gave approximately the same result. Since the models do not contain semidiurnal tidal currents, the measured flow velocity data series were smoothed with a 12 h moving average. It can be seen in Figure 10 that the rapid change in the wind field on 23 November (Figure 2) with the consequent sea level change (Figure 4) caused remarkable changes in the flow regime. The high-speed flow reversed within a short space of time. The coincidence of the measured and simulated along-strait flow speed was high – the correlation coefficient was 0.88. A certain difference can be seen in the case of higher flow speeds.

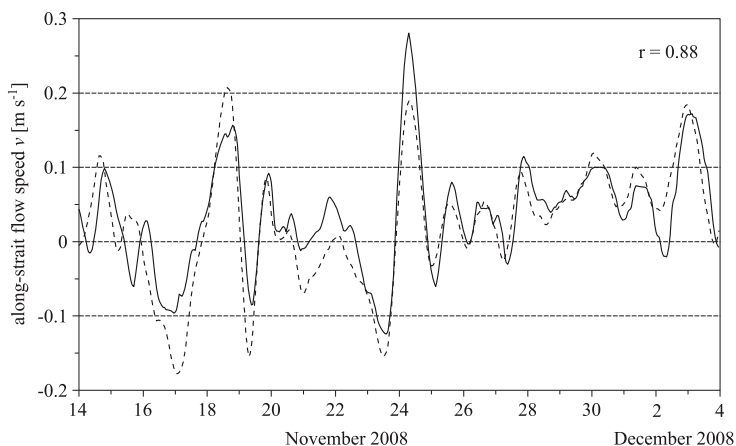


**Figure 10.** A comparison of simulated and measured along-strait flow speed  $v$  in the Suur Strait. Solid curve – measured flow speed, dashed curve – simulated flow speed. The model grid step is 100 m. The measured along-strait flow component  $v$  was smoothed with a 12 h running mean

Re-calculations with the circulation model were performed for November by taking into account wave stress as forcing additional to the wind. The wave stress was obtained from wave model simulations. The r.m.s. difference of the simulated along-strait flow component  $v$  with and without wave stress was  $0.01 \text{ m s}^{-1}$  over the Suur Strait model area. The estimate

was found for 19 November when the significant wave height was the highest (Figure 5a).

Wind-induced currents were much stronger in the strait area, reaching values of up to  $60 \text{ cm s}^{-1}$  (Figure 11), when wave-induced currents were negligible. However, wave-induced currents were essential in the flow field near the south-eastern tip of Muhu Island. The influence of wave stress on water exchange in the Suur Strait is insignificant. Wave-induced currents should be considered when modelling sediment transport in a shallow sea in the case of a long fetch.

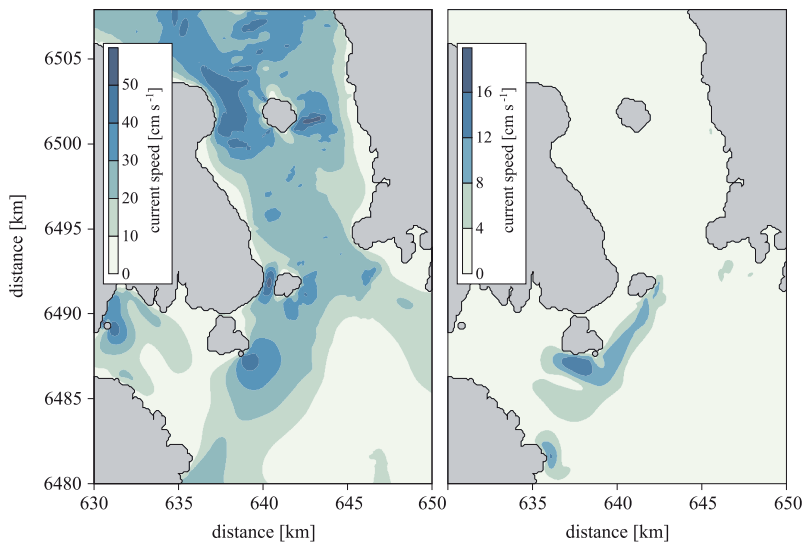


**Figure 11.** Maps of wind induced current speed (left) and wave induced current speed (right) in the Suur Strait at 23:00 UTC on 19 November 2008

The simulations with a validated high resolution circulation model were performed for the whole of 2008. Satellite imagery (Envisat, MERIS, ASAR) showed that the Väinameri region was practically ice free in 2008. The along-strait flow speed and direction were highly variable throughout the year (Figure 12), but water exchange was evidently seasonally variable (Figure 13). Northward flows were dominant from January until the middle of February, resulting in a  $15 \text{ km}^3$  water transport from the Gulf of Riga to the Väinameri.

From mid-February until late April, the cumulative water exchange through the Suur Strait was small, although the instantaneous velocities were not. From May till mid-June outflow from the Väänameri to the Gulf of Riga was dominant, the corresponding cumulative water exchange being  $10 \text{ km}^3$ . From May to July the currents were less variable than during the rest of the year. During the summer months (June, July, August) the periods of outflow from the Gulf of Riga alternated with inflow.

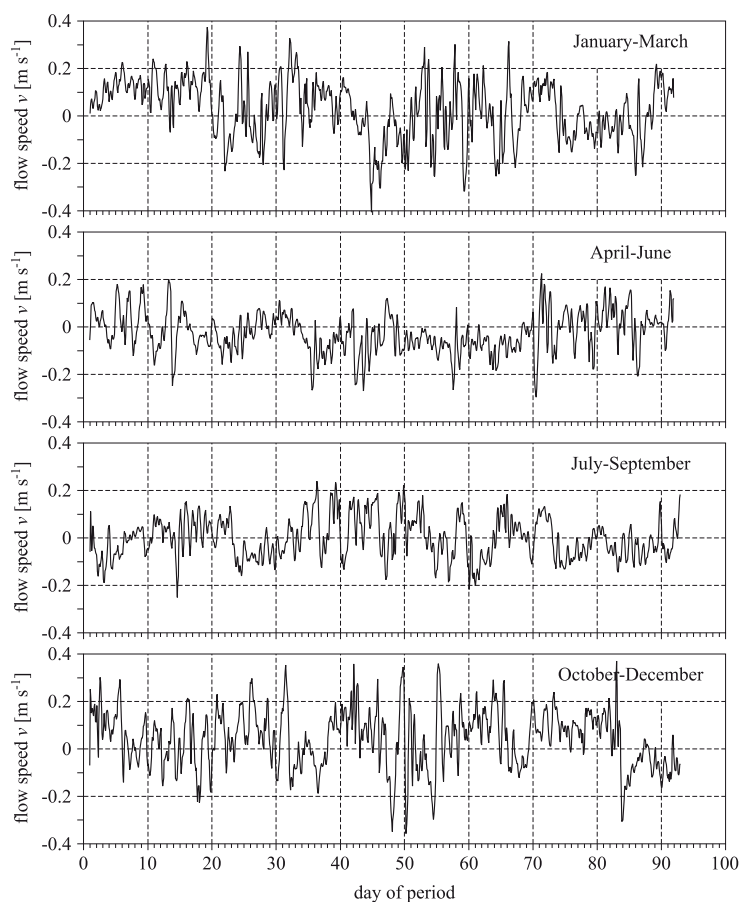


**Figure 12.** The simulated along-strait flow speed  $v$  at the centre of the Virtsu-Kuivastu transect during 2008

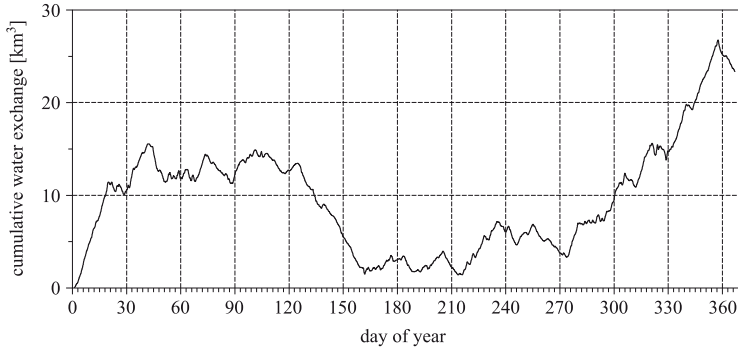


**Figure 13.** Cumulative water exchange through the Virtsu-Kuivastu cross-section during 2008

From October until the end of December there was a gross outflow from the Gulf of Riga to the Väinameri: the corresponding cumulative water exchange was approximately  $20 \text{ km}^3$ . The annual water exchange was about  $23 \text{ km}^3$  from the Gulf of Riga to the Väinameri. To conclude, both the flow speed and the water exchange are characterized by considerable variability.

A dominant outflow from the Gulf of Riga to the Väinameri from late autumn to early spring is characteristic of mild winters (Otsmann et al. 2001). For instance, the winter of 1994/1995 was stormy and ice free, which resulted in a strong outflow into the Suur Strait. October–December 1996 was also windy, resulting in a persistent outflow. In contrast, the winter of 1995/1996 was cold (ice cover in the Suur Strait) and the dominant winds blew from the north. Under these conditions a weak inflow to the Gulf of Riga through the Suur Strait was observed.

#### 4. Conclusions

1. Field measurements showed a certain asymmetry between along-strait wind forcing, flow speed and significant wave height. Because of the longer fetch of southerly waves, the highest significant wave heights (maximum 1.6 m) were observed during southerly wind events.
2. Numerical simulations with added wave stress as forcing demonstrated the minimal influence of wave-induced currents on flow speed and water exchange in the Suur Strait; nevertheless, wave-induced currents should be taken into consideration when modelling nearshore hydrodynamics.

3. Current-induced shear velocities were below the critical value for resuspension, whereas wave-induced shear velocities considerably exceeded it in cases of stronger southerly wind forcing. In general, wave-induced shear velocities were larger in the shallower areas but less than the critical value in the deep waters of the Suur Strait. Hence, the coupled wave-circulation model should be used to estimate sediment resuspension and transport in the area.
4. The simulations for the whole of 2008 showed a clear seasonal cycle with respect to cumulative transport, outflow from the Gulf of Riga during autumn and early winter, and inflow during early spring. There was an gross annual outflow of 23 km<sup>3</sup> from the Gulf of Riga to the Väinameri.

Further studies are needed to quantify material transport through the Suur Strait focusing on the cycling of material between sediments and water.

### Acknowledgements

We thank the anonymous referees for their valuable comments on the manuscript.

### References

- Alari V., Raudsepp U., Kõuts T., 2008, *Wind wave measurements and modelling in Küdema Bay, Estonian Archipelago Sea*, J. Marine Syst., 74 (Suppl. 1), S30–S40.
- Booij N., Ris R.C., Holthuijsen L.H., 1999, *A third-generation wave model for coastal regions. 1. Model description and validation*, J. Geophys. Res., 104 (C4), 7649–7666.
- Holthuijsen L.H., 2007, *Waves in oceanic and coastal waters*, Cambridge Univ. Press, New York, 404 pp.
- Komen G. J., Cavaleri L., Donelan M., Hasselmann S., Janssen P. A. E. M., 1994, *Dynamics and modelling of ocean waves*, Cambridge Univ. Press, Cambridge, 532 pp.
- Kuhrts C., Fennel W., Seifert T., 2004, *Model studies of transport of sedimentary material in the western Baltic*, J. Marine Syst., 52 (1–4), 167–190.
- Launiainen J., Laurila T., 1984, *Marine wind characteristics in the northern Baltic Sea*, Finnish Mar. Res., 250, 52–86.
- Mardiste H., 1995, *Eestit pürava mere hüdroloogilise uurimise ajalugu (kuni 1917 aastani)*, Teaduse ajaloo lehekülgi Eestist, XI, TA Kirjastus, Tallinn, 58–78.
- Mulligan R. P., Hay A. E., Bowen A. J., 2008, *Wave-driven circulation in a coastal bay during the landfall of a hurricane*, J. Geophys. Res., 113, C05026, 1–10.

- Otsmann M., Astok V., Suursaar Ü., 1997, *A model for water exchange between the Baltic Sea and the Gulf of Riga*, Nordic Hydrol., 28 (4–5), 351–364.
- Otsmann M., Suursaar Ü., Kullas T., 2001, *The oscillatory nature of the flows in the system of straits and small semienclosed basins of the Baltic Sea*, Cont. Shelf Res., 21 (15), 1577–1603.
- Seifert T., Fennel W., Kuhrts C., 2009, *High resolution model studies of transport of sedimentary material in the south-western Baltic*, J. Marine Syst., 75 (3–4), 382–396.
- Seifert T., Kayser B., Tauber F., 2001, *Bathymetry data of the Baltic Sea*, Baltic Sea Res. Inst., Warnemünde.
- Sipelgas L., Raudsepp U., Kõuts T., 2006, *Operational monitoring of suspended matter distribution using MODIS images and numerical modelling*, Adv. Space Res., 38 (10), 2182–2188.
- Soomere T., Keevallik S., 2003, *Directional and extreme wind properties in the Gulf of Finland*, Proc. Estonian Acad. Sci. Eng., 9, 73–90.
- SWAN team, 2008, SWAN Cycle III version 40.72.
- Suursaar Ü., Astok V., Alenius P., Kullas T., Otsmann M., 1998, *Thermohaline regime and currents in the Suur Strait and Hari Strait in 1996–1997*, EMI Rep. Ser., 9, 6–22.
- Suursaar Ü., Astok V., Kullas T., Nõmm A., Otsmann M., 1995, *Currents in the Suur Strait and their role in the nutrient exchange between the Gulf of Riga and the Baltic Proper*, Proc. Estonian Acad. Sci. Ecol., 5, 103–123.
- Suursaar Ü., Astok V., Kullas T., Otsmann M., Alenius P., 1996, *Thermohaline regime and currents in the Suur Strait in 1993–1995*, EMI Rep. Ser., 3, 7–58.
- Suursaar Ü., Kullas T., Otsmann M., 2002, *A model study of sea level variations in the Gulf of Riga and the Väinameri Sea*, Cont. Shelf Res., 22 (14), 2001–2019.
- Van Rijn L. C., 2007, *Unified view of sediment transport by currents and waves 1: initiation of motion, bed roughness and bed-load transport*, J. Hydraul. Eng.–ASCE, 133 (6), 649–667.
- Van der Westhuysen A. J., Zijlema M., Battjes J. A., 2007, *Nonlinear saturation-based whitecapping dissipation in SWAN for deep and shallow water*, Coast. Eng., 54 (2), 151–170.

## **Paper IV**

Alari, V., Raudsepp, U. 2010. Depth induced breaking of wind generated surface gravity waves in Estonian coastal waters. *Boreal Environment Research*, 15 (3), pp. 295-300.



# Depth induced breaking of wind generated surface gravity waves in Estonian coastal waters

Victor Alari and Urmas Raudsepp

*Marine Systems Institute at Tallinn University of Technology, Akadeemia Rd. 21, 12618 Tallinn, Estonia*

*Received 1 Mar. 2008, accepted 29 May 2009 (Editor in charge of this article: Timo Huttula)*

Alari, V. & Raudsepp, U. 2010: Depth induced breaking of wind generated surface gravity waves in Estonian coastal waters. *Boreal Env. Res.* 15: 295–300.

Depth-induced wave breaking is a key term for wave energy dissipation in the action balance equation of the third generation spectral wave models, and becomes an essential consideration in modelling wave behaviour in shallow water and near the coast. Neglecting this sink function leads to an overestimation of significant wave heights. Current paper addresses the importance of depth induced wave breaking, using the SWAN wave model, at two locations in Estonian coastal waters in case of NNW storms — the first site is the Harilaiu Bank, situated in the north-west of the Saaremaa Island while the other one is Tallinn Bay. We performed simulations using SWAN with two different setups, i.e. the depth induced wave-breaking accounted and not accounted. The computed wave height in the first case was smaller than in the second case with maximum difference of 4.8 m in the Harilaiu Bank and 2.3 m in Tallinn Bay. Previous studies using the WAM model suggest that remarkable wave maxima exist in these regions due to focusing of wave rays e.g. due to topographic refraction of surface waves. As these maxima were reproduced by SWAN when depth-induced wave breaking was turned-off, we conclude that the maxima simulated by WAM can be an artefact of the model.

## Introduction

The length of the Estonian coastline is about 3780 km. Although the coast of Estonia is not as staggered as are the Finnish and Swedish coasts, it still contains numerous shallows and islands. Consequently, modelling the wave regime of Estonian coastal waters requires a model that is capable of modelling the processes involved in shallow water wave propagation and dissipation over complex bathymetry. The least understood aspect of the physics of wave evolution, as it pertains to spectral modelling, is the dissipation source function. In shallow water, three terms contribute to the dissipation source function: dissipation due

to surface processes (white-capping), dissipation due to bottom friction and depth-induced wave breaking. Understanding and modelling depth induced wave breaking and other processes are thus critically important in achieving an accurate representation of the principal sink function in the energy (or action) balance equation.

Soomere (2003, 2005) analyzed the typical and extreme wave regimes off the north-western Saaremaa Island and Tallinn Bay using a third generation spectral wave model WAM (Komen 1994). The extreme storm in the former case was  $25 \text{ m s}^{-1}$  NNW wind blowing steadily over the Baltic Sea within eight hours. The latter case was NNW wind with the speed of  $23 \text{ m s}^{-1}$  blowing

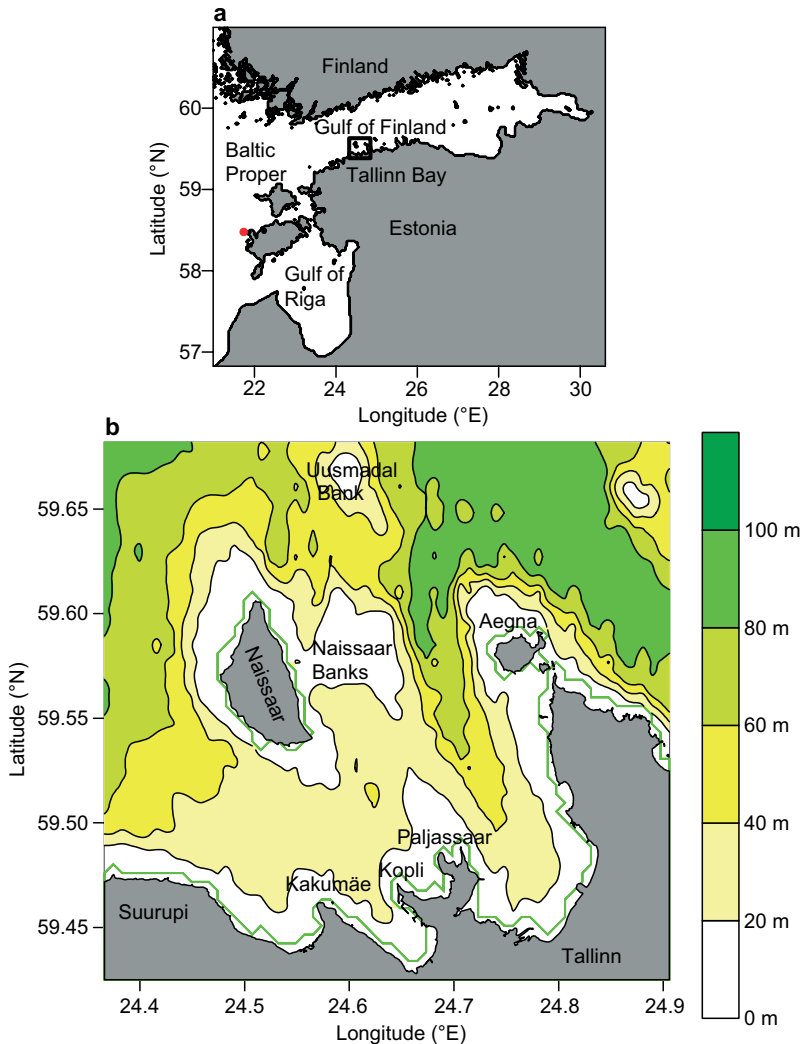


**Fig. 1.** (a) Location of the Harilau Bank (red dot). (b) Bathymetry of Tallinn Bay.

steadily for six hours. Soomere (2003) found that several wave height maxima occurred near the Saaremaa and Hiiumaa Islands with the most intensive ones occurring at the Harilau Bank (Fig. 1), where significant wave heights grew up to 9.8 m. In Tallinn Bay, several wave height related maxima occurred near the Aegna Island, Paljassaare and Kopli Peninsulas and at shallows in Tallinn Bay (Fig. 1). He explained these maxima as topographic refraction of the surface waves. However, the WAM wave model does not include a sink function for depth-induced wave breaking (Komen 1994) and the effect of triads is also not considered — although less significant than depth-induced wave breaking in the present case.

The objective of this study was to repeat numerical experiments of Soomere (2003, 2005) in Estonian coastal waters using the SWAN model — a third-generation spectral shallow water wave model (Booij 1999, Holthuijsen 2007) — and to compare obtained results with those of Soomere obtained with the WAM model (Soomere 2003, 2005). Wave patterns at the Harilau Bank and Tallinn Bay are of great importance. The Harilau Bank is close to the Kiipsaare Cape, a peninsula which is being fast eroded due to beach processes induced by wave activity. Tallinn Bay on the other hand has the most intense shipping activity in Estonia and, therefore, an accurate presentation of its typical and extreme wave properties are of great

importance. The SWAN model was validated for significant wave heights in small K udema Bay, (north-western Saaremaa Island) by Alari *et al.* (2008).

## Numerical model

SWAN is a third-generation phase-averaged spectral wave model developed at the Delft University of Technology, the Netherlands (Booij *et al.* 1999). In SWAN, the waves are described with the two-dimensional wave action density spectrum, whereas the evolution of the action density,  $N$ , is governed by the time-dependent wave action balance equation, which in Cartesian coordinates reads:

$$\frac{\partial N}{\partial t} + (\vec{c}_g + \vec{U}) \nabla N + \frac{\partial c_\sigma N}{\partial \sigma} + \frac{\partial c_\theta N}{\partial \theta} = \frac{S_{\text{tot}}}{\sigma} \quad (1)$$

The first term represents the local rate of change in action density; the second term denotes the propagation of wave energy in the two-dimensional geographical space with  $c_g$  being the group velocity and  $U$  the ambient current. The third term represents the effect of shifting the relative frequency due to variations in depth and mean currents. The fourth term represents the depth-induced and current-induced refraction. The quantities  $c_\sigma$  and  $c_\theta$  are the propagation velocities in spectral space ( $\sigma$ ,  $\theta$ ) with  $\sigma$  and  $\theta$  representing the relative frequency and the direction of propagation respectively. The right-hand side contains the source term  $S_{\text{tot}}$  that represents all physical processes that generate, dissipate or redistribute wave energy. In shallow water, six processes contribute to  $S_{\text{tot}}$ :

$$S_{\text{tot}} = S_{\text{wind}} + S_{\text{nl3}} + S_{\text{nl4}} + S_{\text{wc}} + S_{\text{bot}} + S_{\text{db}} \quad (2)$$

These terms denote respectively the energy input by wind ( $S_{\text{wind}}$ ), the non-linear transfer of wave energy through three-wave ( $S_{\text{nl3}}$ ) and four-wave interactions ( $S_{\text{nl4}}$ ), and the decay of waves due to white-capping ( $S_{\text{wc}}$ ), bottom friction ( $S_{\text{bot}}$ ) and depth-induced wave breaking ( $S_{\text{db}}$ ).

In the surf zone, the dissipation of wave energy due to depth-induced wave breaking becomes stronger than the wave decay due to bottom friction or percolation (Massel 1996).

The modelling of energy dissipation, due to breaking in the wave train, is usually based on four main assumptions (Massel 1996): (1) dissipation is equivalent to dissipation in a bore connecting two regions of uniform flow; (2) dissipation is proportional to the difference between the local energy flux and the stable energy flux; (3) the breaking wave height is saturated, i.e. the wave height is proportional to the local water depth and the proportionality coefficient is assumed to be constant across the surf zone; (4) dissipation is controlled by the presence of surface roller.

Following the previous, in SWAN total dissipation due to depth-induced wave breaking is modelled as dissipation of a bore, applied to the breaking waves in a random field in shallow water. The wave period used is calculated from zero and the first moment of the variance density spectrum. The tunable coefficient e.g. the breaking parameter is set to 0.73. (Holthuijsen 2007).

For the north-western coast of Estonia, the model is exposed to NNW wind (direction 330 ) having the strength of 25 m s<sup>-1</sup> blowing steadily over the Baltic Sea. The model topography is based on Seifert *et al.* (2001) with the resolution of 1' along latitudes and 2' along longitudes. The number of spectral frequencies is 40. The spectral frequencies are distributed logarithmically on the frequency range of 0.04–1 Hz and 12 spectral directions are also used.

Calculations of Tallinn Bay wave field were carried out using a triple nested model. The coarse Baltic Sea model had resolution of 1' along latitudes and 2' along longitudes. The medium grid for the Gulf of Finland (GOF) had a resolution of 0.5' along latitudes and 1' along longitudes, with the boundary conditions obtained from the coarse Baltic Sea model. The high resolution Tallinn Bay model is 0.25' along latitudes and 0.5' along longitudes and the boundary conditions were obtained from GOF model. The model is forced with the NNW wind blowing at 23 m s<sup>-1</sup>. The spectral resolution is the same as for north-western Estonia. In the case of the high resolution Tallinn Bay model, the number of spectral directions is 24.

Two calculations for north-western Estonia and Tallinn Bay were made. The first calculation was with depth-induced breaking activated and

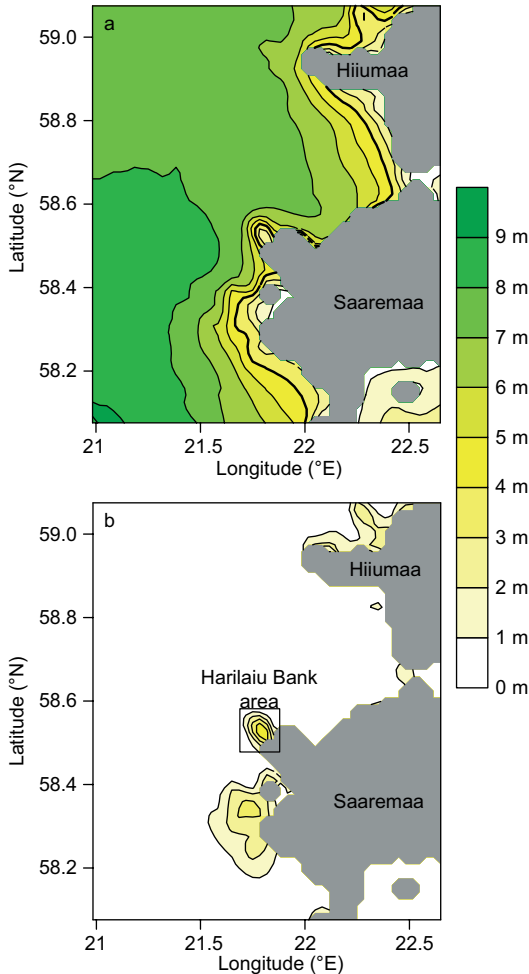


**Fig. 2.** (a) Significant wave height in the coastal zone of the Hiiumaa and Saaremaa Islands in case of an extreme ( $25 \text{ m s}^{-1}$ ) NNW storm. (b) Difference between depth induced breaking not activated and depth induced breaking activated. The 4 m isoline is contoured bold. Colour bar holds for **b** as well.

the second one was with depth-induced breaking not-activated. The analyzed and visualized fields represent saturated wave fields.

## Results

### Harilau Bank

The significant wave height can grow as high as 8 m offshore and even 9 m when moving farther towards the open sea (Fig. 2). Approaching

the coast, the significant wave height decreases. Only in some parts of the NW Saaremaa Island, the significant wave height remains over 6 m. When comparing the topography of this region with the other areas where the significant wave height starts to decrease farther away from coast, it becomes clear, that here large water depths are closer to the coast.

Calculations with depth-induced breaking turned off presents areas near the coast where the significant wave height increases (Fig. 2b). The largest increase in the significant wave height up to 4.8 m forms at the Harilau Bank. It means that the maximum significant wave height at the Harilau Bank is 7.4 m in the case of depth-induced wave breaking turned off. South of the Harilau Bank forms an area where the significant wave height grows more than 3 m in the case of depth-induced breaking turned off. Third area where an increase in the significant wave height is seen is located NW of the Hiiumaa Island, where the increase is over 1 m. Other coastal areas do not show an increase of the significant wave height. As the water depth in the other areas starts to decrease quite far away from the coast and smoothly (no significant slope), we may conclude that bottom friction mainly dissipates waves there instead of depth-induced wave breaking. On the open sea, the difference between the calculations with depth-induced wave breaking and without it is, as expected, negligible.

The wave-height maxima as depicted in Soomere (2001: fig. 2, 2003: fig. 4) are not present in calculations with SWAN (Fig. 2a) in the case of activated depth-induced wave breaking. In Soomere (2001, 2003), the maximum significant wave height grew up to 9.8 m and 10.5 m at the Harilau Bank, respectively. Calculations with SWAN in present work show that the maximum significant wave height near the Harilau Bank does not exceed 3 m, but grows to 9 m on the open sea. The latter coincides well with Soomere (2001, 2003).

Soomere (2001, 2003) also reports that the maximum wave heights owing to topographic refraction accumulate in a certain time phase of a storm. The analysis of time series of the significant wave height at the Harilau Bank (Fig. 3) calculated with the non-stationary mode of

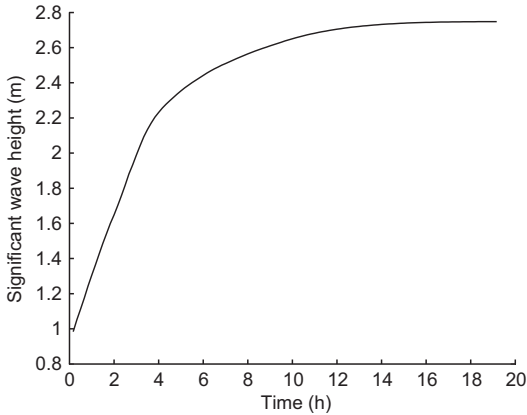


**Fig. 3.** Dependence of significant wave height on wind duration at the Harilaiu Bank.

SWAN does not show any anomalous wave-height growth at any time. The wave height grows to 2.6 m within about 9 hours and then becomes saturated.

### Tallinn Bay

Although Tallinn Bay is well sheltered by two islands (Naissaar and Aegna) and many shallows (*see* Fig. 1), high waves may penetrate into the bay in case of NNW winds (Fig. 4a). The significant wave height may be as high as 3 m in the bay interior and up to 4 m to the west of the Naissaar Island, which is about 1 m less than reported by Soomere (2005). Areas north of the Aegna Island and shallows between Aegna and Naissaar islands exhibit significant wave heights less than 3 m. Areas near the peninsulas of Suurupi, Kakumäe, Kopli and Paljassaar exhibit the significant wave heights less than 2.5 m. The lowest significant wave heights, less than 1 m, occur between the mainland and the Aegna Island. In general, the significant wave height calculated for the Tallinn Bay interior with SWAN is about 0.5 m smaller than in Soomere (2005).

The results of using the SWAN model with depth-induced breaking inactive show an increase in wave height north of the Aegna Island and on the north-western coast of the Naissaar Island, near the peninsulas of Kopli, Paljassaar and Kakumäe, and at Naissaar Bank and the Uusmadal Bank, as well as at Suurupi

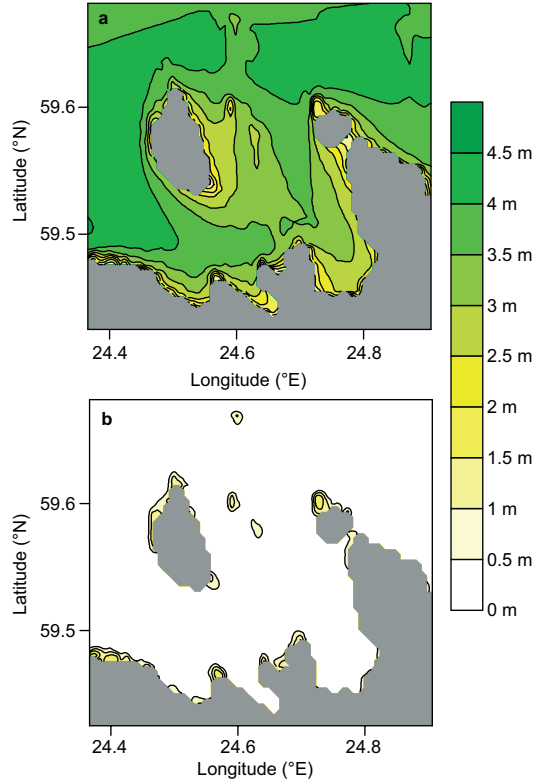


**Fig. 4.** (a) Significant wave height in Tallinn Bay and adjacent sea area in case of an extreme ( $23 \text{ m s}^{-1}$ ) NNW storm. (b) Difference between depth induced breaking not activated and depth induced breaking activated. Color bar holds for **b** as well.

(Fig. 4b; *see* also Fig. 1 for exact locations). The increase in the significant wave height north of Aegna is 1.8 m, 1.1 m at the Keskmadal Bank, 1.4 m at the Naissaar Bank, 2 m at the Kakumäe Peninsula, 1.5 m at the Kopli and Paljassaare peninsulas. The highest increase occurs near the Suurupi Peninsula, where the non-breaking case presents significant wave height increase of 2.3 m. Central Tallinn Bay, also west of the Naissaar Island and other areas, where the water depth is greater than 20 m do not show increase in the significant wave height. As compared with the increase of the significant wave at the Harilaiu Bank in case of depth-induced breaking turned off, Tallinn Bay exhibits almost two times lower increase, however, there are more areas where the significant wave height increases. The lower increase of the significant wave height is probably due to lower background values of the

significant wave height in Tallinn Bay (and in the Gulf of Finland) as compared with those at the Harilaiu Bank (and in the Baltic Proper).

## Conclusions

Three possible sources of errors in wave modelling suggested by Komen *et al.* (1994) are: (1) inadequate wind input, (2) inadequate numerical schemes and resolutions, and finally (3) inadequate model physics. In this paper, we compared SWAN wave model results with and without depth-induced wave breaking to address the effect of depth-induced wave breaking in the Estonian coastal waters.

The results of modelling with SWAN indicate that depth-induced wave breaking plays a key role in the dissipation of waves at the Harilaiu Bank and in Tallinn Bay. In the case of NNW storms, depth-induced wave breaking reduces the significant wave height up to 4.8 m at the Harilaiu Bank and up to 2.3 m in Tallinn Bay. Hence, the maxima in these areas are not caused by topographic refraction, as suggested by Soomere (2003, 2005). Although WAM is a widely used and verified model against measurements in deep water (Komen *et al.* 1994), it does not reproduce the wave fields near shore, as shown here. The WAM model is intended for deep water applications, and cannot be realistically applied to coastal regions with horizontal scales smaller than 20–30 km and water depth smaller than 20–30 m (e.g. Booij 1999). The reduction of the significant wave heights due to depth-induced breaking at the Harilaiu Bank and in Tallinn Bay clearly shows that the results obtained with WAM can lead to large overestimation of wave heights, as WAM can not be expected to obtain realistic values in this kind of depths, especially in extreme conditions.

In conclusion, the wave height maxima at the Harilaiu Bank and Tallinn Bay (Soomere 2003, 2005) are an artefact of the WAM model — confirming the fact that WAM was never intended to reproduce wave fields near shore. Let us remind ourselves that maximum wave heights can be up to 1.8 times larger than significant wave heights, hence the calculations by Soomere (2001, 2003) lead to the maximum wave height of 18 m at the Harilaiu Bank. Thus the conclusions by Soomere are likely incomplete.

*Acknowledgments:* We are grateful to Dr. Gennadi Lessin and Kai Ristikivi for the help in preparing the figures, and to anonymous referees for their crucial comments and suggestions.

## References

- Alari V., Raudsepp U. & Kõuts T. 2008. Wind wave measurements and modelling in Küdema Bay, Estonian Archipelago Sea. *J. Mar. Syst.* 74: S30–S40.
- Booij N., Ris R.C. & Holthuijsen L.H. 1999. A third-generation wave model for coastal regions. 1. Model description and validation. *J. Geophys. Res.* C104: 7649–7666.
- Holthuijsen L.H. 2007. *Waves in oceanic and coastal waters*. Cambridge University Press, Cambridge.
- Komen G.J., Cavaleri L., Donelan M., Hasselmann K., Hasselmann S. & Janssen P.A.E.M. 1994. *Dynamics and modelling of ocean waves*. Cambridge University Press, Cambridge.
- Massel S. 1996. *Ocean surface waves: their physics and prediction*. World Scientific Publication, Singapore.
- Seifert T., Kayser B. & Tauber F. 2001. A high resolution spherical grid topography of the Baltic Sea, revised edition. In: *Baltic Sea Science Congress 2001: Past, Present and Future — A Joint Venture*, Abstract Volume, Stockholm University, p. 298.
- Soomere T. 2001. Wave regimes and anomalies off north-western Saaremaa Island. *Proc. Estonian Acad. Sci. Eng.* 7: 157–173.
- Soomere T. 2003. Anisotropy of wind and wave regimes in the Baltic Proper. *J. Sea Res.* 49: 305–316.
- Soomere T. 2005. Wind wave statistics in Tallinn Bay. *Boreal Env. Res.* 10: 103–118.

## **Paper V**

Alari, V., Raudsepp, U., Kõuts, T. 2008. Wind wave measurements and modelling in Küdema Bay, Estonian Archipelago Sea. *Journal of Marine Systems*, 74 (SUPPL.), pp. S30-S40.





## Wind wave measurements and modelling in Küdema Bay, Estonian Archipelago Sea

Victor Alari\*, Urmas Raudsepp, Tarmo Kõuts

Marine Systems Institute at Tallinn University of Technology, 12618 Akadeemia Rd. 21, Tallinn, Estonia

### ARTICLE INFO

#### Article history:

Received 31 August 2007

Received in revised form 19 November 2007

Accepted 25 November 2007

Available online 21 October 2008

#### Keywords:

Baltic Sea

Küdema Bay

Small semi-enclosed bay

Wave measurements

SWAN

### ABSTRACT

The wind wave climate of the Küdema Bay, situated northwest of Saaremaa Island, has been analyzed on the basis of wave measurements carried out in the summer and autumn of 2005, with the use of the third-generation spectral wave model SWAN. The analysis of wave data sets has shown that the wind waves in the Küdema Bay were dominated by locally generated fetch-limited wind waves. The average significant wave height was 16 cm for summer deployment, and 24 cm for autumn deployment, respectively. That low wave climate mainly results from the climatic conditions where the winds are frequently blowing from the mainland, and when fetch length of waves is less than 2 nmi. The strongest wave event, where significant wave height reached 1.5 m, was associated with the north-westerly winds with speeds of up to 13.3 m/s. Significant wave heights obtained with the wave model were well correlated with the measured ones, whereas the model strongly underestimated the peak-periods of waves. It can be concluded that the typical wave climate of the bay is rather soft, but high waves are expected with north-westerly winds.

© 2008 Elsevier B.V. All rights reserved.

### 1. Introduction

The observation, analysis and prediction of wind-generated surface gravity waves in ocean environments, shelf seas and coastal areas have been a subject of interest for oceanographers, scientists, engineers etc. for quite a long time now. During that period the measurement techniques have developed from visual observations made by an observer (Soomere and references therein, 2005) to remote sensing techniques with the use of satellites (Holthuijsen, 2007). The analyses of waves have evolved from the simple (statistical) description of their properties, to the discovery of the advanced concept of two-dimensional wavenumber-direction spectrum, first introduced in the 1950s (Liu, 2000). During the 20th century, numerical wave models have evolved from the 1st generation model to more advanced 3rd generation numerical models (Komen et al., 1994).

Although several wave experiments have been carried out in small and medium sized bays, e.g. bearing in mind the

growth of waves in a narrow bay (Pettersson, 2004), or in fetch and depth-limited lakes (Breugem, 2003), the majority of measurements cover only deep water and open seas. In the latter case the interaction of waves with the sea basin is neglected; also the growth and decay of waves are dictated only by wind pressure, whitecapping and quadruplet non-linear transfer. As the waves propagate towards coast and shallower areas, the wave field transforms and the decay and growth of the waves are controlled by complicated physical processes. These processes include nonlinear energy transfer between wave triads, depth-induced wave breaking, shoaling of waves, and decay of waves by bottom friction. Thus the complex wave field common to coastal environments is evolved.

Even though basic knowledge admits that wind waves in small semi-enclosed basins are small and have high frequencies, the waves have an important impact on defining the shape of the coastline (Soomere, 2005); storm waves induce high sediment re-suspension (Jönsson, 2006) and also, the functioning of marine ecosystem is dependent on waves (Jönsson, 2006). Therefore, an accurate picture of a typical and extreme wave regime is necessary.

\* Corresponding author. Tel.: +372 6204318; fax: +372 6204301.  
E-mail address: [victor.alari@phys.sea.ee](mailto:victor.alari@phys.sea.ee) (V. Alari).

The objective of this paper is to analyze the wave regime of a small semi-enclosed bay, and the Küdema Bay was chosen for this purpose. The determination of the bay's wave regime is also important from an engineering point of view – in 2005 a new deep sea harbour was built on the west coast of the Küdema Bay, despite the fact that during the last 100 years, the harbour had been demolished by northerly storms on two occasions. The Küdema Bay is situated on the north-western side of Estonia's largest island Saaremaa, between the Peninsulas of Panga and Ninase (Fig. 1). The mean width of the bay is 1.5 nmi (west–east direction) and its length is 4 nmi (north–south direction), with a mean depth of 7.5 m. The bay is an attractive study object due to its coastline, because on the northern side of the bay the water depth is already 20 m at only about 400 m from the shore, so the high waves may penetrate into the bay.

The typical wave regime of the bay was analyzed on the basis of wave measurements, which were carried out using submerged pressure transducers, and with the use of a third-generation spectral wave model SWAN (Booij et al., 1999), which is more suitable for coastal areas than the well-known and verified model for deep waters WAM (Komen et al., 1994).

The structure of this article is as follows: In Section 2 data of wave and wind measurements are presented, and the method for determining the basic wave parameters from sub-surface pressure is described, in Section 3 the description of the wave model and setup of the model is introduced; results are presented in Section 4 and the discussion is presented in Section 5; main conclusions are drawn in Section 6.

## 2. Data and method

### 2.1. Wind and wave data sets

Wave measurements were made twice in 2005 in the Küdema Bay near the Saaremaa (historically known as Tamme) Harbour site (Fig. 1) at the location 58°32.375' N and 22°14.477' E. The first period of measurements was from July 27 to August 19, and the second period of measurements

was from the October 29 to November 21. Wave data sets were collected with sub-surface pressure transducer (wave gauge) developed by PTR group, Estonia. The pressure sensor of the gauge was 12 m above the bottom; the water depth at the site was about 17 m. The gauge was set to take samples at 4 Hz.

There are two reasons why the wave gauge was put so deep respect to free water surface: (1) With NW storms the significant wave heights can be up to 5 m at the entrance of the bay (Soomere, 2001a), so in order to prevent the gauge from remaining “dry,” it had to be mounted sufficiently deep; (2) Since there was some navigation going on in the bay, the gauge had to be placed deeper than the draught of the navigating vessels in order for it not to be damaged by vessels.

Soomere (2001b, 2003) suggests that Vilsandi's wind data constitutes a good representation of the scalar and directional properties of the wind regime off the coast of Saaremaa, and also in the Baltic Proper. Vilsandi's weather station is situated 30 km SW of the Küdema Bay. For the interpretation of wave height and period variability, and also as an input for the wave model, wind parameters measured by the Vilsandi meteorological station, such as average wind speed and direction, were used. The parameters were recorded on an hourly basis. Vilsandi's data is considered to be precise enough, since small errors in atmospheric data can result in large errors in modelled oceanographic data (Signell et al., 2005).

### 2.2. Converting sub-surface pressure to spectral wave parameters

Sub-surface pressure transducers measure the instantaneous pressure that is the sum of the air pressure, hydrostatic pressure and wave-induced dynamical pressure. When the air pressure and hydrostatic pressure are assumed to remain constant, the dynamic pressure under water is expressed with equations derived from linear wave theory (Tsai et al., 2005). That pressure is a function of three parameters: the height of the pressure sensor from the seabed, the wave frequency and the water depth. In intermediate water depth, the pressure decreases hyperbolically with the depth, so a sub-surface

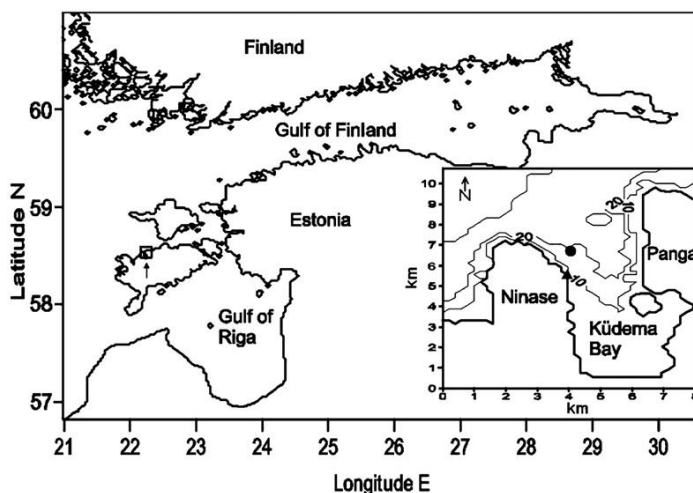


Fig. 1. Bathymetry of Küdema Bay (depth in metres) with wave observation site (●) and Saaremaa harbour (▲).

attenuation coefficient therefore has to be applied in order to get a realistic picture of the wave height.

The method to derive the surface wave height from the sub-surface pressure is the following:

First, the measured time series is divided into twenty-minute long sections, called wave packets. This kind of packet length performs well, since smaller packet length introduces a large statistical scatter (WMO, 1998). Additionally, the packet is de-averaged and de-trended. Mean value is used in order to calculate the gauge depth, which is needed for the calculation of the attenuation coefficient. Further on, the power spectral density is estimated by using a Welch method, and a Hanning window is used to smooth the spectrum. Obtained subsurface pressure spectra ( $S_p$ ) were converted to surface elevation spectra ( $S_\eta$ ) using linear wave theory by:

$$S_\eta = S_p \left( \frac{\cosh kd}{\rho g \cosh k(d+z)} \right)^2, \tag{1}$$

with  $k$  the wave-number calculated from the linear dispersion equation,  $d$  the water depth,  $z$  elevation of the pressure gauge relative to the mean water surface,  $\rho$  the water density and  $g$  the acceleration due to gravity.

The wave steepness at the measurement location is greatly under 0.1 with a median of 0.02. Also, the water depth at the measurement location belongs to a transitional water depth and therefore linear transformation formulae are suggested to perform well.

During the measurement campaigns, the height of the water column above the wave gauge varied from 4.9 m to 5.25 m in the summer measurement period, and from 4.1 m to 4.6 m in the autumn measurement period, so waves with frequencies lower than 0.3855 Hz were measurable. Also, an

attenuation rate of 5 was accepted to eliminate the higher frequencies.

From the wind wave spectrum, the zero moment was calculated (the energy variance or equivalently, the area under the spectrum) and the significant wave height was derived from that ( $H_{m0}$ ). The mean zero-crossing period ( $T_{m02}$ ) was also calculated from the wave spectrum.

### 3. Model description and setup

#### 3.1. Model description

The SWAN wave model was implemented to describe the wave characteristics in the K udema Bay. SWAN is a third-generation phase averaged spectral wave model developed at Delft University of Technology (Booij et al., 1999). In SWAN, the waves are described with the two-dimensional wave action density spectrum, whereas the evolution of the action density  $N$  is governed by the time-dependent wave action balance equation, which in Cartesian coordinates reads:

$$\frac{\partial N}{\partial t} + (\vec{c}_g + \vec{U}) \cdot \nabla N + \frac{\partial c_{\theta} N}{\partial \sigma} + \frac{\partial c_{\theta} N}{\partial \theta} = \frac{S_{tot}}{\sigma}. \tag{2}$$

The first term represents the local rate of change in action density; the second term denotes the propagation of wave energy in the two-dimensional geographical space with  $\vec{c}_g$  the group velocity, and  $\vec{U}$  the ambient current. This term can be recast in Cartesian, spherical or curvy-linear coordinates. The third term represents the effect of shifting the relative frequency due to variations in depth and mean currents. The fourth term represents the depth-induced and current-

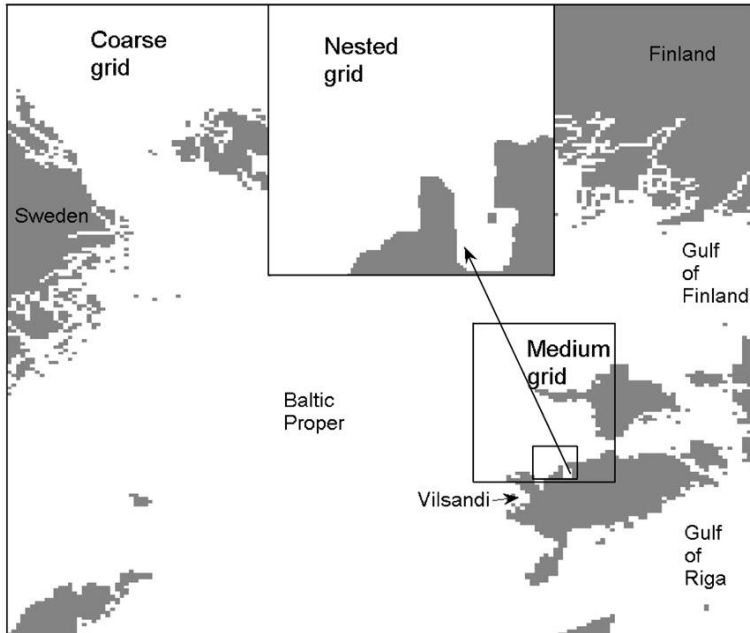


Fig. 2. The coarse, medium and nested wave model grids.

induced refraction. The quantities  $c_\sigma$  and  $c_\theta$  are the propagation velocities in spectral space  $(\sigma, \theta)$  with  $\sigma$  and  $\theta$  representing the relative frequency and the direction of propagation, respectively. The right-hand side contains the source term  $S_{\text{tot}}$  that represents all physical processes that generate, dissipate or redistribute wave energy. In shallow water, six processes contribute to  $S_{\text{tot}}$ :

$$S_{\text{tot}} = S_{\text{wind}} + S_{\text{nl3}} + S_{\text{nl4}} + S_{\text{wc}} + S_{\text{bot}} + S_{\text{db}}. \quad (3)$$

These terms denote respectively the energy input by wind ( $S_{\text{wind}}$ ), the nonlinear transfer of wave energy through three-wave ( $S_{\text{nl3}}$ ) and four-wave interactions ( $S_{\text{nl4}}$ ), and the decay of waves due to whitecapping ( $S_{\text{wc}}$ ), bottom friction ( $S_{\text{bot}}$ ) and depth-induced wave breaking ( $S_{\text{db}}$ ). Extensive details on the formulations of these processes can be found e.g. in Komen et al. (1994).

### 3.2. Model setup

For the present calculations with SWAN, the third-generation model respect to wind-input, quadruplet interactions and whitecapping was used. Triads, bottom friction and depth-induced breaking were also activated. For wind-input and whitecapping dissipation, the formulation by Komen (Komen et al., 1994) was used; in case of wind-input only the exponential growth term was activated. The quadruplet interaction was approximated using the Discrete Interaction Approximation (DIA). The breaking of waves is controlled by the ratio of maximum individual wave height over depth and is set to be 0.73. Semi-empirical expression for bottom friction (see Holthuijsen, 2007) was activated.

Since the K udema Bay is open at the northern side, the wave field generated by northerly winds in the Baltic Proper radiates to the bay, and therefore it is important to take into account the wave calculations of the Baltic Proper. The Bay of Bothnia was not taken into account, because it is expected that waves in Bay of Bothnia do not affect the wave regime in K udema Bay. A medium grid between the coarse Baltic Proper area and the small K udema Bay area was also introduced into the computations as a transitional area for waves. This was needed, since when interpolating spectrum data from coarser resolution to a finer resolution, interpolation errors may occur (Booij et al., 2004). Consequently a triple nested model was used (Fig. 2). The details of the computation area are summarized in Table 1.

The high-resolution bottom topography of the K udema Bay and adjacent sea area was manually digitized from marine chart No 13 submitted by the Estonian Maritime Board. The water depths were interpolated to a model grid using Kriging, a very popular method in geophysical statistics (Cressie, 1993). Although the marine chart is not a precise source of the depth data (last measurements date from the 1980s), it still is the best available data source for the water depths. The data for Baltic Proper was extrapolated from the Baltic Sea topography presented by Seifert et al. (2001).

The model was forced with the Vilsandi's wind data provided by Estonian Meteorological and Hydrological Institute. The wind speeds and directions were interpolated to model time steps: for the coarse run it was 30 min, for the medium run it was 10 min, and for the K udema Bay it was

**Table 1**

Location of origin of the computational grid, number of meshes of the computational grid, mesh sizes of the computational grid, model time step, spectral directions and spectral frequencies

	Coarse grid	Medium grid	Nested grid
Location of origin of $x$ -direction ( $^\circ$ )	18.3167	21.6167	22.035
Location of origin of $y$ -direction ( $^\circ$ )	57.6583	58.4717	58.485
Nr. of meshes in $x$ -direction	160	100	94
Nr. of meshes in $y$ -direction	200	167	104
Mesh size in $x$ -direction ( $^\circ$ )	0.0333	0.01	0.00333
Mesh size in $y$ -direction ( $^\circ$ )	0.0167	0.005	0.0016667
Model time step (min)	30	10	5
Spectral directions	24	24	24
Spectral frequencies	40	40	40

5 min. Because SWAN numerical techniques are implicit, abovementioned time steps suit well.

In every computational grid point, wave energies were calculated for 24 propagation directions and for 40 different frequencies distributed logarithmically on the range of 0.05–1 Hz. The waves that can be simulated with resolutions mentioned latter may have peak periods from 20–1 s.

## 4. Results

### 4.1. Results of the summer measurement campaign

The time series of the significant wave height and the mean zero-crossing period during the summer measurement period are shown on Fig. 3a and b. Mean significant wave height in the summer measurement period was 16 cm. Minimum perturbation was found to be 2 cm, and the maximum significant wave height was 151 cm. The significant wave height was below 20 cm in 77% of the wave packets. However, in the context of small wave heights 1–2-day long wave events could be distinguished, where significant wave height increased over 20 cm. Average wave period was 4.1 s. The shortest period was 3.1 s, and the longest period was 6.2 s. Also, there were periods around 4–5 s during the first half of the measurement period, with the corresponding wave heights rather small (below 4 cm). These periods occurred because the pressure sensor was not reliable for measuring the periods of very small waves. The maximum period was measured on the 10th of August, and the corresponding significant wave height was 20 cm. Associated wind speed was 2 m/s.

In the middle of the summer measurement period (8–9 August) a wave event took place where maximum significant wave height reached 151 cm. Wind speeds during this event rose from 4.5 m/s to 13.3 m/s in 5 h, and the wind was blowing from NNW (Fig. 3c and d). The wave period during the event increased from 3.3 s (at the beginning of the event) to a maximum of 5.3 s.

The mean wind speed during the summer measurement period was 4.4 m/s. Several medium strength wind events (6 m/s to 10 m/s) occurred with corresponding wave heights below 40 cm. Wind was blowing more or less from SE to SW during these events, indicating that land winds generate low waves.

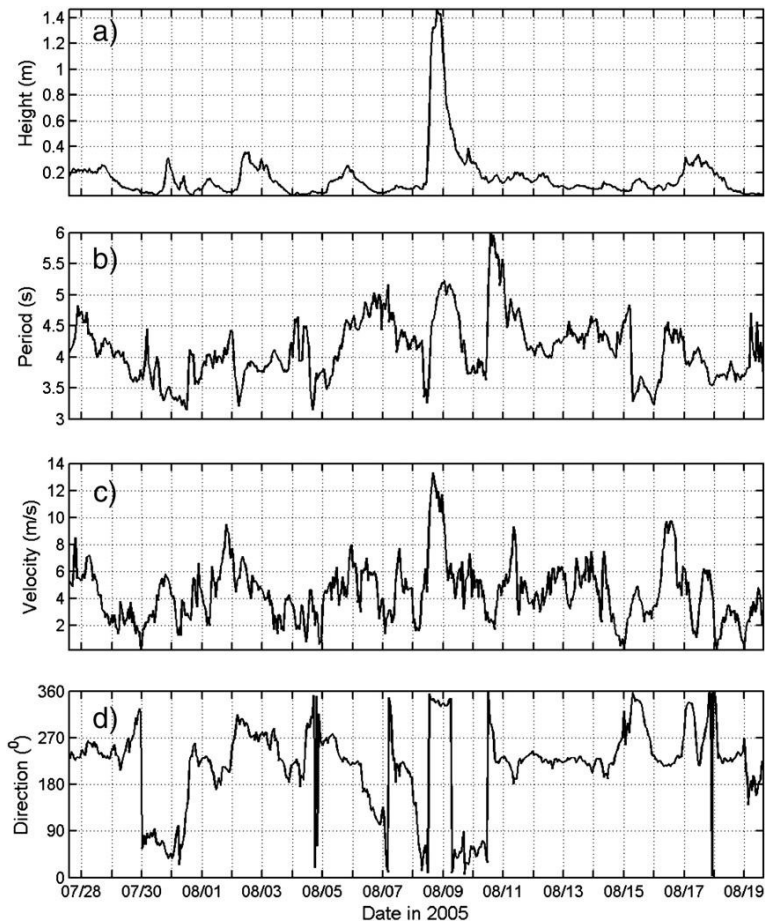


**Fig. 3.** The time series of measured wind and wave data for the deployment from July 27 to August 19, 2005. (a) Significant wave height, (b) Mean zero-crossing period, (c) Vilsandi raw wind speed and (d) Vilsandi raw wind direction.

#### 4.2. Results of the autumn measurement campaign

In the autumn measurement period the mean significant wave height was 24 cm (Fig. 4a). Smallest significant wave height was 5 cm and biggest significant wave height was 120 cm. The mean wave height during the autumn measurement period was higher than in the summer period because the mean wind speed was 3.5 m/s higher, whereas during the summer measurement period the dominating winds were low. Mean wave period in autumn was 4.7 s, the shortest wave period was 2.7 s, and the longest wave period 7.5 s was associated with higher wave activity in the second half of the measurement period.

In the context of medium noise two wave events could be distinguished, where in the first case the wave height was 120 cm, and in the second case it was 97 cm. The first wave event that actually consisted of two events took place from November 13 to 16. At first, the wave height grew from 20 cm to an average of 50 cm. The wind speed was almost 20 m/s (Fig. 4c) and it was blowing from between SSW and W (Fig. 4d). Further on the wind speeds remained below 15 m/s, the wind shortly

blew from the direction of 300–330°, and the significant wave height was almost 120 cm. Second wave event took place from November 18 to 20. The wind speeds remained below 10 m/s, the wind blew from the direction of 350–300°, and the significant wave height reached almost 100 cm.

From the beginning of the measurements through to 14 of November the wind direction fluctuated between S and W, and the wind speed was 5–12 m/s. The significant wave height during this time was mainly under 20 cm, with some exceptions, when wind speed grew over 10 m/s resulting in a wave height up to 40 cm.

#### 4.3. Model data comparison

In Fig. 5 the modelled and measured significant wave height for the summer period are shown. The model is an accurate reproduction of the two wave events at the beginning of the measurement period. The third wave event that occurred on the 2nd of August is slightly overestimated by the model. It is also obvious that the modelled significant wave heights and the measured significant wave heights form

a similar pattern, but occasionally with some time lag. The correlation coefficient between modelled and measured wave heights is 0.92. The root mean square error (RMSE) is 9 cm. The highest wave event was reproduced accurately by the model. The growth and decay of significant wave height between model and measured data coincided fine during this event. The modelled event maximum was at 136 cm, whereas the measured maximum was 151 cm, and the time lag between maxima was 20 min. One remarkable item is that at the decay phase of the significant wave height, there was some growth of measured waves, which was also almost exactly reproduced by the model.

The time series comparisons of modelled and measured peak periods in the summer measurement campaign are shown in Fig. 6. It can be seen that the measured peak periods are always higher than the modelled ones, which is indicated by the RMSE of 2.6 s. It is hard to see any regular patterns between measured and modelled data during the periods of land winds. Only during the highest wave event, the pattern between modelled and measured peak periods is obvious, and at the maxima of that event, the modelled peak period is only 1 s lower than the measured one.

In Fig. 7 the modelled significant wave height and the measured one of the second measurement period are illustrated. During the period of low wave activity the modelled significant wave height is systematically higher than the measured one. This is also emphasized by the mean bias, which is 18 cm. The RMSE is 22 cm, and the correlation coefficient is 0.58, showing less similarity between model and data than in the summer period. The first wave event shows some differences in the structure of the event between model and data. In the measurements the increase of significant wave height was cut off during the first half of the development, while it grew continuously in the model. The peak value was reached simultaneously in the model and the measurements, but the latter had a value that was 15 cm lower. The drops of significant wave height coincide in time. The second wave event was well reproduced by the model in terms of timing, but was underestimated in terms of height.

The modelled peak periods and measured ones are compared for the autumn measurements campaign (Fig. 8). The modelled peak periods are much lower than the measured ones during the period of low wave activity. The

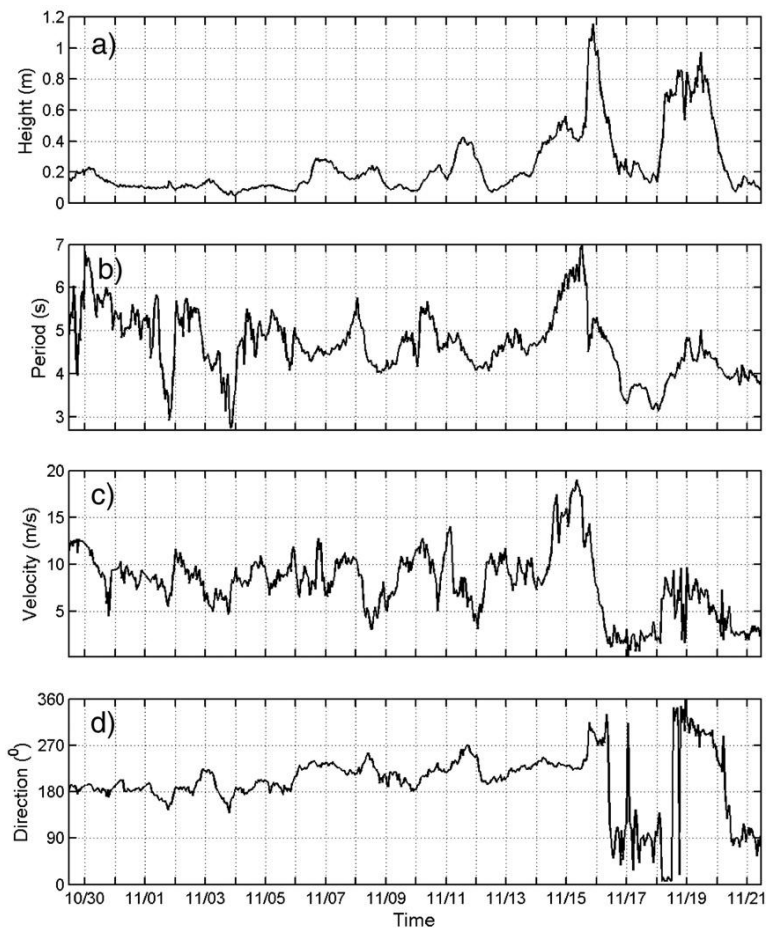
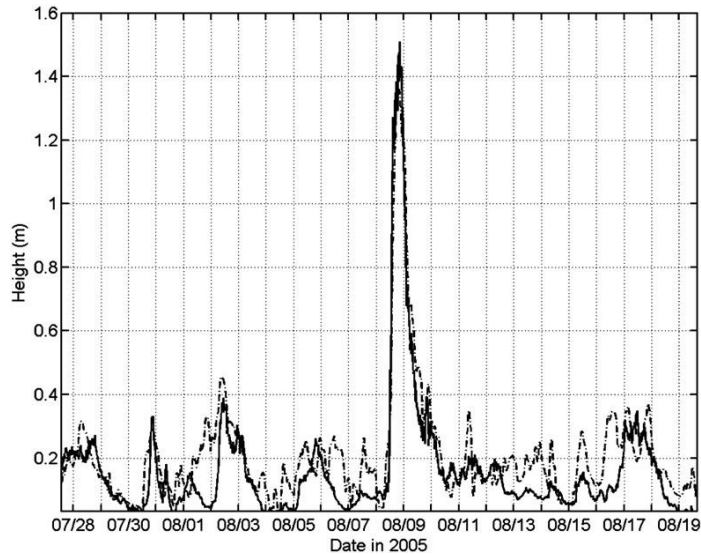


Fig. 4. Same as Fig. 3 but the deployment was from October 29 to November 21.



**Fig. 5.** Time series comparison of significant wave height between SWAN (dashed line) hindcast and the measured data (solid line) for summer measurement period.

mean bias is 3.6 s, and RMSE is 4 s for the whole measurement period. The comparison improves during the wave events.

#### 4.4. Typical and extreme wave heights based on modelling

The distribution of the modelled significant wave height on the 8th of August at 17:00 (UTC) is shown in Fig. 9. This corresponds to the maximum of the modelled wave field, which was created by NNW winds blowing as high as 13.3 m/s. It is clear that the significant wave height at the entrance of the

bay is 1.5 m. As the waves propagate south, the wave height decays due to bottom friction. Therefore the northern part of the bay exhibits higher waves than the southern (lower) part of the bay.

An average of the time integrated wave field of the modelled wave heights from 30th October to 14th November is presented in Fig. 10. This distribution represents the typical situation occurring in the bay in case of S–SW moderate winds, which are prevailing. The high values of wave heights in the lower part of the bay are not realistic. Significant wave height in the centre of

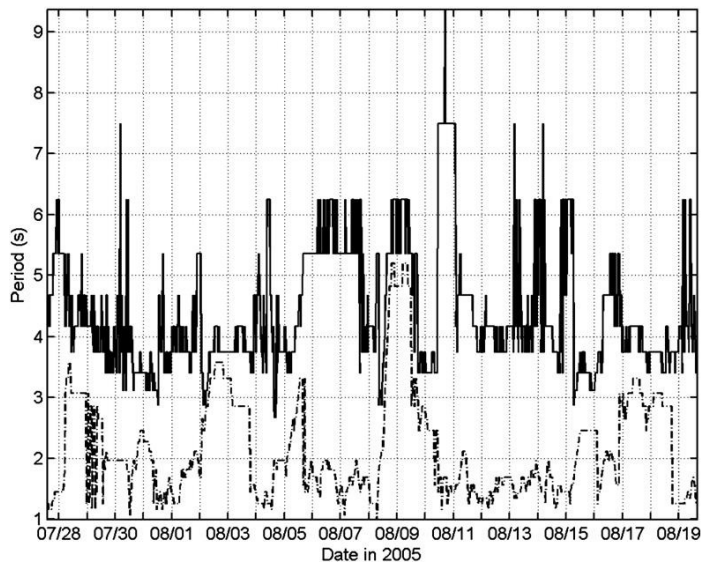


**Fig. 6.** Time series comparison of peak periods between SWAN (dashed line) hindcast and the measured data (solid line) for summer measurement period.

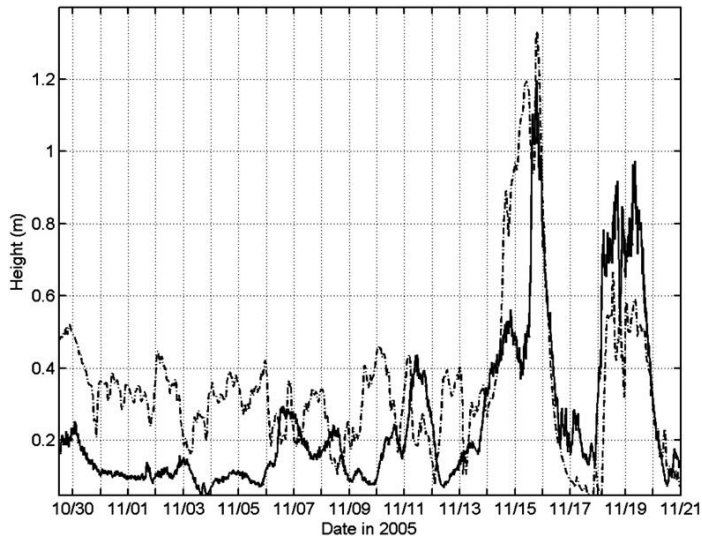


Fig. 7. Same as Fig. 5 but for autumn measurement period.

the bay is 30–40 cm, and increases to 60 cm as one move further away from the bay. Due to the wind direction, the east coast exhibits higher waves than the west coast.

## 5. Discussion

The wind regime in the Baltic Proper area is more or less anisotropic (Soomere, 2003), which also leads to an anisotropy of waves. Based on the measurements conducted at Vilsandi during the summer and autumn measurement campaigns, the distribution of wind direction did not differ significantly from the long-term direction. The most frequent winds were blowing either from south or southwest. South,

south-westerly winds have a short fetch length and therefore the waves in the bay were small, which is also indicated by the measurements. During the measurement campaigns the mean speeds of land winds were below 15 m/s, and the corresponding wave heights during the time were below 40 cm.

Fetch plays an important role in the growth of waves. The best illustration is when two wave events are compared. During the first measurement period, the highest wave height was 151 cm, the greatest wind speed was 13.3 m/s, and its direction was NNW. The bay is fully open to that direction, and the fetch length is about 100 nmi. During the second measurement period, the wave height reached 55 cm. The

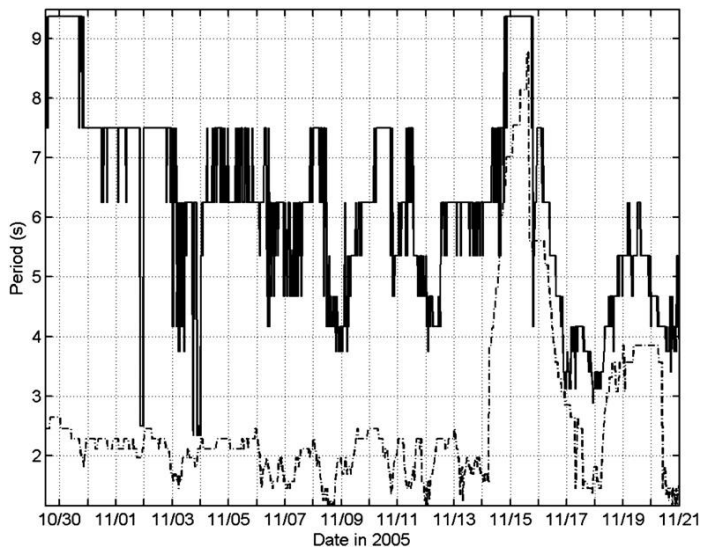


Fig. 8. Same as Fig. 6 but for autumn measurement period.

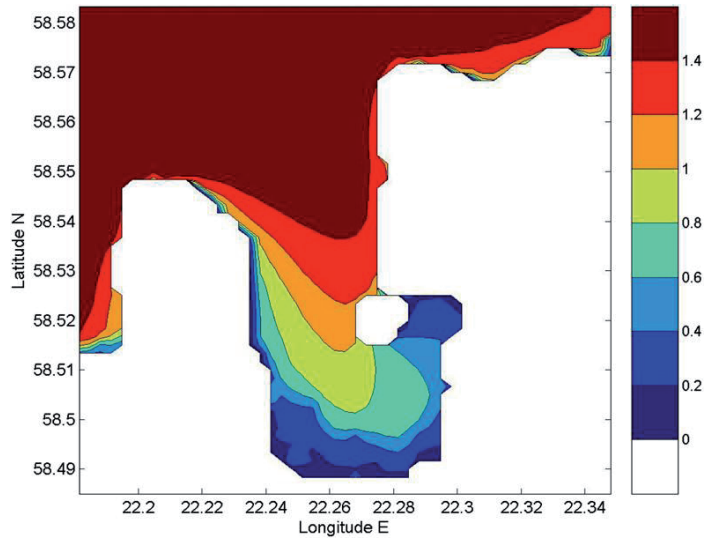


Fig. 9. The  $H_{m0}$  field distribution by SWAN for August 8, 2005 at 1700 UTC. Contour levels are in metres.

associated wind speed was almost 20 m/s blowing from SSW. The fetch was 2 nmi at most.

The wave periods in Küdema Bay are somewhat longer than usual. As for comparison, in the Tallinn Bay (Soomere, 2005), the mean periods of wind waves are 2 s, or for a more distant example, in the Chesapeake Bay (Lin et al., 2002), the mean peak periods are around 2–4 s. The time series contour plots of the spectral densities of the summer and autumn measurement campaigns are shown in Figs. 11 and 12, respectively. Most of the wave energy is concentrated in the range of 0.2 to 0.3 Hz. During the wave events the spectral peak shifts to lower frequencies; the latter is consistent with linear wave theory, and is observed frequently. In contrast,

during the first measurement period, on the 10th of August, the mean period grew to 6 s. This is also indicated in the spectrum, where a group of higher energy is at low values (Fig. 11). The spectral width parameter  $\epsilon$  (WMA, 1998) during this event was 0.55, indicating that the spectrum was broad and swell was not present.

Model data comparison reveals that SWAN represents quite well the significant wave heights in Küdema Bay. The model predicted very well the wave events occurring in summer, and the first wave event in autumn, but underestimated the second wave event occurring in autumn. In case of land winds the model frequently overestimated the measured ones. The Küdema Bay is sheltered with a bluff,

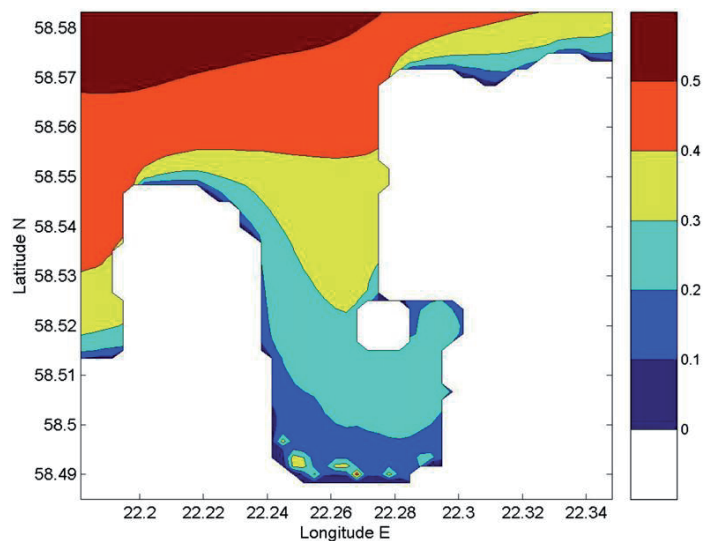


Fig. 10. The averaged  $H_{m0}$  field distribution by SWAN from October 29 till November 14. Contour levels are in metres.

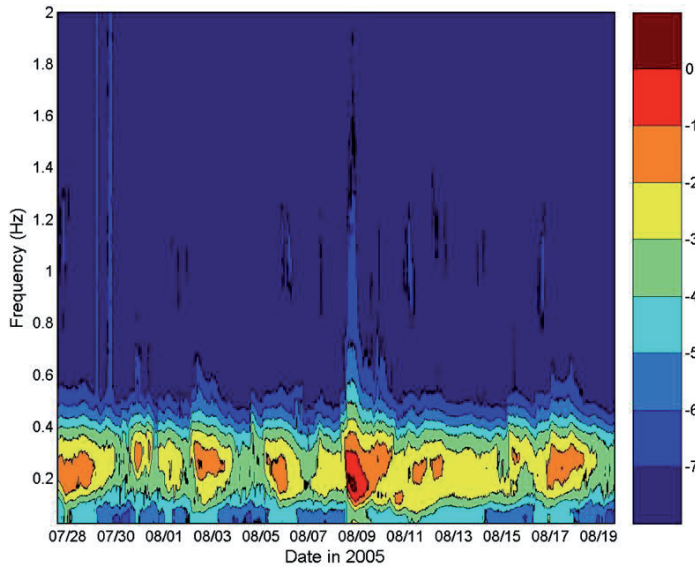


Fig. 11. Time series of the power spectrum density of summer measurement period. The unit of energy density is ( $\text{m}^2/\text{Hz}$ ) and the scale is logarithmic.

and it is estimated that the cause of the modelled wave height being higher with land winds is due to the screening effect that the bluff has upon winds blowing from shore. This screening effect has been reported earlier by Elken et al. (2001).

The model strongly underestimates the peak wave periods. This underestimation has long been known in the SWAN. For pure wind sea, the energy density at lower frequencies is typically underestimated, whereas energy levels in tail are generally overestimated. These leave both

the peak and mean periods underestimated (Westhuysen et al., 2007). There are several explanations for that. For example, Westhuysen et al. (2007) demonstrate that the peak period underestimation by SWAN is partly due to the use of DIA, which is an approximation of the complete set of quadruplet interactions. Another explanation is based on the definition of the whitecapping source term, which is currently represented in SWAN by the pulse-based, quasi-linear model (Booij et al., 1999). Westhuysen et al. (2007) suggest a new saturation-based model, which leads to more accurate results.

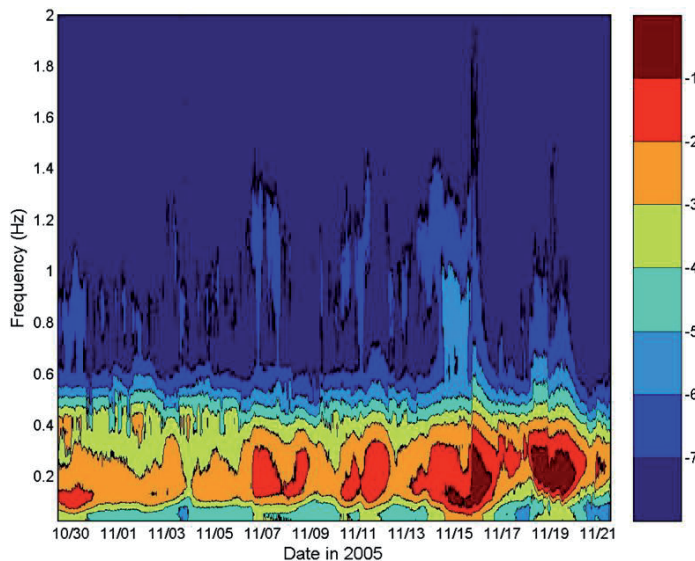


Fig. 12. Same as Fig. 11 but of autumn measurement period.

Model results of typical and extreme wave fields in the bay show some spatial variability of waves in the bay. During NWW storms significant wave heights are high in the entrance of the bay, and decay while penetrating into the bay. Also, near the harbour the wave heights during NWW storms are comparable to those in the centre of the bay. Consequently, the sea area adjacent to the harbour exhibits high wave activity during storms. The soft wave activity in the bay (Fig. 10) is a direct result of winds, since prevailing winds come from S, SSW or SW and therefore the fetch length is small.

## 6. Conclusions

The wave regime of the Küdema Bay was analysed on the basis of wave measurements, and with the use of numerical modelling. The measurements were conducted during two seasons, in summer and in autumn, which represent different wind regimes. Although the measurement period was shorter than used in studies of the wave regime of oceanic environments, it is long enough to characterize the typical wind wave regime of the Küdema Bay, since the wind regime in the Baltic Proper and adjacent sea area is anisotropic. This anisotropy was also prevailing in the wind measurements made in the summer and the autumn of 2005. The conclusions are:

- Wind waves in the Küdema Bay are dominated by locally-generated fetch-limited wind waves.
- Land winds with speeds of up to 15 m/s do not generate significant wave heights higher than 40 cm.
- North-westerly winds of up to 13 m/s are able to generate waves as high as 1.5 m at the measurement site.
- Typical wind wave periods in the bay are between 3 and 5 s.
- The wind speed and direction are both equally important for the wave growth in the bay.
- Modelled significant wave heights and measured ones correlated well, and therefore SWAN gives good representation of the significant wave heights.
- SWAN does not adequately represent the spectral shape of the waves, resulting thus in large underestimation of peak periods.
- The overall wave regime indicated by measurements and modelling is modest, but with strong NWW storms high waves may penetrate into the bay.

## Acknowledgments

We are grateful to the Estonian Meteorological and Hydrological Institute (EMHI) for providing the wind data from Vilsandi's weather station. This work was supported by Tallinn Port through contract nr. 544L.

## References

- Booij, N., Ris, R.C., Holthuijsen, L.H., 1999. A third-generation wave model for coastal regions. 1. Model description and validation. *J. Geophys. Res.* C104, 7649–7666.
- Booij, N., Haagsma, I.J.G., Holthuijsen, L.H., Kieftenburg, A.T.M.M., Westhuysen, A.J. van der, Zijlema, M., 2004. SWAN Cycle III version 40.41 User Manual. Delft University of Technology.
- Breugem, A. 2003. A reanalysis of the wave observations in Lake Georgia. Master's thesis, Delft University of Technology.
- Cressie, N.A.C., 1993. *Statistics for spatial data*. Wiley.
- Elken, J., Kask, J., Kõuts, T., Liiv, U., Perens, R., Soomere, T., 2001. Hydrodynamical and geological investigations of possible deep harbour sites in north-western Saaremaa Island: overview and conclusions. *Proc. Est. Acad. Sci., Eng.* 7 (2), 85–98.
- Holthuijsen, L.H., 2007. *Waves in oceanic and coastal waters*. Cambridge University Press.
- Jönsson, A., 2006. A model study of suspended sand due to surface waves during a storm in the Baltic Proper. *J. Mar. Syst.* 63, 91–104.
- Komen, G.J., Cavaleri, L., Donelan, M., Hasselmann, K., Hasselmann, S., Janssen, P.A.E.M., 1994. *Dynamics and modelling of ocean waves*. Cambridge University Press.
- Lin, W., Sanford, L.P., Suttles, S.E., 2002. Wave measurement and modeling in Chesapeake Bay. *Cont. Shelf Res.* 22, 2673–2686.
- Liu, P.C., 2000. Is the wind wave frequency spectrum outdated. *Ocean Eng.* 27, 577–588.
- Pettersson, H. 2004. Wave growth in a narrow bay. Ph.D. thesis, Finnish Institute of Marine Research. Contributions no. 9.
- Seifert, T., Kayser, B., Tauber, F., 2001. Bathymetry data of the Baltic Sea. Baltic Sea Research Institute, Warnemünde.
- Signell, R.P., Carniel, S., Cavaleri, L., Chiggiato, J., Doyle, J.D., Pullen, J., Scavo, M., 2005. Assessment of wind quality for oceanographic modelling in semi-enclosed basins. *J. Mar. Syst.* 53, 217–233.
- Soomere, T., 2001a. Wave regimes and anomalies off north-western Saaremaa Island. *Proc. Est. Acad. Sci., Eng.* 7 (2), 157–173.
- Soomere, T., 2001b. Extreme wind speeds and spatially uniform wind events in the Baltic Proper. *Proc. Est. Acad. Sci., Eng.* 7 (3), 195–211.
- Soomere, T., 2003. Anisotropy of wind and wave regimes in the Baltic Proper. *J. Sea Res.* 49, 305–316.
- Soomere, T., 2005. Wind wave statistics in Tallinn Bay. *Boreal Environ. Res.* 10, 103–118.
- Tsai, Cheng-Han, Huang, Min-Chih, Young, Fu-Ji, Lin, Yin-Chern, Li, Hsien-Wen, 2005. On the recovery of surface wave by pressure transfer function. *Ocean Eng.* 32, 1247–1259.
- Westhuysen, van der A.J., Zijlema, M., Battjes, J.A., 2007. Nonlinear saturation-based whitecapping dissipation in SWAN for deep and shallow water. *Coast. Eng.* 54, 151–170.
- World Meteorological Association, 1998. *Guide to wave analysis and forecasting*.



## ACKNOWLEDGEMENTS

“Life is not easy for any of us. But what of that?  
We must have perseverance and above all confidence in ourselves.  
We must believe that we are gifted for something and that this thing must be  
attained.”

*Marie Curie*

I would like to share gratitude and deep respect upon my scientific advisor and a friend, Dr. Urmas Raudsepp. It was a brave step for him to start supervising me 8.5 years ago, when I was just a school-kid, knowing zero of science. Thank you for believing in me!

Ilja my pal, you are the only person in the world to whom I can turn to when everybody else have lost their head. I'm privileged to know you.

It is of no secrets that Marine Systems Institute has become my second home, literally, and the nice people working there my second family. I would like to thank the whole staff but especially the leader, Prof. Jüri Elken, for being a real gentleman, as this is a rare characteristic among topguns. Senior staff who have broadened and enriched my view of (scientific) life are: Dr. Kõuts, Dr. Erm, Dr. I.Lips, Prof. U.Lips, Dr. Laanemets, Dr. Lilover, Dr. Lessin, Dr. Pärn, Prof. Keevallik. Young scientists and graduate students, who have to tolerate me: Dr. Uiboupin, Dr. Lagemaa, Dr. Väli, G. Haran, E. Soosaar, L. Raag, S.Rikka, N. Kolesova, F. Buschmann, Jaak Karjane. My students Marili and Ingvar have forced me to Really study and understand waves. Peeter Laas, thank you for the inspiring discussions on biology and other issues.

Friends – Madis L., Silver S. and Aleksander V., thank you! Friends from Delft University of Technology – thank you for making my visit memorable and nice!

The work was financially supported through Estonian Science Foundation grant ETF8968. The author wishes to thank SA Archimedes, who has made possible my stay at Delft University of Technology. Estonian Meteorological and Hydrological Institute is appreciated for providing meteorological data. The papers forming this thesis are reprinted with the kind permission from the publishers.

Finally, the two most important persons in my life: Aelica Alari and Kai Ristikivi. Without your cognitive and emotional support would I be where I am? No.

## ABSTRACT

The aim of this thesis was to improve the knowledge of near-coastal wave field variability in the Baltic Sea. The focus was on studying depth-induced wave breaking, whitecapping dissipation and temporally varying water level and to quantify wave-induced flow and set-up. The effect of arrays of small obstacles to wave field evolution was also studied. The Simulating Waves Nearshore (SWAN) model covering multiple spatial scales (grid size varying from 2 km down to 25 m) was used to achieve the aims. The SWAN model coupled to a phase-resolving wave model and to a hydrodynamic model allowed estimation of wave-induced set-up and flow, respectively. It was shown that near-coastal wave fields were heterogeneous on spatial scales, as well as in temporal scales.

Effects of surge upon wave field evolution and wave-induced set-up were studied during cyclone Gudrun (January 2005) in a shallow bay. Significant wave height increases by taking into account the additional deepening of water due to surge. The increase in significant wave height is correlated with water depth and surge. During peak surge (2.7 m) wave height increases maximally 0.3 m in areas where water is deeper than 10 m, but up to 1 m when water is shallower than 5 m. During low surge (< 1 m) wave height increase is not so profound. The transformation of sea state with initial conditions of 1.8 m significant wave height and 5.2 s peak period results in wave induced setup of 0.51 m and additional inundation of 130 m at the Pärnu coast, as calculated by the phase-resolving wave model.

Depth-induced wave breaking is an important mechanism in dissipating wave energy in shallow water. In the case of a  $23 \text{ m s}^{-1}$  NNW storm the depth induced wave breaking reduced significant wave height up to 2.3 m in a semi-sheltered bay, compared to a situation when this source term is inactive. Considerable dissipation due to depth-induced breaking in high winds commences in the Baltic Sea when water depth is less than 20 m. Wave breaking dissipation was up to five times as intense in depth range between 4-10 m during cyclone Gudrun compared to dissipation due to bottom friction.

Calculations with two wind speeds of  $8 \text{ m s}^{-1}$  and  $15 \text{ m s}^{-1}$  with varying fetches were made to assess the influence of arrays of obstacles (wind turbines) to significant wave height. Obstacles influenced wave field marginally, reducing significant wave heights in the nearby surf zone less than 1 %. This stems from the low obstacle-to-crest ratio in the particular cases, which limited the diffraction, scattering and breaking of incident wave field.

The effect of the whitecapping formulations on peak period was studied. Nonlinear saturation based whitecapping reduced the difference between modeled and measured peak periods to 3 %, while the quasi-linear pulse based model underestimated peak period by 18 %.

Wave induced near-bed orbital flow and currents resulting from spatial gradients in wave energy were investigated in the Suur Strait under non-

stationary wind in November 2008. Numerical simulations with added wave stress as forcing in a hydrodynamic model showed a minor influence of wave field to overall water exchange. This was the case in a narrow channel dominated by barotropic currents. However, wave induced currents were dominating over wind driven currents at local scales. The maximum wave induced current speed was  $16 \text{ cm s}^{-1}$ . Wave induced shear velocities considerably exceeded the threshold for resuspension in a narrow channel at instances, when current induced shear velocity favored deposition.

## RESÜMEE

Käesolevas töös uuriti rannalähedaste laineväljade muutlikkust Läänemeres. Fookuses oli merepõhja indutseeritud murdumise, *whitecapping*'u ja ajas muutuva veetaseme mõju uurimine laineväljade arengus ning lainetuse tekitatud lisaveetaseme tõusu ning hoovuste kvantifitseerimine. Lisaks uuriti grupeeritud väikeste objektide (tuuleturbiinid) mõju laineväljade kujunemisele. Töö eesmärkide saavutamiseks kasutati spektraalset lainemudelit SWAN, kus mudeli võrgusamm varieerus kahest kilomeetrist kuni 25 meetrini. Lainetuse tekitatud lisaveetaseme tõusu kvantifitseerimiseks kasutati kombineeritud spektraalset ja faasilahutusega lainemudeleid. Lainetuse indutseeritud hoovused arvutati kombineeritud spektraalset lainemudelit ning kahemõõtmelist hüdrodünaamika mudelit kasutades. Näidati, et rannikulähedased laineväljad on väga heterogeensed nii ruumis kui ajas.

Hinnati 2005. aasta jaanuaritormi tekitatud veetaseme tõusu mõju olulise lainekõrguse muutlikkusele Pärnu lahes ning samas lainetuse tekitatud lisaveetaseme-tõusu. Oluline lainekõrgus kasvab, kui võtta arvesse tuulest tingitud veetaseme tõus ning lainekõrguse kasv sõltub veesügavusest ja veetaseme tõusust. Maksimaalse veetaseme tõusu korral (2,7 m) suurenes oluline lainekõrgus kuni 0,3 m merealadel, kus veesügavus oli üle 10 m. Alla 5 m veesügavusega kohtades suurenes oluline lainekõrgus kuni 1 m. Väikese veetaseme tõusu mõju ( $< 1$  m) lainekõrguse kasvule oli tagasihoidlik. Lainetusest tingitud lisaveetaseme tõus 2005. aasta jaanuaritormi ajal Pärnu rannas oli 0,51 m ning üleujutatud ala kaugus rannast 130 m. See toimus oludes, kus enne murdumist oli oluline lainekõrgus 1,8 m ning piigi periood 5,2 s.

Merepõhja indutseeritud tuulelainetuse murdumine on oluline laineenergiat vähendav mehhanism madalas vees.  $23 \text{ m s}^{-1}$  puhuva põhjaloo tormi ajal vähendas merepõhja indutseeritud murdumine poolsuletud lahes olulist lainekõrgust kuni 2,3 m. Läänemeres tuleb arvestada merepõhja indutseeritud murdumisega piirkondades, kus veesügavus on väiksem kui 20 m. Veesügavusvahemikus 4–10 m oli merepõhja indutseeritud murdumine 2005. a. jaanuaritormi ajal viis korda intensiivsem kui põhjahõrdest tingitud energia vähenemine.

Paljude väikeste objektide mõju olulise lainekõrguse muutumisele hinnati  $8 \text{ m s}^{-1}$  ja  $15 \text{ m s}^{-1}$  puhuvate tuulte korral. Oluline lainekõrgus vähenes kuni 1% takistustest allatuult jääval rannalähedasel merealal. Marginaalne mõju oli tingitud väikesest takistuse diameetri ja lainepikkuse suhtest, mistõttu lainevälja difraktsioon ja hajumine olid väikesed.

Kahe erineva *whitecapping*'u formuleeringu võrdlemisel selgus, et piigi periood on paremini hinnatud, kui kasutada *whitecapping*'u formuleeringul lokaalset lainearvu keskmise lainearvu asemel, mõõtmistega võrreldes oli erinevus vastavalt 3% ja 18%.

Lainetuse tekitatud põhjalähedasi nihkekiirusi ning lainetusest tingitud

hoovusi uuriti Suures Väinas mittestatsionaarsete tuulte korral. Arvutused näitasid, et lainetuse tingitud hoovused ei oma olulist rolli üldise veevahetuse kujunemisel väinas, kus barotroopsed hoovused on domineerivad. Samas olid lainetuse tekitatud hoovused lokaalselt olulised, ulatudes kuni  $16 \text{ cm s}^{-1}$ . Lainetuse tekitatud nihkekiirused ületasid tunduvalt resuspensiooniks vajaliku läve ajamomentidel, kui barotroopsete hoovuste nihkekiirus polnud piisav resuspensiooni tekitamiseks.

## ELULOOKIRJELDUS

### 1. Isikuandmed

Ees- ja perekonnanimi Victor Alari  
Sünniaeg ja -koht 01.04.1989 Tallinn, Eesti  
Kodakondsus Eestlane

### 2. Kontaktandmed

Aadress Akadeemia tee 15a, Tallinn, Eesti  
Telefon +372 6204307  
E-posti aadress victor.alari@msi.ttu.ee

### 3. Hariduskäik

Õppeasutus (nimetus lõpetamise ajal)	Lõpetamise aeg	Haridus (eriala/kraad)
Tallinna Tehnikaülikool	2012	Maa-teadused/Magistrikraad
Tallinna Tehnikaülikool	2011	Tehniline füüsika/Bakalaureuse kraad
Tallinna Vanalinna Täiskasvanute Gümnaasium	2009	Keskharidus

### 4. Keelteoskus (alg-, kesk- või kõrgtase)

Keel	Tase
Eesti	Emakeel
Inglise	Kõrgtase
Vene	Algtase

### 5. Täiendusõpe

Õppimise aeg	Täiendusõppe läbiviija nimetus

### 6. Teenistuskäik

Töötamise aeg	Tööandja nimetus	Ametikoht
2013-...	Tallinna Tehnikaülikooli Meresüsteemide Instituut	Nooremteadur

2013	Delfti Tehnikaülikool, Holland	Stażöör
2011-2012	Tallinna Tehnikaülikooli Üliõpilasesindus	Teadusspetsialist
2006-2012	Tallinna Tehnikaülikooli Meresüsteemide Instituut	Tehnik

7. Teadustegevus - publikatsioonid Eesti Teadusinfosüsteemi klassifikaatori 1.1, 1.2 ja 3.1 järgi

1.1

- **Alari, V.**, Raudsepp, U. 2012. Simulation of wave damping near coast due to offshore wind farms. *Journal of Coastal Research*. 28(1), 143-148.
- Erm, A., **Alari, V.**, Lips, I., Kask, J. 2011. Resuspension of sediment in a semi-sheltered bay due to wind waves and fast ferry wakes. *Boreal Environment Research*. 16, 149-163.
- Raudsepp, U., Laanemets, J., Haran, G., **Alari, V.**, Pavelson, J., Kõuts, T. 2011. Flow, waves and water exchange in the Suur Strait, the Gulf of Riga in 2008. *Oceanologia*, 53(1), 35-56
- **Alari, V.**, Raudsepp, U. 2010. Depth induced breaking of wind generated surface waves in Estonian coastal waters. *Boreal Environment Research*, 15, 295-300.
- **Alari V**, Raudsepp U, Kõuts T. 2008. Wind wave measurements and modelling in Küdema Bay, Estonian Archipelago Sea, *Journal of Marine Systems*, 74, S30-S40.

1.2

- Erm, A., **Alari, V.**, Madis, L. 2009. Monitoring wave-induced sediment resuspension. *Estonian Journal of Engineering*, 15(3), 196 - 211.

3.1

- **Alari, V.**, Kõuts, T. 2012. Simulating wave-surge interaction in a non-tidal bay during cyclone Gudrun in January 2005. *IEEE/OES Baltic 2012 International Symposium: May 8-11, 2012, Klaipeda, Lithuania*.
- Buschmann, F., Erm, A., **Alari, V.**, Listak, M., Rebane, J., Toming, G. 2012. Monitoring sediment transport in the coastal zone of Tallinn Bay. *IEEE/OES Baltic 2012 International Symposium: May 8-11, 2012, Klaipeda, Lithuania*.
- **Alari, V.**, Raudsepp, U. 2010. Comparison of ADV measured near bed orbital speed and latter derived from wave gauge measurements at intermediate water depths. *IEEE/OES Baltic 2010 International Symposium: August 25-27, 2010, Riga, Latvia*.
- Erm, A., **Alari, V.**, Buschmann, F., Kõuts, T., Raudsepp, U., Loitjäär, K. 2010. Near bottom velocity and turbidity measurements in coastal

waters of NW Estonia. *IEEE/OES Baltic 2010 International Symposium: August 25-27, 2010, Riga, Latvia.*

- Haran, G., Raudsepp, U., **Alari, V.**, Uiboupin, R., Sipelgas, L., Erm, A. 2010. Operational observations methods during offshore sand mining – case study in Tallinn Bay, southern Gulf of Finland. *IEEE/OES Baltic 2010 International Symposium: August 25-27, 2010, Riga, Latvia.*
- Kolesova, N., Raudsepp, U., **Alari, V.** 2010. Dominant zoobenthic species in the northwestern coastal sea of Estonia – potential role of abiotic stresses. *IEEE/OES Baltic 2010 International Symposium: August 25-27, 2010, Riga, Latvia.*
- Erm, A., **Alari, V.**, Kõuts, T. 2008. Transport of sediments resuspended by ferries. *IEEE/OES Baltic 2008 International Symposium: May 27-29, 2008, Tallinn, Estonia.*
- **Alari, V.**, Erm, A., Väli, G., Lips, I., Lips, U. 2008. Optical properties of North-Eastern Baltic Sea in spring and summer 2007. *IEEE/OES Baltic 2008 International Symposium: May 27-29, 2008, Tallinn, Estonia.*

#### Teaduspreemiad ja -tunnustused

2011, Victor Alari; Eesti Teaduste Akadeemia teadusauhind üliõpilastele  
2011, Victor Alari; TalveAkadeemia teadusartiklite konkurss; I preemia bakalaureuse ja magistrantuuri astmes  
2010, Victor Alari; TTÜ Üliõpilaste Teadustööde Konkurss; I preemia loodus- ja täppisteaduste valdkonnas  
2010, Victor Alari; Üliõpilaste teadustööde riiklik konkurss. I preemia loodusteaduste ja tehnika valdkonnas bakalaureuse kategoorias.  
2006, Victor Alari; Õpilaste teadustööde riikliku konkursi I preemia põhikooli astmes.

#### Teadustöö põhisuunad

Tuulelainete mõõtmine ja numbriline modelleerimine. Lainetuse indutseeritud setete resuspensioon ja transport. Lainetuse interaktsioon vesiehitistega. Lainetuse tekitatud veetaseme tõus ja hoovused. Lainetuse operatiivne prognoos. Lainekliima analüüs. Lainemudelite arendamine. Mittestruktureeritud võrgud.

#### Uurimisprojektid

Kokku üle 30 teadus/insenertehnilise projekti, loetelus ainult käimasolevad

*Eesti teadusfondi grandid*

-Lainetuse tekitatud hoovused ja meretaseme tõus rannikumers (2011-2014)

*Siseriiklikud projektid*

-Eesti kliima ja keskkonnaseisundi võimalike muutuste hindamine atmosfääri-, mere- ja jõgede äravoolu dünaamiliste mudelite tulemuste põhjal (KESTA, 2011-2014)

*Rahvusvahelised projektid*

-Innovaatiline lainetuse prognoosisüsteem laevade ohutuks navigatsiooniks (EUROSTARS, 2011-2014)

# CURRICULUM VITAE

## 1. Personal data

Name Victor Alari  
Date and place of birth 01 April 1989, Tallinn, Estonia

## 2. Contact information

Address Akadeemia Rd. 15a, Tallinn  
Phone +372 6204307  
E-mail victor.alari@msi.ttu.ee

## 3. Education

Educational institution	Graduation year	Education (field of study/degree)
Tallinn University of Technology	2012	Earth sciences/Masters degree
Tallinn University of Technology	2011	Engineering physics/Bachelor degree

## 4. Language competence/skills (fluent; average, basic skills)

Language	Level
Estonian	Native
English	Fluent
Russian	Basic skills

## 5. Special Courses

Period	Educational or other organisation

## 6. Professional Employment

Period	Organisation	Position
2013-...	Tallinn University of Technology, Marine Systems Institute	Junior research fellow
2013	Delft University of Technology	Trainee
2006-2012	Tallinn University of Technology, Marine Systems Institute	Other staff

## 7. Scientific work - Publications according to Estonian Research Information System

### 1.1 (Articles indexed by the ISI WEB of Science)

- **Alari, V.**, Raudsepp, U. 2012. Simulation of wave damping near coast due to offshore wind farms. *Journal of Coastal Research*. 28(1), 143-148.
- Erm, A., **Alari, V.**, Lips, I., Kask, J. 2011. Resuspension of sediment in a semi-sheltered bay due to wind waves and fast ferry wakes. *Boreal Environment Research*. 16, 149-163.
- Raudsepp, U., Laanemets, J., Haran, G., **Alari, V.**, Pavelson, J., Kõuts, T. 2011. Flow, waves and water exchange in the Suur Strait, the Gulf of Riga in 2008. *Oceanologia*, 53(1), 35-56
- **Alari, V.**, Raudsepp, U. 2010. Depth induced breaking of wind generated surface waves in Estonian coastal waters. *Boreal Environment Research*, 15, 295-300.
- **Alari V.**, Raudsepp U, Kõuts T. 2008. Wind wave measurements and modelling in Küdema Bay, Estonian Archipelago Sea, *Journal of Marine Systems*, 74, S30-S40.

### 1.2 (Pre-reviewed articles in other international research journals)

- Erm, A., **Alari, V.**, Madis, L. 2009. Monitoring wave-induced sediment resuspension. *Estonian Journal of Engineering*, 15(3), 196 – 211.

### 3.1 (Articles in proceedings indexed by the ISI WEB of Science)

- **Alari, V.**, Kõuts, T. 2012. Simulating wave-surge interaction in a non-tidal bay during cyclone Gudrun in January 2005. *IEEE/OES Baltic 2012 International Symposium: May 8-11, 2012, Klaipeda, Lithuania*.
- Buschmann, F., Erm, A., **Alari, V.**, Listak, M., Rebane, J., Toming, G. 2012. Monitoring sediment transport in the coastal zone of Tallinn Bay.

*IEEE/OES Baltic 2012 International Symposium: May 8-11, 2012, Klaipeda, Lithuania.*

- **Alari, V.**, Raudsepp, U. 2010. Comparison of ADV measured near bed orbital speed and latter derived from wave gauge measurements at intermediate water depths. *IEEE/OES Baltic 2010 International Symposium: August 25-27, 2010, Riga, Latvia.*
- Erm, A., **Alari, V.**, Buschmann, F., Kõuts, T., Raudsepp, U., Loitjäär, K. 2010. Near bottom velocity and turbidity measurements in coastal waters of NW Estonia. *IEEE/OES Baltic 2010 International Symposium: August 25-27, 2010, Riga, Latvia.*
- Haran, G., Raudsepp, U., **Alari, V.**, Uiboupin, R., Sipelgas, L., Erm, A. 2010. Operational observations methods during offshore sand mining – case study in Tallinn Bay, southern Gulf of Finland. *IEEE/OES Baltic 2010 International Symposium: August 25-27, 2010, Riga, Latvia.*
- Kolesova, N., Raudsepp, U., **Alari, V.** 2010. Dominant zoobenthic species in the northwestern coastal sea of Estonia – potential role of abiotic stresses. *IEEE/OES Baltic 2010 International Symposium: August 25-27, 2010, Riga, Latvia.*
- Erm, A., **Alari, V.**, Kõuts, T. 2008. Transport of sediments resuspended by ferries. *IEEE/OES Baltic 2008 International Symposium: May 27-29, 2008, Tallinn, Estonia.*
- **Alari, V.**, Erm, A., Väli, G., Lips, I., Lips, U. 2008. Optical properties of North-Eastern Baltic Sea in spring and summer 2007. *IEEE/OES Baltic 2008 International Symposium: May 27-29, 2008, Tallinn, Estonia.*

#### Honours & Awards

2011, Victor Alari; Estonian Academy of Sciences, science award for high-school students

2011, Victor Alari; WinterAcademy contest of research papers; I price at undergraduate level

2010, Victor Alari; Science contest for high school students at TUT; I price in category of exact and natural sciences

2010, Victor Alari; Estonian national science contest for high-school students. I prize in natural sciences at undergraduate level

2006, Victor Alari; Estonian National Contest for Young Scientists at secondary school level, I Prize at basic school level

#### Main areas of scientific work

Wind wave measurements and numerical modeling. Wave induced sediment resuspension and transport. Wave interactions with marine infrastructure. Wave induced currents and setup. Operational forecast of waves. Wave climatology. Development of wave models. Unstructured grids.

## Research projects

Have participated in more than 30 projects. Listed are ongoing projects:

### *Estonian Science Foundation Grants*

-Wave induced currents and sea level setup in the coastal sea

### *National projects*

-Assessment of possible changes of Estonian climate and environmental status on the basis of dynamical modeling of atmosphere, ocean and river runoff (EstKliima).

### *International projects*

-Advanced wave forecast for safe navigation of small vessels

**DISSERTATIONS DEFENDED AT  
TALLINN UNIVERSITY OF TECHNOLOGY ON  
NATURAL AND EXACT SCIENCES**

1. **Olav Kongas**. Nonlinear Dynamics in Modeling Cardiac Arrhythmias. 1998.
2. **Kalju Vanatalu**. Optimization of Processes of Microbial Biosynthesis of Isotopically Labeled Biomolecules and Their Complexes. 1999.
3. **Ahto Buldas**. An Algebraic Approach to the Structure of Graphs. 1999.
4. **Monika Drews**. A Metabolic Study of Insect Cells in Batch and Continuous Culture: Application of Chemostat and Turbidostat to the Production of Recombinant Proteins. 1999.
5. **Eola Valdre**. Endothelial-Specific Regulation of Vessel Formation: Role of Receptor Tyrosine Kinases. 2000.
6. **Kalju Lott**. Doping and Defect Thermodynamic Equilibrium in ZnS. 2000.
7. **Reet Koljak**. Novel Fatty Acid Dioxygenases from the Corals *Plexaura homomalla* and *Gersemia fruticosa*. 2001.
8. **Anne Paju**. Asymmetric oxidation of Prochiral and Racemic Ketones by Using Sharpless Catalyst. 2001.
9. **Marko Vendelin**. Cardiac Mechanoenergetics *in silico*. 2001.
10. **Pearu Peterson**. Multi-Soliton Interactions and the Inverse Problem of Wave Crest. 2001.
11. **Anne Menert**. Microcalorimetry of Anaerobic Digestion. 2001.
12. **Toomas Tiivel**. The Role of the Mitochondrial Outer Membrane in *in vivo* Regulation of Respiration in Normal Heart and Skeletal Muscle Cell. 2002.
13. **Olle Hints**. Ordovician Scolecodonts of Estonia and Neighbouring Areas: Taxonomy, Distribution, Palaeoecology, and Application. 2002.
14. **Jaak Nõlvak**. Chitinozoan Biostratigraphy in the Ordovician of Baltoscandia. 2002.
15. **Liivi Kluge**. On Algebraic Structure of Pre-Operad. 2002.
16. **Jaanus Lass**. Biosignal Interpretation: Study of Cardiac Arrhythmias and Electromagnetic Field Effects on Human Nervous System. 2002.
17. **Janek Peterson**. Synthesis, Structural Characterization and Modification of PAMAM Dendrimers. 2002.
18. **Merike Vaher**. Room Temperature Ionic Liquids as Background Electrolyte Additives in Capillary Electrophoresis. 2002.
19. **Valdek Mikli**. Electron Microscopy and Image Analysis Study of Powdered Hardmetal Materials and Optoelectronic Thin Films. 2003.
20. **Mart Viljus**. The Microstructure and Properties of Fine-Grained Cermets. 2003.
21. **Signe Kask**. Identification and Characterization of Dairy-Related *Lactobacillus*. 2003.
22. **Tiiu-Mai Laht**. Influence of Microstructure of the Curd on Enzymatic and Microbiological Processes in Swiss-Type Cheese. 2003.
23. **Anne Kuusksalu**. 2–5A Synthetase in the Marine Sponge *Geodia cydonium*. 2003.
24. **Sergei Bereznev**. Solar Cells Based on Polycrystalline Copper-Indium

- Chalcogenides and Conductive Polymers. 2003.
25. **Kadri Kriis**. Asymmetric Synthesis of C<sub>2</sub>-Symmetric Bimorpholines and Their Application as Chiral Ligands in the Transfer Hydrogenation of Aromatic Ketones. 2004.
  26. **Jekaterina Reut**. Polypyrrole Coatings on Conducting and Insulating Substrates. 2004.
  27. **Sven Nõmm**. Realization and Identification of Discrete-Time Nonlinear Systems. 2004.
  28. **Olga Kijatkina**. Deposition of Copper Indium Disulphide Films by Chemical Spray Pyrolysis. 2004.
  29. **Gert Tamberg**. On Sampling Operators Defined by Rogosinski, Hann and Blackman Windows. 2004.
  30. **Monika Übner**. Interaction of Humic Substances with Metal Cations. 2004.
  31. **Kaarel Adamberg**. Growth Characteristics of Non-Starter Lactic Acid Bacteria from Cheese. 2004.
  32. **Imre Vallikivi**. Lipase-Catalysed Reactions of Prostaglandins. 2004.
  33. **Merike Peld**. Substituted Apatites as Sorbents for Heavy Metals. 2005.
  34. **Vitali Syritski**. Study of Synthesis and Redox Switching of Polypyrrole and Poly(3,4-ethylenedioxythiophene) by Using *in-situ* Techniques. 2004.
  35. **Lee Põllumaa**. Evaluation of Ecotoxicological Effects Related to Oil Shale Industry. 2004.
  36. **Riina Aav**. Synthesis of 9,11-Secosterols Intermediates. 2005.
  37. **Andres Braunbrück**. Wave Interaction in Weakly Inhomogeneous Materials. 2005.
  38. **Robert Kitt**. Generalised Scale-Invariance in Financial Time Series. 2005.
  39. **Juss Pavelson**. Mesoscale Physical Processes and the Related Impact on the Summer Nutrient Fields and Phytoplankton Blooms in the Western Gulf of Finland. 2005.
  40. **Olari Ilison**. Solitons and Solitary Waves in Media with Higher Order Dispersive and Nonlinear Effects. 2005.
  41. **Maksim Säkki**. Intermittency and Long-Range Structurization of Heart Rate. 2005.
  42. **Enli Kiipli**. Modelling Seawater Chemistry of the East Baltic Basin in the Late Ordovician–Early Silurian. 2005.
  43. **Igor Golovtsov**. Modification of Conductive Properties and Processability of Polyparaphenylene, Polypyrrole and polyaniline. 2005.
  44. **Katrin Laos**. Interaction Between Furcellaran and the Globular Proteins (Bovine Serum Albumin  $\beta$ -Lactoglobulin). 2005.
  45. **Arvo Mere**. Structural and Electrical Properties of Spray Deposited Copper Indium Disulphide Films for Solar Cells. 2006.
  46. **Sille Ehala**. Development and Application of Various On- and Off-Line Analytical Methods for the Analysis of Bioactive Compounds. 2006.
  47. **Maria Kulp**. Capillary Electrophoretic Monitoring of Biochemical Reaction Kinetics. 2006.
  48. **Anu Aaspõllu**. Proteinases from *Vipera lebetina* Snake Venom Affecting Hemostasis. 2006.

49. **Lyudmila Chekulayeva.** Photosensitized Inactivation of Tumor Cells by Porphyrins and Chlorins. 2006.
50. **Merle Uudsemaa.** Quantum-Chemical Modeling of Solvated First Row Transition Metal Ions. 2006.
51. **Tagli Pitsi.** Nutrition Situation of Pre-School Children in Estonia from 1995 to 2004. 2006.
52. **Angela Ivask.** Luminescent Recombinant Sensor Bacteria for the Analysis of Bioavailable Heavy Metals. 2006.
53. **Tiina Lõugas.** Study on Physico-Chemical Properties and Some Bioactive Compounds of Sea Buckthorn (*Hippophae rhamnoides* L.). 2006.
54. **Kaja Kasemets.** Effect of Changing Environmental Conditions on the Fermentative Growth of *Saccharomyces cerevisiae* S288C: Auxo-accelerostat Study. 2006.
55. **Ildar Nisamedtinov.** Application of  $^{13}\text{C}$  and Fluorescence Labeling in Metabolic Studies of *Saccharomyces* spp. 2006.
56. **Alar Leibak.** On Additive Generalisation of Voronoï's Theory of Perfect Forms over Algebraic Number Fields. 2006.
57. **Andri Jagomägi.** Photoluminescence of Chalcopyrite Tellurides. 2006.
58. **Tõnu Martma.** Application of Carbon Isotopes to the Study of the Ordovician and Silurian of the Baltic. 2006.
59. **Marit Kauk.** Chemical Composition of  $\text{CuInSe}_2$  Monograin Powders for Solar Cell Application. 2006.
60. **Julia Kois.** Electrochemical Deposition of  $\text{CuInSe}_2$  Thin Films for Photovoltaic Applications. 2006.
61. **Ilona Oja Açıık.** Sol-Gel Deposition of Titanium Dioxide Films. 2007.
62. **Tiia Anmann.** Integrated and Organized Cellular Bioenergetic Systems in Heart and Brain. 2007.
63. **Katrin Trummal.** Purification, Characterization and Specificity Studies of Metalloproteinases from *Vipera lebetina* Snake Venom. 2007.
64. **Gennadi Lessin.** Biochemical Definition of Coastal Zone Using Numerical Modeling and Measurement Data. 2007.
65. **Enno Pais.** Inverse problems to determine non-homogeneous degenerate memory kernels in heat flow. 2007.
66. **Maria Borissova.** Capillary Electrophoresis on Alkylimidazolium Salts. 2007.
67. **Karin Valmsen.** Prostaglandin Synthesis in the Coral *Plexaura homomalla*: Control of Prostaglandin Stereochemistry at Carbon 15 by Cyclooxygenases. 2007.
68. **Kristjan Piirimäe.** Long-Term Changes of Nutrient Fluxes in the Drainage Basin of the Gulf of Finland – Application of the PolFlow Model. 2007.
69. **Tatjana Dedova.** Chemical Spray Pyrolysis Deposition of Zinc Sulfide Thin Films and Zinc Oxide Nanostructured Layers. 2007.
70. **Katrin Tomson.** Production of Labelled Recombinant Proteins in Fed-Batch Systems in *Escherichia coli*. 2007.
71. **Cecilia Sarmiento.** Suppressors of RNA Silencing in Plants. 2008.
72. **Vilja Mardla.** Inhibition of Platelet Aggregation with Combination of Antiplatelet Agents. 2008.
73. **Maie Bachmann.** Effect of Modulated Microwave Radiation on Human

- Resting Electroencephalographic Signal. 2008.
74. **Dan Hvonen.** Terahertz Spectroscopy of Low-Dimensional Spin Systems. 2008.
  75. **Ly Villo.** Stereoselective Chemoenzymatic Synthesis of Deoxy Sugar Esters Involving *Candida antarctica* Lipase B. 2008.
  76. **Johan Anton.** Technology of Integrated Photoelasticity for Residual Stress Measurement in Glass Articles of Axisymmetric Shape. 2008.
  77. **Olga Volobujeva.** SEM Study of Selenization of Different Thin Metallic Films. 2008.
  78. **Artur Jgi.** Synthesis of 4'-Substituted 2,3'-dideoxynucleoside Analogues. 2008.
  79. **Mario Kadastik.** Doubly Charged Higgs Boson Decays and Implications on Neutrino Physics. 2008.
  80. **Fernando Prez-Caballero.** Carbon Aerogels from 5-Methylresorcinol-Formaldehyde Gels. 2008.
  81. **Sirje Vaask.** The Comparability, Reproducibility and Validity of Estonian Food Consumption Surveys. 2008.
  82. **Anna Menaker.** Electrosynthesized Conducting Polymers, Polypyrrole and Poly(3,4-ethylenedioxythiophene), for Molecular Imprinting. 2009.
  83. **Lauri Ilison.** Solitons and Solitary Waves in Hierarchical Korteweg-de Vries Type Systems. 2009.
  84. **Kaia Ernits.** Study of In<sub>2</sub>S<sub>3</sub> and ZnS Thin Films Deposited by Ultrasonic Spray Pyrolysis and Chemical Deposition. 2009.
  85. **Veljo Sinivee.** Portable Spectrometer for Ionizing Radiation "Gammamapper". 2009.
  86. **Jri Virkepu.** On Lagrange Formalism for Lie Theory and Operadic Harmonic Oscillator in Low Dimensions. 2009.
  87. **Marko Piirsoo.** Deciphering Molecular Basis of Schwann Cell Development. 2009.
  88. **Kati Helmja.** Determination of Phenolic Compounds and Their Antioxidative Capability in Plant Extracts. 2010.
  89. **Merike Smera.** Sobemoviruses: Genomic Organization, Potential for Recombination and Necessity of P1 in Systemic Infection. 2010.
  90. **Kristjan Laes.** Preparation and Impedance Spectroscopy of Hybrid Structures Based on CuIn<sub>3</sub>Se<sub>5</sub> Photoabsorber. 2010.
  91. **Kristin Lippur.** Asymmetric Synthesis of 2,2'-Bimorpholine and its 5,5'-Substituted Derivatives. 2010.
  92. **Merike Luman.** Dialysis Dose and Nutrition Assessment by an Optical Method. 2010.
  93. **Mihhail Berezovski.** Numerical Simulation of Wave Propagation in Heterogeneous and Microstructured Materials. 2010.
  94. **Tamara Aid-Pavlidis.** Structure and Regulation of BDNF Gene. 2010.
  95. **Olga Bragina.** The Role of Sonic Hedgehog Pathway in Neuro- and Tumorigenesis. 2010.
  96. **Merle Randrt.** Wave Propagation in Microstructured Solids: Solitary and Periodic Waves. 2010.

97. **Marju Laars.** Asymmetric Organocatalytic Michael and Aldol Reactions Mediated by Cyclic Amines. 2010.
98. **Maarja Grossberg.** Optical Properties of Multinary Semiconductor Compounds for Photovoltaic Applications. 2010.
99. **Alla Maloverjan.** Vertebrate Homologues of Drosophila Fused Kinase and Their Role in Sonic Hedgehog Signalling Pathway. 2010.
100. **Priit Pruunsild.** Neuronal Activity-Dependent Transcription Factors and Regulation of Human *BDNF* Gene. 2010.
101. **Tatjana Knjazeva.** New Approaches in Capillary Electrophoresis for Separation and Study of Proteins. 2011.
102. **Atanas Katerski.** Chemical Composition of Sprayed Copper Indium Disulfide Films for Nanostructured Solar Cells. 2011.
103. **Kristi Timmo.** Formation of Properties of  $\text{CuInSe}_2$  and  $\text{Cu}_2\text{ZnSn}(\text{S},\text{Se})_4$  Monograin Powders Synthesized in Molten KI. 2011.
104. **Kert Tamm.** Wave Propagation and Interaction in Mindlin-Type Microstructured Solids: Numerical Simulation. 2011.
105. **Adrian Popp.** Ordovician Proetid Trilobites in Baltoscandia and Germany. 2011.
106. **Ove Pärn.** Sea Ice Deformation Events in the Gulf of Finland and This Impact on Shipping. 2011.
107. **Germo Väli.** Numerical Experiments on Matter Transport in the Baltic Sea. 2011.
108. **Andrus Seiman.** Point-of-Care Analyser Based on Capillary Electrophoresis. 2011.
109. **Olga Katargina.** Tick-Borne Pathogens Circulating in Estonia (Tick-Borne Encephalitis Virus, *Anaplasma phagocytophilum*, *Babesia* Species): Their Prevalence and Genetic Characterization. 2011.
110. **Ingrid Sumeri.** The Study of Probiotic Bacteria in Human Gastrointestinal Tract Simulator. 2011.
111. **Kairit Zovo.** Functional Characterization of Cellular Copper Proteome. 2011.
112. **Natalja Makarytsheva.** Analysis of Organic Species in Sediments and Soil by High Performance Separation Methods. 2011.
113. **Monika Mortimer.** Evaluation of the Biological Effects of Engineered Nanoparticles on Unicellular Pro- and Eukaryotic Organisms. 2011.
114. **Kersti Tepp.** Molecular System Bioenergetics of Cardiac Cells: Quantitative Analysis of Structure-Function Relationship. 2011.
115. **Anna-Liisa Peikolainen.** Organic Aerogels Based on 5-Methylresorcinol. 2011.
116. **Leeli Amon.** Palaeoecological Reconstruction of Late-Glacial Vegetation Dynamics in Eastern Baltic Area: A View Based on Plant Macrofossil Analysis. 2011.
117. **Tanel Peets.** Dispersion Analysis of Wave Motion in Microstructured Solids. 2011.
118. **Liina Kaupmees.** Selenization of Molybdenum as Contact Material in Solar Cells. 2011.
119. **Allan Olsper.** Properties of VPg and Coat Protein of Sobemoviruses. 2011.

120. **Kadri Koppel**. Food Category Appraisal Using Sensory Methods. 2011.
121. **Jelena Gorbatšova**. Development of Methods for CE Analysis of Plant Phenolics and Vitamins. 2011.
122. **Karin Viipsi**. Impact of EDTA and Humic Substances on the Removal of Cd and Zn from Aqueous Solutions by Apatite. 2012.
123. **David Schryer**. Metabolic Flux Analysis of Compartmentalized Systems Using Dynamic Isotopologue Modeling. 2012.
124. **Ardo Illaste**. Analysis of Molecular Movements in Cardiac Myocytes. 2012.
125. **Indrek Reile**. 3-Alkylcyclopentane-1,2-Diones in Asymmetric Oxidation and Alkylation Reactions. 2012.
126. **Tatjana Tamberg**. Some Classes of Finite 2-Groups and Their Endomorphism Semigroups. 2012.
127. **Taavi Liblik**. Variability of Thermohaline Structure in the Gulf of Finland in Summer. 2012.
128. **Priidik Lagemaa**. Operational Forecasting in Estonian Marine Waters. 2012.
129. **Andrei Errapart**. Photoelastic Tomography in Linear and Non-linear Approximation. 2012.
130. **Külliki Krabbi**. Biochemical Diagnosis of Classical Galactosemia and Mucopolysaccharidoses in Estonia. 2012.
131. **Kristel Kaseleht**. Identification of Aroma Compounds in Food using SPME-GC/MS and GC-Olfactometry. 2012.
132. **Kristel Kodar**. Immunoglobulin G Glycosylation Profiling in Patients with Gastric Cancer. 2012.
133. **Kai Rosin**. Solar Radiation and Wind as Agents of the Formation of the Radiation Regime in Water Bodies. 2012.
134. **Ann Tiiman**. Interactions of Alzheimer's Amyloid-Beta Peptides with Zn(II) and Cu(II) Ions. 2012.
135. **Olga Gavrilova**. Application and Elaboration of Accounting Approaches for Sustainable Development. 2012.
136. **Olesja Bondarenko**. Development of Bacterial Biosensors and Human Stem Cell-Based *In Vitro* Assays for the Toxicological Profiling of Synthetic Nanoparticles. 2012.
137. **Katri Muska**. Study of Composition and Thermal Treatments of Quaternary Compounds for Monograin Layer Solar Cells. 2012.
138. **Ranno Nahku**. Validation of Critical Factors for the Quantitative Characterization of Bacterial Physiology in Accelerostat Cultures. 2012.
139. **Petri-Jaan Lahtvee**. Quantitative Omics-level Analysis of Growth Rate Dependent Energy Metabolism in *Lactococcus lactis*. 2012.
140. **Kerti Orumets**. Molecular Mechanisms Controlling Intracellular Glutathione Levels in Baker's Yeast *Saccharomyces cerevisiae* and its Random Mutagenized Glutathione Over-Accumulating Isolate. 2012.
141. **Loreida Timberg**. Spice-Cured Sprats Ripening, Sensory Parameters Development, and Quality Indicators. 2012.
142. **Anna Mihhalevski**. Rye Sourdough Fermentation and Bread Stability. 2012.
143. **Liisa Arike**. Quantitative Proteomics of *Escherichia coli*: From Relative to Absolute Scale. 2012.

144. **Kairi Otto**. Deposition of  $\text{In}_2\text{S}_3$  Thin Films by Chemical Spray Pyrolysis. 2012.
145. **Mari Sepp**. Functions of the Basic Helix-Loop-Helix Transcription Factor TCF4 in Health and Disease. 2012.
146. **Anna Suhhova**. Detection of the Effect of Weak Stressors on Human Resting Electroencephalographic Signal. 2012.
147. **Aram Kazarjan**. Development and Production of Extruded Food and Feed Products Containing Probiotic Microorganisms. 2012.
148. **Rivo Uiboupin**. Application of Remote Sensing Methods for the Investigation of Spatio-Temporal Variability of Sea Surface Temperature and Chlorophyll Fields in the Gulf of Finland. 2013.
149. **Tiina Kriščiunaite**. A Study of Milk Coagulability. 2013.
150. **Tuuli Levandi**. Comparative Study of Cereal Varieties by Analytical Separation Methods and Chemometrics. 2013.
151. **Natalja Kabanova**. Development of a Microcalorimetric Method for the Study of Fermentation Processes. 2013.
152. **Himani Khanduri**. Magnetic Properties of Functional Oxides. 2013.
153. **Julia Smirnova**. Investigation of Properties and Reaction Mechanisms of Redox-Active Proteins by ESI MS. 2013.